UNIVERSITÀ DEGLI STUDI DI PARMA

Dottorato di Ricerca in Tecnologie dell'Informazione

XXI Ciclo

EFFICIENT DISTRIBUTED DETECTION
FOR WIRELESS SENSOR NETWORKS

Coordinatore:

Chiar.mo Prof. Carlo Morandi

Tutor:

Chiar.mo Prof. Gianluigi Ferrari

Dottorando: *Marco Martalò*

Gennaio 2009

To my family
For their unconditioned support

Longum iter est per praecepta,
breve et efficax per exempla
(Lucio Anneo Seneca, Epistulae morales ad Lucilium)

Contents

List of Figures

List of Tables

Introduction

Recent years have witnessed an exponential growth of micro device manufacturing techniques and, in particular, of powerful sensor devices. The costs of these sensors have dropped, leading to an increasing interest on sensor networks for civilian applications, e.g., environmental monitoring. The use of sensor networks in the military field has, on the other hand, a long history.

In all cases, the goal of a sensor network is to identify the status of a phenomenon of interest through a collaborative action of the sensors. An istance of this collaborative action is given by *distributed detection*. The increasing interest for sensor networks has, therefore, spurred a significant activity on the design of efficient distributed detection techniques.

In this thesis, we investigate how the structural properties of the physical phenomenon under observation can be taken into account in designing distributed detection algorithms for sensor networks. After an accurate literature survey (Chapter 1), this thesis will be structured around the following themes.

- Distributed detection of spatially *constant* phenomena, i.e., phenomena with the same status across the sensors (Chapter 2). We first present an analytical framework for performance evaluation of multihop clustered sensor networks, with multi-level information fusion. In this case, a simple reclustering procedure is proposed to prolong the network lifetime. Finally, our framework is extended to scenarios with non-constant observation SNR and possible joint decoding/fusion strategies at the access point (AP).

- Distributed detection of a phenomenon whose status changes *independently*

from sensor to sensor (Chapter 3). In this case, the goal of the AP is to re-construct the overall phenomenon status. Thereofore, heuristic detection algorithms with reduced computational complexity are proposed and compared to the optimum minimum mean square error (MMSE) strategy.

- Distributed detection of spatially *correlated* sources (Chapter 4). In this case, we design distributed detection algorithms which take into account the spatial correlation among the sensors in scenarios with or without an intermediate relay. Moreover, the impact of simple power control strategies is evaluated.

In all cases, a lot of emphasis is put on the negative impact of the noise in the communication channels and proper techniques are incorporated into the proposed algorithms to counter-act this limitation. Moreover, simulation and experimental results, relative to IEEE 802.15.4 sensor networks, are provided, in order to validate our analytical framework also in these more realistic scenarios.

Chapter 1

Literature Analysis and Motivations

1.1 Introduction

Recent years have witnessed an increasing interest for the use of distributed detection techniques in sensor networks [2], especially for civilian applications [3], e.g., environmental monitoring [4]. The application of distributed detection techniques in the military field has, on the other hand, a long history. In all cases, the goal of a sensor network with distributed detection is to identify the status of a phenomenon of interest through a collaborative action of the sensors [5]. The increasing interest for sensor networks has, therefore, spurred a significant activity on the design of efficient distributed detection techniques, in order to obtain fault-tolerant networks with the longest possible lifetime [6].

This chapter is structured as follows. In Section 1.2, we review the literature related to the distributed detection of spatially constant phenomena, i.e., phenomena with the same status across all the sensors. In Section 1.3, we focus on the techniques proposed in the literature for distributed detection of spatially non-constant phenomena, i.e., phenomena changing independently their status from sensor to sensor. Finally, in Section 1.4 we focus on techniques which exploit the spatial correlation

of the observed phenomenon.

1.2 Detection of Spatially Constant Phenomena

Several communication-theoretic-oriented approaches have been proposed to study decentralized detection [7–14]. In [15], the authors follow a Bayesian approach for the minimization of the probability of decision error at the AP and study optimal fusion rules. Most of the proposed approaches are based on the assumption of *ideal* communication links between the sensors and the AP. However, in a realistic communication scenario, these links are likely to be *noisy* [16]. The impact of noisy communication links on the design of optimal fusion rules is evaluated in [17–21]. A practical and widely used model for the noisy communication links is the binary symmetric channel (BSC) [17–21]. In [21], a few techniques are proposed to make the system more robust against the noise. In [13], the author considers MMSE parameter estimation in sensor networks. Use of censoring algorithms at the sensors has also been studied for the design of decentralized detection schemes [22]. In [23] the authors analyze aspects related to compression of observed data (using distributed source coding) and data transmission.

Information-theoretic approaches have also been proposed for the study of sensor networks with decentralized detection. In [12], the authors propose a framework to characterize a sensor network in terms of its entropy and false alarm/missed detection probabilities. Information theory has also been used to tackle the problem of optimally placing sensors over a given surface to meet the chosen design criterion. In [24], the mutual information is evaluated in a scenario with censoring sensors which transmit their local likelihood ratios, by maximizing the probability of correct decision [25]. In order to optimally place the sensors over a given surface, system entropy and mutual information are considered in [26] and [27], respectively. In [28], an information-theoretic approach is proposed to solve, with limited complexity, the problem of sensor selection and placement for target localization and tracking. Decentralized detection algorithms, based on the evaluation of the sensor network mutual information, have also been proposed to design intelligent systems

that recognize, in a robust manner, a target in a scene which rapidly changes [29].

The impact of communication constraints, e.g., limited bandwidth and presence of noise, is considered in [30], where a randomization paradigm for decentralized detection is proposed to overcome the communication bottle-neck. In [31], the authors consider the problem of decentralized detection in *wireless* sensor networks where communication links are affected by fading. In the latter scenario, the optimal distributed detection strategy is first derived, on the basis of the integration of the communication and fusion phases, and then suboptimal (requiring a limited a priori knowledge of the channel state) strategies are developed. This approach is further extended in [17], where the authors optimize the local decision strategy in sensor networks with fading, and in [32], where the authors propose a decentralized detection strategy based on censoring sensors, which transmit only when their local likelihood ratios are sufficiently large.

One of the critical issues in designing sensor networks is their energy efficiency, especially in wireless scenarios, where sensors may be battery-powered. Motivated by recent theoretical results in the area of network coding [33–38], significant research activity has been devoted to the development of specific channel coding strategies. Although preliminary works focus on scenarios with ideal communication channels, the impact of communication noise has also been investigated [39]. Moreover, distributed network coding strategies for the multi-access relay channel, i.e., a channel where source nodes can send their information to the destination through a common relay node, have been investigated [40, 41].

The problem of extending the sensor network lifetime is a direct consequence of the energy efficiency in scenarios with battery-powered nodes. In particular, the derivation of upper bounds for the sensor network lifetime has been exploited. In [42–50], various analyses are carried out according to the particular sensor network architecture and the definition of sensor network lifetime. In [51], a simple formula, independent of these parameters, is provided for the computation of the sensor network lifetime and a medium access control (MAC) protocol is proposed to maximize the sensor network lifetime. In [52], a distributed MAC protocol is designed in order to maximize the network lifetime. In [53], network lifetime maximization is considered

as the main criterion for the design of sensor networks with data gathering. In [54], the authors consider a realistic sensor network with nodes equipped with TinyOS, an event-based operating system for networked sensor motes. In this scenario, the network lifetime is evaluated as a function of the average distance of the sensors from the central data collector. In [55], an analytical framework, based on the Chen-Stein method of Poisson approximation, is proposed in order to find the critical time at which isolated nodes, i.e., nodes without neighbors in the network, begin to appear, due to the deaths of other nodes. Although this method is derived for generic networks where nodes are randomly deployed and can die in a random manner, this can also be applied to sensor networks. Finally, an important area of application of wireless sensor networking is the medical field. In [56], an analysis of network lifetime using IEEE 802.15.4 sensor networks [57] is derived for this kind of applications.

In several situations, the sensors might observe the *same* phenomenon with *varying quality*. In other words, while some sensors might have direct access to the phenomenon (e.g., they are close to a monitored source of heat), other sensors might not (e.g., there is an obstruction between them and the target source of heat). Therefore, a relevant problem, with practical implications, consists in evaluating the performance of distributed detection schemes with non-constant observation quality at the sensors.

1.3   Detection of Spatially Non-Constant Phenomena

While in Section 1.2 we surveyed the literature on decentralized detection of a phenomenon *common* for all sensors, it is of interest to analyze cases where the status of the phenomenon may vary from sensor to sensor. In [58], the authors consider a scenario with a single phenomenon status change (denoted, in the following, as *boundary*) and propose a framework, based on minimum mean square error (MMSE) estimation, to determine the position of this boundary. In [59], under the assumption of proper regularity of the observed boundary, a reduced-complexity MMSE decoder is proposed. In [60], the authors show that an MMSE decoder is unfeasible for large scale sensor networks, due to its computational complexity, and propose a distributed detection strategy based on factor graphs and the sum-product algorithm. Moreover, MMSE-

based distributed detection schemes have also been investigated in scenarios with a common binary phenomenon under observation and bandwidth constraints [61]. Finally, in [62, 63] the authors examine the problem of determining boundaries of natural phenomena through proper processing of data collected by sensor networks. In those papers, particular attention is devoted to the estimation accuracy, given in terms of the confidence interval of the results obtained with the proposed framework.

1.4 Detection of Correlated Sources

In the previous sections, we focused on scenarios where the phenomenon under observation is *common* for all sensors or may change *independently* across them. However, in a more general case, the phenomenon status observed at each sensor can be *correlated*. In the case of a single collector node (the AP), this problem is often referred to as the reach-back channel problem [64–67]. In its simplest form, it can be summarized as follows: two independent nodes have to transmit correlated sensed data to a collector node by spending the minimum possible energy, i.e., by exploiting in some way the implicit correlation among the data. In the case of orthogonal additive white Gaussian noise (AWGN) channels, the separation between source and channel coding is optimal [67, 68]. This means that the theoretical limit can be achieved by, first, compressing each source up to the Slepian-Wolf (SW) limit and, then, utilizing two independent capacity-achieving channel codes (one per source). However, implementing a practical system based on separation, i.e., distributed source coding (DSC), is not straightforward [69–73]. In particular, the problem of designing good practical codes for correlated sources is still an open issue [74] and, moreover, separation between source and channel coding may lead to catastrophic error propagation.

An alternative approach to exploiting the correlation between sources is represented by joint source-channel coding (JSCC). In this case, the correlated sources are not source-encoded but only channel-encoded. If we compare, for a given information rate, a JSCC system with a system based on source/channel separation, the channel codes used in the JSCC system must be less powerful (i.e., with higher rate).

This weakness can be compensated by exploiting the correlation between sources at the joint decoder, making the overall performance approach the theoretical limits. Note that in the JSCC approach, the sources are encoded independently of each other (i.e., for a given source neither the realizations from the other sources nor the correlation model are available at the encoder site) and transmitted through the channel. Correlation between the sources, instead, must be assumed to be known or accurately estimated at the (common) receiver, which aims at the reconstruction of the two sources. Works dealing with JSCC schemes have so far considered turbo or low-density parity-check (LDPC) codes [75–77], in such a way that the decoder can exploit the correlation among sources by performing proper message passing between the two decoders. Recently, the application of rateless coding has also been considered to improve the performance of multiple access systems [78, 79].

In [80], the authors consider LDPC coding at the sources and network coding at the relay, and their goal is to derive an overall Tanner graph to describe the joint LDPC/network code and implement message-passing decoding. Moreover, in [80] scenarios with only two sources are considered, whereas our framework is applicable to scenarios with any number of sources. Note also that relay networks with a single source (and not correlated sources) and single destination have been thoroughly investigated [81, 82]. Although cooperative coding [83, 84] has also been applied to relayed schemes [85, 86], we underline that our focus is on *non-cooperative* schemes, i.e., schemes where the sources do not cooperate directly with each other.

The performance of multiple access schemes can be improved by the use of feedback. In general terms, the collector can provide the sources with supplementary information (e.g., on the links' states) to allow them to counter-act the effects of channel noise. From an information-theoretic viewpoint, while feedback does not increase the capacity of a memoryless channel with one sender and one receiver [87], it is well known that the capacity region of multiple access channels increases through the use of feedback [88, 89]. In [90, 91], the authors devise joint source-channel coding strategies for multiple-access channels with feedback and correlated sources.

Chapter 2

Distributed Detection of Spatially Constant Phenomena

2.1 Introduction

In this chapter, we analyze the problem of distributed detection of a spatially constant phenomenon in wireless sensor networks. We first present a communication-theoretic framework on distributed detection in clustered sensor networks where hierarchical multi-level fusion is considered. The sensor nodes observe a binary phenomenon and transmit their own data to an AP, possibly through intermediate fusion centers (FCs), which perform majority-like fusion strategies. We investigate the impact of uniform and non-uniform clustering on the system performance, evaluated in terms of probability of decision error on the phenomenon status at the AP. Our results show that uniform clustering leads to minimum performance degradation, which depends only on the number of decision levels, rather than on the specific clustered topology.

Since the uniform clustering topology allows to reduce the performance loss incurred by multi-level information fusion, we then investigate the benefits, in terms of longer network lifetime, of *adaptive reclustering*. In particular, the lifetime is studied under a physical layer quality of service (QoS) constraint, given by the maximum tolerable probability of decision error at the AP. On the other hand, *absence of re-*

clustering leads to a shorter network lifetime, and we show the impact of various clustering configurations under different QoS conditions. Our results show that the organization of sensors in a *few big clusters* is the winning strategy to maximize the network lifetime. Moreover, the observation of the phenomenon should be *frequent* in order to limit the penalties associated with the reclustering procedure.

Although our analysis in based on the assumption of constant signal-to-noise ratio (SNR) at the sensors, we show how to extend it to sensor networks characterized by *non-constant* observation SNRs at the sensors. Furthermore, we show *how* the impact of communication noise in the links between the sensors and the AP depends on the sensor SNR profile (i.e., the spatial distribution of the observation noise). More precisely, different sensor SNR profiles are compared under two alternative assumptions: (i) common *maximum* sensor SNR or (ii) common *average* sensor SNR.

Finally, we study how to combine decoding and fusion at the AP in sensor networks for distributed detection to improve the performance in scenarios where the sensors communicate to the AP through *noisy* communication links. Simple distributed channel coding strategies are analyzed, either using repetition coding at each sensor (i.e., multiple observations) or distributed (network-wide) systematic block channel coding. In the latter case, the use of a relay is proposed. In all cases, the system performance is analyzed *separating* or *joining* the decoding and fusion operations at the AP. Our results show that the schemes with joint decoding and fusion show a significant performance improvement with respect to that of schemes with separate decoding and fusion and the use of *multiple observations* is often the winning choice at practical values of the probability of decision error.

Throughout this chapter, the analytical approach is extended to realistic sensor networks, based on commercial protocols. In particular, simulation (relative to Zigbee networks) and experimental (relative to IEEE 802.15.4-based networks) results, which confirm the analytical predictions, are presented, enriching the proposed analytical framework and showing how typical networking performance metrics (such as throughput and delay) are influenced by the probability of decision error.

This chapter is structured as follows. In Section 2.2, we present the analytical framework to analyze the peformance of clustered sensor networks. In Section 2.3,

we analyze the sensor network lifetime in the presence of the proposed distributed detection startegies. In Section 2.4, we extend our framework to take into account possible non-constant SNR spatial distributions at the sensors. In Section 2.5, we extend the framework also to take into account the presence of different detection/fusion strategies. Finally, in Section 2.6 concluding remarks are given.

2.2 Distributed Detection in Clustered Sensor Networks

2.2.1 Preliminaries on Distributed Binary Detection

We consider a network scenario where n sensors observe a *common binary phenomenon* whose status is defined as follows:

$$H = \begin{cases} H_0 & \text{with probability } p_0 \\ H_1 & \text{with probability } 1 - p_0 \end{cases}$$

where $p_0 \triangleq P(H = H_0)$. In the remainder of this thesis, if no otherwise stated, we will focus on a scenario with equal a priori probabilities of the phenomenon, i.e., $p_0 = p_1 = 1/2$. However, similar results can be derived for a scenario with $p_0 \neq 1/2$. The sensors are clustered into $n_c < n$ groups, and each sensor can communicate only with its local first-level FC. The first-level FCs collect data from the sensors in their corresponding clusters and make local decisions on the status of the binary phenomenon. In a scenario with two levels of information fusion, each local FC transmits to the AP, which makes the final decision. A logical representation of this architecture is shown in Figure 2.1. The observed signal at the i-th sensor can be expressed as

$$r_i = c_E + n_i \qquad i = 1, \dots, n \tag{2.1}$$

where

$$c_E \triangleq \begin{cases} 0 & \text{if } H = H_0 \\ s & \text{if } H = H_1 \end{cases}$$

and $\{n_i\}$ are additive noise samples. Assuming that the noise samples $\{n_i\}$ are independent with the same Gaussian distribution $\mathcal{N}(0, \sigma^2)$, the common signal-to-noise
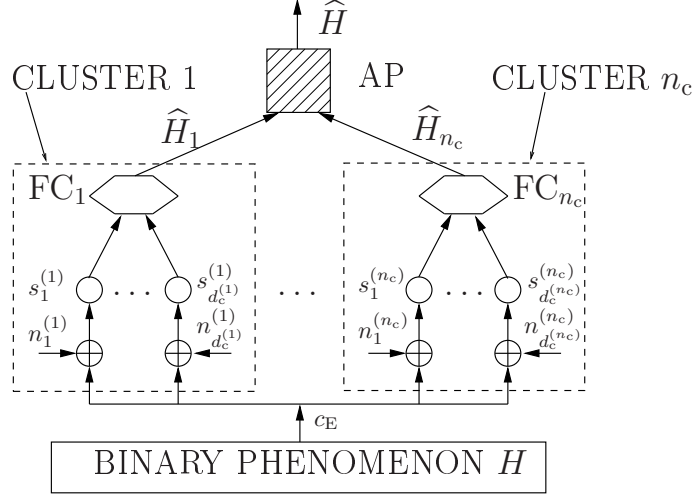
Figure 2.1: Block diagram of a clustered sensor network with distributed binary detection and two decision levels.

ratio (SNR) at the sensors can be defined as follows:

$$\text{SNR}_{\text{sensor}} = \frac{[\mathbb{E}\{c_{\text{E}}|H_1\} - \mathbb{E}\{c_{\text{E}}|H_0\}]^2}{\sigma^2} = \frac{s^2}{\sigma^2}. \tag{2.2}$$

Each sensor makes a decision comparing its observation r_i with a threshold value τ_i and computes a local decision $u_i = U(r_i - \tau_i)$, where $U(\cdot)$ is the unit step function. In order to optimize the system performance, the thresholds $\{\tau_i\}$ need to be optimized. Even though, in general, a common value of the decision threshold for all sensors might not be the best choice, in the following we assume that all sensors use the same decision threshold τ. While in a scenario with no clustering and ideal communication links between the sensors and the AP the relation between the optimized value of τ and s is well known [15], in the presence of clustering it is not. In the following, the value of τ will be optimized in all considered scenarios. More precisely, we consider a possible (discrete) set of values which can be assumed by $\tau : \{\tau_{\min}, \tau_{\min} + \Delta\tau, \tau_{\min} + 2\Delta\tau, \ldots, \tau_{\max}\}$. In other words, τ can assume values in $[\tau_{\min}, \tau_{\max}]$ at regular steps of (sufficiently small) width $\Delta\tau$. For a given sensor SNR, the probability of decision

error is evaluated for each possible value of τ, and the minimizing value is selected as threshold. In all considered cases, the optimized value of the common threshold is around $\sqrt{\text{SNR}_{\text{sensor}}}/2$, as already observed in [15, 92].

In a scenario with noisy communication links, modeled as BSCs, the decision u_i sent by the i-th sensor can be *flipped* with a probability corresponding to the crossover probability of the BSC model and denoted as p [21]. The received bit at the fusion point (either an FC for clustered networks or directly the AP in the absence of clustering), referred to as $u_i^{(\text{r})}$, can be expressed as

$$u_i^{(\text{r})} = \begin{cases} u_i & \text{with probability } 1-p \\ 1-u_i & \text{with probability } p. \end{cases}$$

In the presence of noisy links, the value of the optimized local threshold τ, fixed for all sensors, might be different from that in a scenario with ideal communication links. As for the case with ideal communication links, this optimization will be carried out, for given SNR and clustering configuration, by minimizing the probability of decision error, as outlined at the end of the previous paragraph. Note that the best strategy would consist in using a properly optimized set of decision thresholds $\{\tau_i\}$ at the sensors. In particular, in a more general scenario where the type of event perceived by the sensor might vary, a more refined per-cluster optimization of the sensor decision threshold could be considered. However, since we are interested in monitoring a spatially constant binary phenomenon, we consider a simpler optimization approach, where the same threshold is used at all sensors.

While the communication links between sensors and first level FCs can be noisy, we assume that the other communication links in the network (i.e., from each FC to higher level FCs or the AP) are ideal. The rationale behind the assumption of ideal high-level links lies in the fact that in practical sensor network design the FCs are likely to be placed relatively close to the AP. Therefore, under the assumption of a robust access control mechanism, one can assume that these links are ideal. The proposed analytical framework can be extended to encompass the presence of higher level noisy links. Moreover, realistic sensor network scenarios (with collisions) will be analyzed, through simulations and experiments, in Section 2.2.5.
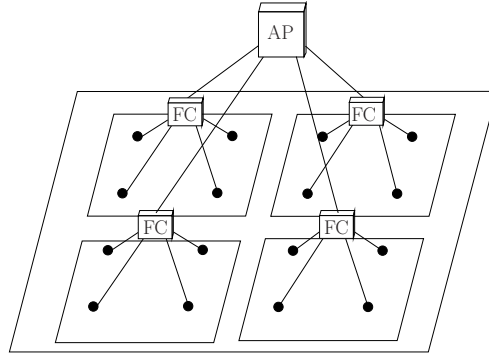
Figure 2.2: An example of a uniformly clustered sensor network with $n = 16$ sensors. There are $n_c = 4$ clusters with $d_c = 4$ sensors each.

We point out that the specific topologies of the considered networks are not explicitly taken into account. For instance, the distances between nodes are not explicitly mentioned. This corresponds to the assumption of modelling all noisy communication links as BSCs with the same cross-over probability. In order to extend our analytical framework, while still keeping the simple BSC-based link modelling, one can consider different cross-over probabilities (they could be associated with a specific network topology). This motivates the use of weighing fusion schemes, where the decisions to be fused together are weighed by the corresponding link qualities [93].

2.2.2   An Analytical Framework for Distributed Detection in Clustered Sensor Networks

Uniform Clustering

In a scenario with *uniform* clustering, the sensors are grouped into identical clusters, i.e., each of the n_c clusters contains d_c sensors, with $n_c \cdot d_c = n$. A pictorial description of a uniformly clustered sensor network with $n = 16$ sensors and 2 decision levels is shown in Figure 2.2: there are $n_c = 4$ clusters with $d_c = 4$ sensors each.

According to the assumption of majority-like information fusion considered in

this chapter, the j-th FC ($j = 1, \ldots, n_c$) computes a local decision using the following rule:

$$\widehat{H}_j = \Gamma\left(u_1^{(j)}, \ldots, u_{d_c}^{(j)}\right) = \begin{cases} 0 & \text{if } \sum_{m=1}^{d_c} u_m^{(j)} < k \\ 1 & \text{if } \sum_{m=1}^{d_c} u_m^{(j)} \geq k \end{cases} \tag{2.3}$$

where $u_m^{(j)}$ is the $m-$th decision of a sensor in the $j-$th cluster and k is the FC decision threshold—since the clusters have the same dimension, the threshold $k = \lfloor d_c/2 \rfloor + 1$ is the same at all FCs. The AP decides with the following majority-like rule based on the local FC decisions $\{\widehat{H}_j\}$:

$$\widehat{H} = \Psi\left(\widehat{H}_1, \ldots, \widehat{H}_{n_c}\right) = \begin{cases} H_0 & \text{if } \sum_{j=1}^{n_c} \widehat{H}_j < k_f \\ H_1 & \text{if } \sum_{j=1}^{n_c} \widehat{H}_j \geq k_f \end{cases} \tag{2.4}$$

where $k_f = \lfloor n_c/2 \rfloor + 1$ is the fusion threshold at the AP. Using a combinatorial approach (based on the repeated trials formula [94]) and taking into account the decision rules (2.3) and (2.4), the probability of decision error at the AP can be expressed as follows:

$$\begin{aligned} P_e &= P(\widehat{H} = H_1 | H_0)P(H_0) + P(\widehat{H} = H_0 | H_1)P(H_1) \tag{2.5} \\ &= p_0 \, \text{bin}(k_f, n_c, n_c, \text{bin}(k, d_c, d_c, Q(\tau))) \\ &\quad + (1 - p_0) \, \text{bin}(0, k_f - 1, n_c, \text{bin}(k, d_c, d_c, Q(\tau - s))) \tag{2.6} \end{aligned}$$

where $Q(x) \triangleq \int_x^\infty \frac{1}{\sqrt{2\pi}} \exp(-y^2/2) \, \mathrm{d}y$ and

$$\text{bin}(a, b, n, z) \triangleq \sum_{i=a}^{b} \binom{n}{i} z^i (1 - z)^{(n-i)} \tag{2.7}$$

where $a, b, n \in \mathbb{N}$ and $z \in (0, 1)$. If $n_c = k_f = 1$ and $d_c = n$, i.e., there is no clustering, the probability of decision error (2.6) reduces to that derived in [21].

We point out that the majority fusion rule (2.3) with FC decision threshold $k = \lfloor d_c/2 \rfloor + 1$ is exact for *odd* values of k. For *even* values of k, the proposed fusion strategy tends to favor a final decision equal to '0.' For example, if $d_c = 2$, then only the received sequence 11 leads to a final decision in favor of '1.' However, since in all considered scenarios the two statuses of the binary phenomenon are equiprobable,
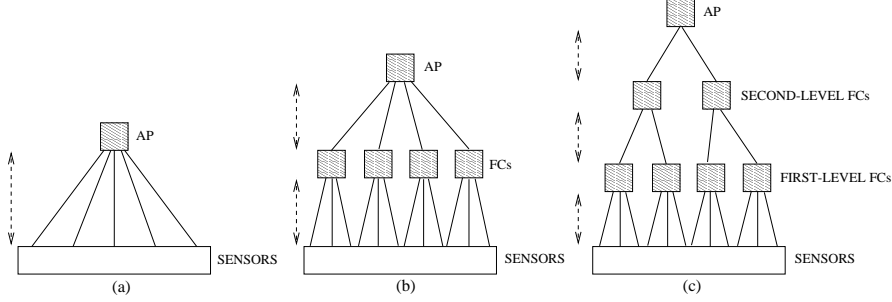
Figure 2.3: Basic structures for sensor networks with distributed detection. Three cases are shown: (a) absence of clustering, (b) uniform clustering with two levels of information fusion, and (c) uniform clustering with three levels of information fusion.

setting k to $\lfloor d_c/2 \rfloor$ would unbalance the decision towards '1,' but, *on average*, the final performance would be the same.

Although we have previously derived the probability of decision error in a scenario with uniform clustering and two levels of information fusion, this analysis can be extended to a scenario with three levels of information fusion. In Figure 2.3 (c), the logical structure of a sensor network with three decision levels is illustrated. For comparison, in the same figure the schemes with (a) no clustering and (b) two decision level uniform clustering are also shown. One should note that Figure 2.3 (b) is logically equivalent to the network schemes shown in Figure 2.1 and Figure 2.2.

In a three decision level scenario the probability of decision error at the AP becomes

$$
\begin{aligned}
P_e \; = \; & p_0 \, \mathrm{bin}(k_f, n_{c_2}, n_{c_2}, \mathrm{bin}(k_2, d_{c_2}, d_{c_2}, \mathrm{bin}(k_1, d_{c_1}, d_{c_1}, Q(\tau)))) \\
& + (1 - p_0) \, \mathrm{bin}(0, k_f - 1, n_{c_2}, \mathrm{bin}(k_2, d_{c_2}, d_{c_2}, \mathrm{bin}(k_1, d_{c_1}, d_{c_1}, Q(\tau - s)))))). \quad (2.8)
\end{aligned}
$$

We remark that the above derivation can be straightforwardly extended to a scenario with a generic number of fusion levels. As for the scenario with uniform clustering and one decision level, the thresholds $\{k_i\}$ can be optimized by minimizing the probability of decision error at the AP.

Non-Uniform Clustering

Assuming a two-level sensor network topology, the probability of decision error in a generic scenario with non-uniform clustering can be evaluated as follows. Define the cluster size vector $\mathscr{D} \triangleq \{d_c^{(1)}, d_c^{(2)}, \ldots, d_c^{(n_c)}\}$, where $d_c^{(i)}$ is the number of sensors in the i-th cluster ($i = 1, \ldots, n_c$) and $\sum_{i=1}^{n_c} d_c^{(i)} = n$. Furthermore, define also the following two probability vectors:

$$\mathscr{P}^{1|1} \triangleq \left\{ p_1^{1|1}, p_2^{1|1}, \ldots, p_{n_c}^{1|1} \right\} \qquad\qquad \mathscr{P}^{1|0} \triangleq \left\{ p_1^{1|0}, p_2^{1|0}, \ldots, p_{n_c}^{1|0} \right\}$$

where $p_\ell^{1|1}$ ($p_\ell^{1|0}$, respectively) is the probability that the ℓ-th FC decides for H_1 when H_1 (H_0, respectively) has happened. We still consider the use of a common threshold τ at the sensors, and its value is optimized as described in Section 2.2.1. The elements of $\mathscr{P}^{1|1}$ (equivalently, the elements of $\mathscr{P}^{1|0}$) are, in general, different from each other and depend on the particular distribution of the sensors among the clusters. In [93], it is shown that the probability of decision error can be expressed as follows:

$$
\begin{aligned}
P_e \;=\; & p_0 \sum_{i=k_f}^{n_c} \sum_{j=1}^{\binom{n_c}{i}} \prod_{\ell=1}^{n_c} \left\{ s_{i,j}(\ell) p_\ell^{1|0} + (1 - s_{i,j}(\ell))(1 - p_\ell^{1|0}) \right\} \\
& + (1 - p_0) \sum_{i=0}^{k_f - 1} \sum_{j=1}^{\binom{n_c}{i}} \prod_{\ell=1}^{n_c} \left\{ s_{i,j}(\ell) p_\ell^{1|1} + (1 - s_{i,j}(\ell))(1 - p_\ell^{1|1}) \right\} \quad (2.9)
\end{aligned}
$$

where $\boldsymbol{s}_{i,j} = (s_{i,j}(1), \ldots, s_{i,j}(n_c))$ is a vector which designates the j-th configuration of the decisions from the first-level FCs in a case with i '1's (and, obviously, $n_c - i$ '0's). In Table 2.1, the possible configurations of $\boldsymbol{s}_{i,j}$ are shown in the presence of $n_c = 3$ clusters. For example, $\boldsymbol{s}_{1,2}$ is the second possible configuration with one '1' (and two '0'): the '1' is the decision of the second FC.

A scenario with *uniform* clustering can be interpreted as a special case of a generic non-uniform scenario. In this case, in fact, the elements of the three vectors $\mathscr{D}$, $\mathscr{P}^{1|1}$, and $\mathscr{P}^{1|0}$, become equal, i.e.:

$$
\begin{cases}
d_c^{(i)} & = \; d_c \\
p_i^{1|1} & = \; \mathrm{bin}(k, d_c, d_c, Q(\tau - s)) \\
p_i^{1|0} & = \; \mathrm{bin}(k, d_c, d_c, Q(\tau))
\end{cases}
$$

Table 2.1: Possible configurations of $s_{i,j}$ in a scenario with $n_c = 3$ clusters.

i	j	$s_{i,j}$
0	1	000
1	1	100
	2	010
	3	001
2	1	110
	2	101
	3	011
3	1	111

$\forall i = 1, \ldots, n_c$. It can be shown that (2.9) reduces to (2.6) in the presence of uniform clustering.

Scenarios with Noisy Communication Links

As described at the end of Section 2.2.1, realistic sensor networks are typically characterized by noisy communication links. In general, a BSC might not be the best modelling choice for a wireless communication link, which might experience block fading [31, 95–97]. However, in the presence of memoryless communication channels the use of a cross-over probability p is accurate. More precisely, p can be given a precise expression depending on the type of channel (with AWGN or bit-by-bit independent fading). Therefore, our simple model can give significant insights into the network behavior in many situations.

In a scenario with non-uniform clustering and two decision levels, the probability of decision error can be derived from (2.9), by replacing the probabilities $\{p_\ell^{1|i}\}_{\ell=1,\ldots,n_c}^{i=0,1}$ with the probabilities $\{p_{\ell,\text{noisy}}^{1|i}\}_{\ell=1,\ldots,n_c}^{i=0,1}$, which take into account the noise in the communication links between sensors and first-level FCs and are defined

as

$$p_{\ell,\text{noisy}}^{1|0} \triangleq \sum_{m=k_\ell}^{d_{\text{c}}^{(\ell)}} \binom{d_{\text{c}}^{(\ell)}}{m} P_{\text{c}_0}^m P_{\text{e}_0}^{d_{\text{c}}^{(\ell)}-m} \tag{2.10}$$

$$p_{\ell,\text{noisy}}^{1|1} \triangleq \sum_{m=k_\ell}^{d_{\text{c}}^{(\ell)}} \binom{d_{\text{c}}^{(\ell)}}{m} P_{\text{c}_1}^m P_{\text{e}_1}^{d_{\text{c}}^{(\ell)}-m}. \tag{2.11}$$

In (2.10), $P_{\text{c}_0} = 1 - P_{\text{e}_0}$ is the probability that a sensor decision sent to a first-level FC is in favor of H_1 when H_0 has happened and can be expressed, according to the BSC model for a noisy communication link, as

$$P_{\text{c}_0} = Q(\tau)(1-p) + [1-Q(\tau)]\,p\,. \tag{2.12}$$

Similarly, in (2.11) $P_{\text{c}_1} = 1 - P_{\text{e}_1}$ represents the probability that a decision sent by a sensor to a first-level FC is in favor of H_1 when H_1 has happened and can be given the following expression:

$$P_{\text{c}_1} = Q(\tau - s)(1-p) + [1-Q(\tau - s)]\,p\,. \tag{2.13}$$

Finally, the probability of decision error in a scenario with noisy communication links becomes

$$\begin{aligned} P_{\text{e}} &= p_0 \sum_{i=k_{\text{f}}}^{n_{\text{c}}} \sum_{j=1}^{\binom{n_{\text{c}}}{i}} \prod_{\ell=1}^{n_{\text{c}}} \{s_{i,j}(\ell)p_{\ell,\text{noisy}}^{1|0} + (1-s_{i,j}(\ell))(1-p_{\ell,\text{noisy}}^{1|0})\} \\ &\quad + (1-p_0) \sum_{i=0}^{k_{\text{f}}-1} \sum_{j=1}^{\binom{n_{\text{c}}}{i}} \prod_{\ell=1}^{n_{\text{c}}} \{s_{i,j}(\ell)p_{\ell,\text{noisy}}^{1|1} + (1-s_{i,j}(\ell))(1-p_{\ell,\text{noisy}}^{1|1})\}. \end{aligned} \tag{2.14}$$

2.2.3 Communication-Theoretic Characterization

Ideal Communication Links

The analytical framework presented in Section 2.2.2 leads to a communication-theoretic characterization of the network performance in terms of probability of decision error at the AP as a function of the sensor SNR and the communication noise level.
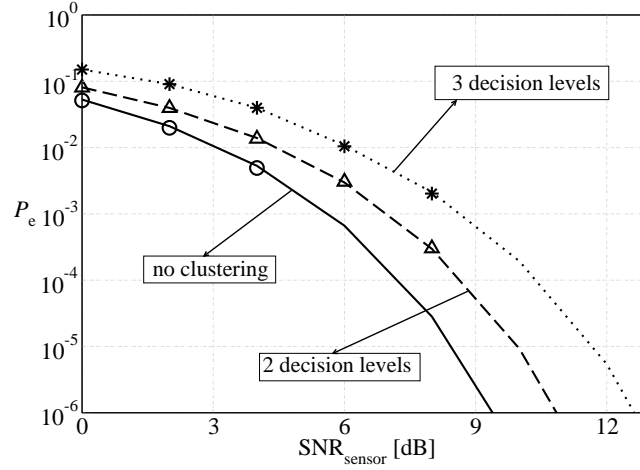
Figure 2.4: Probability of decision error, as a function of the sensor SNR, in a scenario with $n = 16$ sensors and uniform clustering.

In Figure 2.4, the probability of decision error is shown, as a function of the sensor SNR, in the case with $n = 16$ sensors, considering two and three decision levels. In the scenario with two decision levels, the following topologies are possible:

- 8-8 (2 clusters with 8 sensors each);

- 4-4-4-4 (4 clusters with 4 sensors each);

- 2-2-2-2-2-2-2-2 (8 clusters with 2 sensors each).

For a three decision level scenario, the following topologies are considered:

- 4-4-4-4/2-2 (4 first-level FCs, each connected with 4 sensors, and 2 second-level FCs, each connected with 2 first-level FCs);

- 2-2-2-2-2-2-2-2/4-4 (8 first-level FCs, each connected with 2 sensors, and 2 second-level FCs, each connected with 4 first-level FCs);

- 2-2-2-2-2-2-2-2/2-2-2-2 (8 first-level FCs, each connected with 2 sensors, and 4 second-level FCs, each connected with 2 first-level FCs).

Lines and symbols (circles, triangles, and stars) correspond to analytical and simulation results, respectively. For comparison, the probability of decision error with no clustering is also shown. We point out that the simulation results shown in Figure 2.4 and those shown, in the following, in Figure 2.5 are meant to verify the correctness of the analytical framework. In other words, these results are obtained by simulating systems which are identical to those behind the analytical models. Obviously, the agreement between analysis and simulations is perfect. In Section 2.2.5.A, instead, the presented simulation results will refer to realistic Zigbee networks.

In Figure 2.4, only one curve is shown for the scenario with two levels of information fusion, since the performance curves associated with all possible configurations (i.e., 8-8, 4-4-4-4, 2-2-2-2-2-2-2-2) overlap. This implies that one can choose between a uniform network topology with a small number of large clusters and a uniform network topology with a large number of small clusters, still guaranteeing the same performance level. The intuition behind this result is the following.

- If one considers an architecture with small clusters, then fusion at the first-level FCs is not effective. However, many local cluster decisions are then fused together, and this allows to recover (partially) the first-level information loss.

- On the other hand, considering large clusters leads to more reliable local first-level decisions. However, a few of them are then fused together, so that the supplementary (higher-level) refinement is not relevant.

Similar considerations also hold for a three decision level scenario. We point out that in Figure 2.4 the obtained analytical expressions of the probability of decision error are numerically evaluated and verified through simulations. However, we are still working on a simple analytical proof of the identity, for a given number of nodes, of the expressions of the probabilities of decision error for different uniformly clustered scenarios.

Comparing the performance in the absence of clustering with that in the presence of uniform clustering (with either two or three decision levels), one can conclude that the larger is the number of decision levels, the worse is the performance. This is intuitive, since a larger number of decision levels corresponds to a larger number
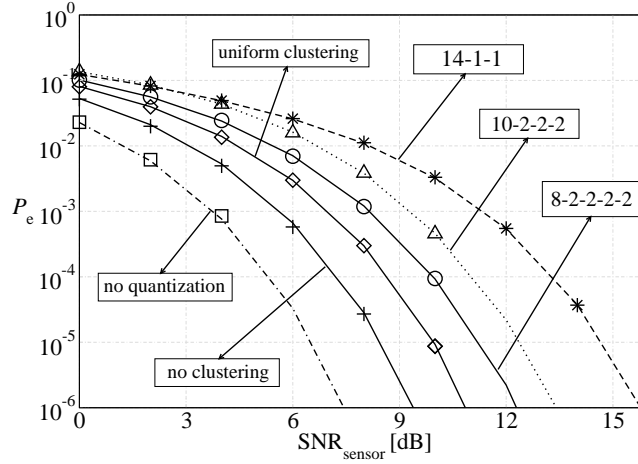
Figure 2.5: Probability of decision error, as a function of the sensor SNR, in a scenario with $n = 16$ sensors. Various configurations are considered.

of partial information losses in correspondence to the fusion operations. However, this holds in scenarios with ideal communication links. In a wireless communication scenario, where some links may be completely obstructed, a sensor network with multiple communication layers might not yield the worst performance.

Although the analytical framework derived in the previous sections is general, the presented results refer to networks with a (relatively) small number of sensors. However, our framework can be extended to scenarios with a large number of sensors. To this regard, in [93] we propose a simple, yet very accurate, approximation of the derived framework based on the application of the De-Moivre Laplace (DML) theorem.

In order to evaluate the impact of non-uniform clustering, we consider a scenario with $n = 16$ sensors and various non-uniform network topologies. In Figure 2.5, the probability of decision error is shown, as a function of the sensor SNR, considering no clustering, two level uniform clustering, and various configurations with two decision levels and non-uniform clustering (explicitly indicated). For comparison, the curve in the absence of quantization at the sensors is also shown. The lines corre-

spond to analytical results, whereas symbols are associated with simulations. In the scenarios with non-uniform clustering, the considered configurations are 8-2-2-2-2 (5 clusters, out of which 4 contain 2 nodes and 1 contains 8 nodes), 10-2-2-2, and 14-1-1. As one can see from Figure 2.5, in the presence of majority-like information fusion the higher is the non-uniformity degree among the clusters, i.e., the more unbalanced is clustering, the worse is the system performance. Consequently, a sensor network designer should avoid non-uniform configurations with one big cluster and remaining small clusters. In general, a two-level uniformly clustered scenario is desirable, since it guarantees the lowest energetic loss with respect to a network with no clustering. However, uniform clustering in a realistic scenario might not be possible, as, for example, in environmental monitoring applications. In fact, the area over which the sensors are distributed could be irregular and, therefore, uniform clustering of the sensors could not be feasible. An interesting application of our framework could consist of the identification of non-uniform clustering "classes," with similar performance per class. This could help significantly a network designer in predicting, for example, the performance degradation caused by the loss of some sensors (e.g., for battery exhaustion).

The above analysis in non-uniformly clustered scenarios applies to situations where the AP does not know the exact distribution of the sensors among the clusters. This is meaningful, for instance, in large networks where only local topology knowledge is possible. If, on the other hand, the distribution is very unbalanced (e.g., 14-1-1 with $n = 16$ sensors) and the AP knows the exact topology, the less reliable decisions originated by small clusters can be ignored. In a scenario with $n = 16$ sensors and the considered 14-1-1 topology, at $P_e = 10^{-4}$ a sensor SNR gain equal to 5.47 dB can be obtained without using, at the AP, the decisions associated with the smaller clusters—this corresponds to the performance of a sensor network with $n = 14$ sensors and no clustering. Therefore, knowledge of the clustering configuration at the AP allows to obtain a performance very close to that in the absence of clustering. In particular, in the previous case with $n = 16$ sensors and 14-1-1 configuration, the sensor SNR loss (with respect to a scenario with no clustering) can be reduced to 0.77 dB by using only the decision sent by the 14-sensor cluster. Our goal, however,
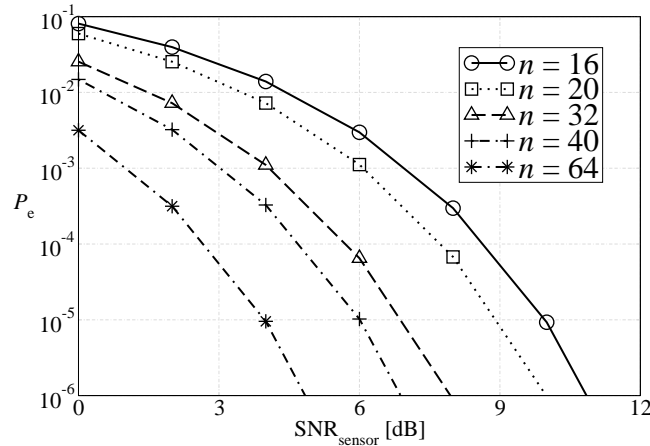
Figure 2.6: Probability of decision error, as a function of the sensor SNR, in a scenario with uniform clustering. Different values of the number of sensors are considered.

is to compare clustering topologies when the AP gives the same weight to all received decisions. This is meaningful for a *dynamic* sensor network scenario, where sensors might die and sensors clusters might become unbalanced. In this case, intelligent re-clustering techniques can be used to improve the system performance, as it will be shown later.

In Figure 2.6, the probability of decision error is shown, as a function of the sensor SNR, for different values of the number of sensors n in a scenario with uniform clustering. In particular, the considered values for n are 16, 20, 32, 40, and 64. Observe that only one curve is associated with each value of n, since we have previously shown that the performance does not depend on the number of clusters (for a given n), as long as clustering is uniform. Obviously, the performance improves (i.e., the probability of decision error decreases) when the number of sensors in the network becomes larger. The results in Figure 2.6 will be used in Section 2.3.1 to compute the sensor network lifetime under a QoS condition on the maximum acceptable probability of decision error.

Noisy Communication Links

While in Section 2.2.3 the performance in scenarios with ideal communication links has been analyzed, we now turn our attention to scenarios with noisy communication links. It is interesting to investigate how the probability of decision error behaves as a function of the communication noise level, i.e., the cross-over probability p. To this end, we introduce a communication-theoretic quality of service (QoS) condition, in terms of the maximum tolerable probability of decision error, denoted as P_e^*. A physical layer-oriented QoS condition can be written as

$$P_e \leq P_e^*. \tag{2.15}$$

Since the probability of decision error is a monotonically decreasing function of the sensor SNR, the QoS condition (2.15) can be equivalently rewritten as

$$\text{SNR}_{\text{sensor}} \geq \text{SNR}_{\text{sensor}}^*$$

where $\text{SNR}_{\text{sensor}}^*$ depends on P_e^*. It is then possible to evaluate the performance under a desired QoS constraint, given by the maximum tolerable probability of decision error P_e^*.

In Figure 2.7, the value of the minimum sensor SNR required to guarantee P_e^*, i.e., $\text{SNR}_{\text{sensor}}^*$, is shown, as a function of the cross-over probability p, in scenarios (i) without clustering and (ii) with clustering and two decision levels, respectively. Two possible values for P_e^* are considered: (i) 10^{-3} (curves with circles) and (ii) 10^{-4} (curves with triangles). As expected, when the noise level increases, the minimum sensor SNR required to guarantee the desired network performance also increases. In fact, since communications become less reliable, a higher accuracy in the observation phase is needed in order to maintain the same overall performance. Besides, one can observe that there exists a vertical asymptote in each curve in Figure 2.7. In other words, there exists a critical value p_{crit} of the noise level, such that: (i) for $p < p_{\text{crit}}$, the sensor network is operative, i.e., there exists a finite value of the sensor SNR which satisfies the desired QoS condition (2.15); (ii) for $p > p_{\text{crit}}$, instead, the network is not operative, i.e., it is not possible to achieve the desired performance level,
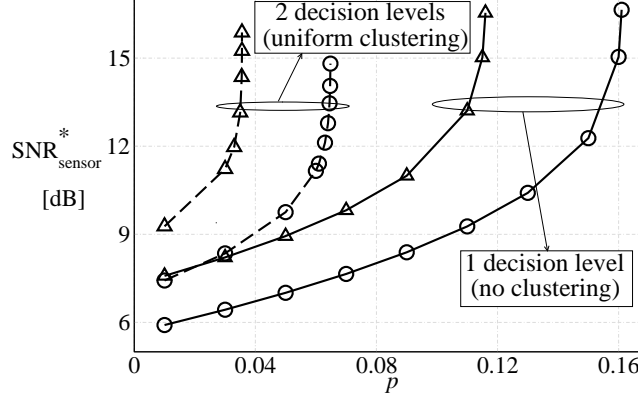
Figure 2.7: Minimum sensor SNR required to obtain a desired QoS, in scenarios with noisy communication links in the cases (i) without clustering and (ii) with uniform clustering and two decision levels. Two possible QoS are considered: (i) $P_{\mathrm{e}}^* = 10^{-3}$ (lines with circles) and (ii) $P_{\mathrm{e}}^* = 10^{-4}$ (lines with triangles).

regardless of the value of the sensor SNR. One could equivalently describe this behavior as *bimodal*. This is a typical behavior of distributed communication networks, such as the bimodal connectivity behavior in ad hoc wireless networks [98–102]. Proper operation of the considered sensor networks with distributed detection can be equivalently interpreted as a symptom of network connectedness. In Figure 2.7, this bimodal behavior is also confirmed in a scenario with uniform clustering and two decision levels. However, in the latter case the impact of the communication noise is stronger with respect to a scenario with no clustering, i.e., the network looses connectivity for smaller values of p. Consequently, the larger is the number of decision levels in the network, the lower is the maximum tolerable communication noise level.

2.2.4   Joint Communication/Information-Theoretic Characterization

The considered sensor network schemes can be modeled as "black boxes" with a binary input (the phenomenon H) and a binary output (the decision $\widehat{H}$ at the AP). Using the model in Figure 2.1, the final decision $\widehat{H}$ can be described as a binary ran-

dom variable[1] with $P_0 \triangleq P(\widehat{H} = H_0)$. In a scenario with two-level uniform clustering and ideal communication links, the parameter P_0 can be rewritten (using the results in Section 2.2.1) as

$$
\begin{aligned}
P_0 &= p_0 \operatorname{bin}(0, k_{\mathrm{f}} - 1, n_{\mathrm{c}}, \operatorname{bin}(k, d_{\mathrm{c}}, d_{\mathrm{c}}, Q(\tau))) \\
&\quad + (1 - p_0) \operatorname{bin}(0, k_{\mathrm{f}} - 1, n_{\mathrm{c}}, \operatorname{bin}(k, d_{\mathrm{c}}, d_{\mathrm{c}}, Q(\tau - s))).
\end{aligned}
\tag{2.16}
$$

We remark that equation (2.16) may look identical to (2.6). In (2.16), however, the term on the right-hand side in the first row corresponds to $P(\widehat{H} = H_0 | H_0)$, whereas in (2.6) it is given by $P(\widehat{H} = H_1 | H_0)$—the second parameter of the function "bin" is, in fact, different in the two cases.

The mutual information of the BIBO sensor network can then be written as [103, ch. 2]

$$
I^{\mathrm{REAL}}(H; \widehat{H}) = H_{\mathrm{e}}^{\mathrm{REAL}}(\widehat{H}) - H_{\mathrm{e}}^{\mathrm{REAL}}(\widehat{H} | H)
$$

where $H_{\mathrm{e}}^{\mathrm{REAL}}(\widehat{H} | H)$ is the conditional entropy of $\widehat{H}$ given H [103]. After a few manipulations, the mutual information becomes

$$
I^{\mathrm{REAL}}(H; \widehat{H}) = H_{\mathrm{e}}\left(p_0(1 - p_{10}) + (1 - p_0)p_{01}\right) - p_0 H_{\mathrm{e}}(p_{10}) - (1 - p_0)H_{\mathrm{e}}(p_{01})
\tag{2.17}
$$

where $p_{ij} \triangleq P(\widehat{H} = H_i | H_j)$, $i, j = 0, 1$.

In Figure 2.8, the probability of decision error is shown, as a function of the *mutual information*, for the same scenario considered in Figure 2.5, i.e., with no clustering (circles), uniform clustering (triangles), and non-uniform clustering (pluses, 14-1-1 configuration), respectively. The communication links are ideal. The curves considered in this figure are parameterized curves, obtained by combining probability of decision error curves with mutual information curves, through the common parameter given by the sensor SNR. As one can see, the curves associated with different sensor network topologies overlap. In other words, for a given value of the mutual information, the probability of decision error is fixed. note, however, that a specific mutual information is obtained in clustered (for example, 4-4-4-4 or 2-2-2-2-2-2-2-2)

---

[1]Note that the definition of $P_0 = P(\widehat{H} = H_0)$ (relative to the decision $\widehat{H}$) is different from that given for the *a priori* probability of the phenomenon $p_0 = P(H = H_0)$ given in Section 2.2.1.
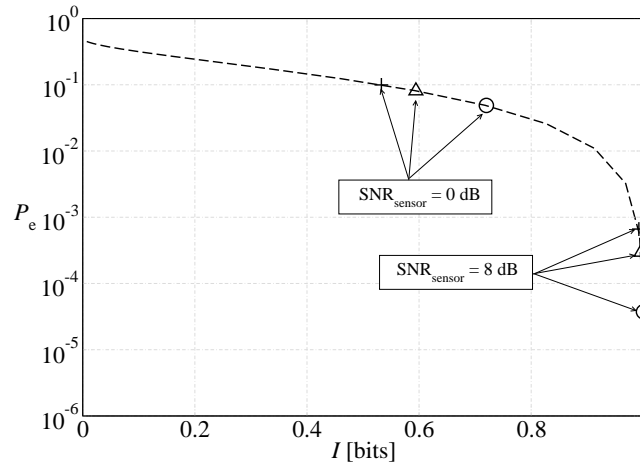
Figure 2.8: Probability of decision error, as a function of the mutual information, in a scenario with $n = 16$ sensors. The operating points for various clustering configurations and two sensor SNRs are shown.

and non-clustered scenarios for different values of the sensor SNR (in the figure, a few representative points associated with two SNRs are highlighted). In other words, for a given mutual information the presence of clustering leads to an *energetic loss* at the sensors (in the observation phase). The loss with non-uniform clustering is higher than with uniform clustering. Similar curves can be derived for the other scenarios considered in this chapter, e.g., for a large number of sensors, with more than two decision levels, and in the presence of noisy communication links between sensors and first-level FCs (with sufficiently low values of the noise level p). However, the network behavior does not change, i.e., for a fixed value of the mutual information, the probability of decision error is uniquely determined.

In Figure 2.9, the probability of decision error is shown, as a function of the mutual information, in a scenario with $n = 16$ sensors and uniform clustering. Communication links between sensors and first-level FCs are noisy, with cross-over probability $p = 0.05$. The limiting (for $\text{SNR}_{\text{sensor}} \to \infty$) operating points over the $P_\text{e} - I$ curve of a BIBO sensor network, corresponding to all possible numbers of decision levels (1,
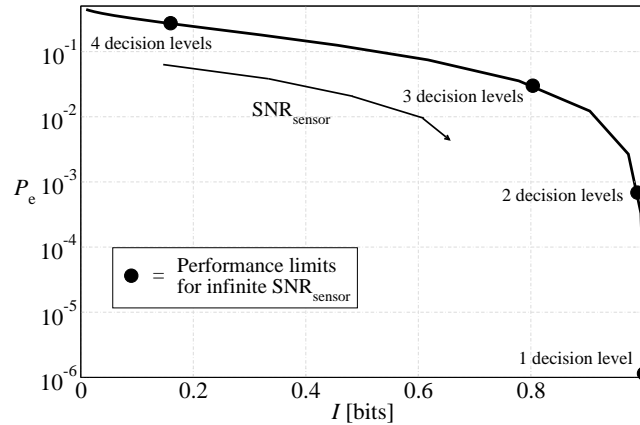
Figure 2.9: Probability of decision error, as a function of the mutual information, in a scenario with $n = 16$ sensors, uniform clustering, and noisy communication links ($p = 0.05$).

2, 3, and 4, respectively), are shown. For a given number of decision levels, the system operating point moves from the position corresponding to $I = 0$ (for very low values of SNR_{sensor}) to the corresponding limiting point, which is asymptotically approached for $SNR_{sensor} \to \infty$. As one can see, the presence of noise over the communication links limits the maximum achievable mutual information, i.e., the maximum information transfer rate accross the network.

In [104], possible simplified expressions for the probability of decision error (as a function of the mutual information), are presented. In particular, (i) polynomial approximations, (ii) asymptotic (for sufficiently large sensor SNR) analytical expressions, and (iii) *bimodal* approximations (valid for all sensor SNRs), are derived.

2.2.5   Realistic Clustered Networks with Data Fusion

In this section, we present *simulation* and *experimental* results which validate our analytical framework in practical sensor networking scenarios, where nodes comply with the Zigbee (simulation results) or IEEE 802.15.4 (experimental results) stan-

dards.

Simulations

The simulations have been carried out with the Opnet Modeler simulator [105] and a built-in Zigbee network model designed at the national Institute of Standards and Technologies (NIST) [106]. This model provides only the first two layers of the ISO/OSI stack, and we have extended it with a simple Opnet model for a FC, which, in addition to providing relaying functionalities, implements the intermediate data fusion mechanisms described in the previous sections. Our Opnet model assumes strong line-of-sight communications between the sensors and the FCs, and between the FCs and the coordinator.

According to the theoretical analysis, the sensors make a noisy observation (affected by AWGN) of a randomly generated binary phenomenon H and make local decisions on the status of the phenomenon. Subsequently, the sensors embed their decisions into proper data packets of length 216 bits,[2] which are sent either to the coordinator (in the absence of clustering) or to the first-level FCs (in the presence of clustering). The decisions are assumed to be either 0 (no phenomenon) or 1 (presence of the phenomenon). Obviously, if some packets are lost due to medium access collisions, decisions (either at the FCs or at the AP) are made only on the received packets (this leads to a reduced reliability of the decisions). If all the packets related to a set of observations of the same phenomenon are lost, instead, the final binary decision is random. Finally, if half of the decisions are in favor of one phenomenon status and the other half are in favor of the other, the coordinator decides for the presence of the phenomenon. More details about the implementation of the data fusion mechanism in Opnet can be found in [107].

In both scenarios, it is possible to evaluate, by simulation, the probability of decision error. Together with the probability of decision error, the simulator allows to evaluate the (i) *packet delivery fraction*, denoted as ξ and defined as the ratio between the number of packets correctly delivered at the coordinator and the number

---

[2]This length corresponds to a payload of 96 bits and a header of 120 bits introduced by physical and MAC layers.
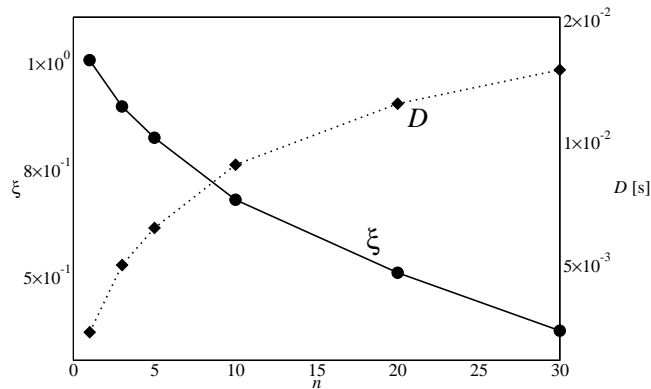
Figure 2.10: Performance analysis in a scenario without clustering: packet delivery fraction and delay performance as functions of the number n of transmitting sensors.

of packets sent by the sensors and (ii) the *delay*, defined as the time interval between the transmission instant and the reception instant of a generic packet. Results about the aggregate throughput (dimension: [pck/s]), defined as $S_{agg} = n \cdot g \cdot \xi$, where n is the number of transmitting sensors and g is the packet generation rate (set to 2 pck/s in all simulation results presented in the remainder of this section), can be found in [107]. Moreover, no acknowledgement (ACK) messages are used to confirm successful transmissions. In order to eliminate possible statistical fluctuations, each simulation performance point is obtained by averaging the results of ten Opnet simulation runs.

In Figure 2.10, the packet delivery fraction and the delay are shown as functions of the number n of transmitting sensors. These curves are obtained considering a fixed observation SNR at the sensors (equal to 0 dB). Our results, however, show that the packet delivery fraction and the delay are not affected by the value of the observation SNR at the sensors. We consider, in fact, ideal communication channels, so that only the observations at sensors are noisy, whereas the packets sent from the sensors to either an FC (clustered schemes) or the coordinator (non-clustered schemes) are received without errors. Consequently, the performance does not depend on the
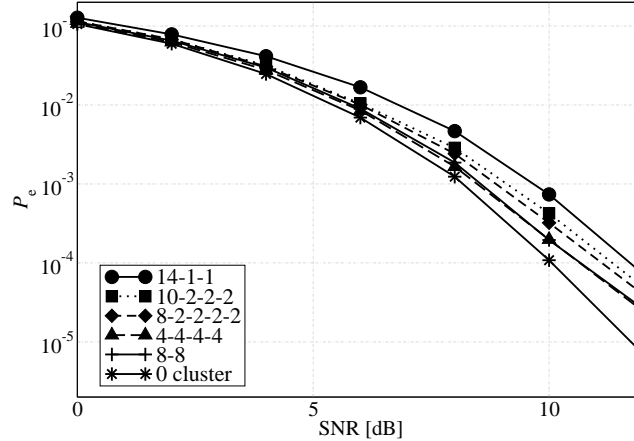
Figure 2.11: BER performance in scenarios with $n = 16$ sensors both in the case of uniform and non-uniform clustering. Various topologies (indicated in the figure) are considered.

considered SNR, since packet delivery fraction and delay are network performance indicators and do not depend on the observation reliability. The packet delivery fraction (solid line with circles) decreases monotonically. In particular, for small values of n, it remains close to 1. When the number of transmitting nodes increases, instead, the number of collisions in the channel increases as well and the packet delivery fraction reduces. In the same figure, the delay (dotted line with diamonds) is also shown. As the intuition suggests, the delay is low for small values of n. When the traffic increases, instead, due to a larger number of collisions, the delay is higher, since the channel is busy for a longer period of time and the probability of finding the channel idle reduces. Finally, for large values of n, the delay seems to start saturating to a maximum value. In this case, in fact, due to the increased offered traffic, at least one sensor is likely to be ready to send its packet as soon as the channel becomes idle.

In Figure 2.11, we analyze the impact of non-uniform clustering on the probability of decision error—as a performance benchmark, the probability of decision error in the case with uniform clustering is also shown. We consider scenarios with

$n = 16$ sensors and the following network configurations: (i) no clustering, (ii) 8-8, (iii) 4-4-4-4 FCs, (iv) 14-1-1, (v) 10-2-2-2, and (vi) 8-2-2-2-2. According to the results in Figure 2.11, the best performance is obtained in the absence of clustering, whereas the worst performance is obtained in the 14-1-1 scenario, i.e., with 3 FCs and non-uniform clustering. From Figure 2.11, one can conclude that, in the presence of non-uniform clustering, the performance improves for relatively balanced clusters (as also predicted by the analytical framework). In this case, in fact, decisions made by intermediate FCs are more reliable, so the final decision made by the coordinator is more likely to be correct. In the case of uniform clustering, instead, the probability of decision error is *not* affected by the number of clusters in the network, as long as the total number of sensors remains the same. In this case, in fact, observing Figure 2.11 one can note that the curves relative to the scenarios with 4 4-sensor clusters and 2 8-sensor clusters are almost overlapped. This is due to the fact that a smaller number of clusters is compensated by a higher quality of the intermediate decisions. This result is in agreement with the theoretical conclusions reached in Section 2.2.3. However, note that the performance in Zigbee scenarios worsens with respect to the analytical case, because the simulator takes into account the losses due to collisions. Since some packets may be lost, the probability of decision error is influenced by the collisions.

Experiments

In order to verify the predictions of the theoretical framework from an experimental perspective, we consider a networking set-up formed by MicaZ nodes [108]. MicaZ platforms include an ATmega128L 7.3 MHz micro-controller [109], FLASH and EEPROM memories, and a 2.4 GHz IEEE 802.15.4 Chipcon CC2420 radio-frequency transceiver [110]. The nodes' operating system is TinyOS. The experimental set-up is characterized by $n = 16$ nodes, organized in uniform clusters, with 2 and 3 decision levels, respectively. In our implementation, each node observes a "0" phenomenon and adds a Gaussian observation noise generated through the function "random" available in the TinyOS environment. According to the local decision threshold, each source node makes a decision on the observed phenomenon and embeds it in a packet to be transmitted. Since each TinyOS packet is formed by a payload
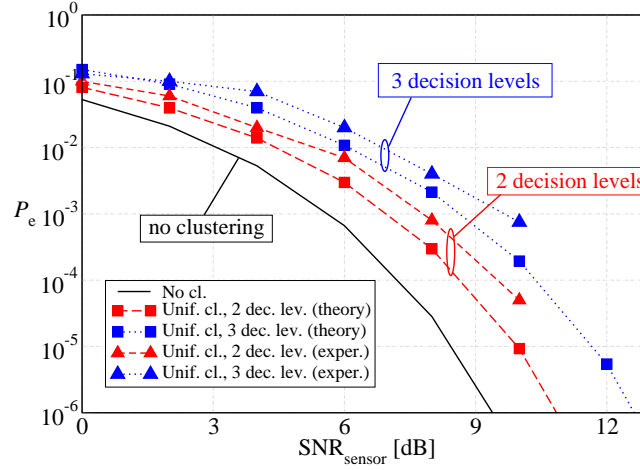
Figure 2.12: Experimental BER performance in scenarios with $n = 16$ sensors and uniform clustering. Two and three decision levels are considered.

of 30 bytes (the first byte contains the dimension and the following 29 the information data), we embed in each packet $29 \times 8 = 232$ consecutive binary decisions. This corresponds to 232 consecutive (time-wise) realizations of the observed binary phenomenon. The packets originated by the source nodes is then transmitted, through the intermediate FCs, to the AP. Note that a packet duration is of the order of 1 ms, and consecutive packet transmissions are separated by approximately 0.1 s. The transmit power is set to -25 dBm and the sensitivity threshold at the receivers is -100 dBm. The distances between communicating nodes (of the order of 2 m) are such that the received power is significantly higher than the sensitivity threshold. The data fusion mechanisms at the intermediate FCs and at the AP follows the majority decision rules described in the analytical framework.

The experimental BER performance is shown in Figure 2.12. In the same figure, for comparison, we also show the corresponding theoretical results extracted from Figure 2.4. As one can see, the experimental results are slightly worse than the theoretical ones (as observed also, in Section 2.2.5 for simulation results), but confirm the trend. This discrepancy is due to the more realistic experimental scenario, where

some packets may get lost because of the wireless communication links. Since the decision rules at the FCs and at the AP do not adapt to the number of received observations, this explains the performance degradation. We point out that in our experiments the packet losses are typically *not* due to collisions, i.e., the traffic load of the considered network scenarios is too low to create problems at the access level. On the opposite, the performance degradation is due to losses of packets due to propagation reasons. An interesting research extension consists in incorporating these effects into our analytical framework.

2.3 Extending the Lifetime of Clustered Sensor Networks

2.3.1 Sensor Network Lifetime under a Physical Layer QoS Condition

In order to evaluate the sensor network lifetime, one needs first to define when the network has to be considered "alive." We assume that the network is "alive" until the QoS condition in (2.15) is satisfied. When a sensor in the network dies (e.g., there is a hardware failure or its battery exhausts), the probability of decision error increases since a lower number of sensors is alive (see, for instance, Figure 2.6). Moreover, the presence of a specific clustering configuration might make the process of network death faster. More precisely, the network dies when the desired QoS condition (2.15) is no longer satisfied, as a consequence of the death of a *critical sensor*. Therefore, the network lifetime corresponds to the lifetime of this critical sensor. Obviously, the criticality of a sensor's death depends on the particular sequence of previous sensors' deaths.

Based on the considerations in the previous paragraph, in order to estimate the *network* lifetime one, first, needs to consider a reasonable model for the *sensor* lifetime. We denote by $F(t) \triangleq P\{T_{\text{sensor}} \leq t\}$ the cumulative distribution function (CDF) of a sensor's lifetime T_{sensor} (the same for all sensors) and we consider the following exponential distribution as representative:

$$F(t) = \left[1 - e^{-t/\mu}\right] U(t) \tag{2.18}$$

where the time t is measured in arbitrary units (dimension: [aU]). We have chosen

the distribution in (2.18) as good models for a sensor lifetime [111, Ch. 8]. Consider-ations about other good models for a sensor lifetime can be found in [112]. Note that the results presented here for an exponential distributions also hold for other allowed distributions in [112].

As mentioned before, we are interested in analyzing the network behavior when the QoS condition (2.15) is satisfied. More precisely, in the following sections we evaluate the sensor network lifetime in scenarios with (A) ideal reclustering and (B) no reclustering. The obtained results are then commented.

Analysis with Ideal Reclustering

In the case of *ideal reclustering*, the network dynamically reconfigures its topology, immediately after a sensor death, in order to recreate a uniform configuration. Ob-viously, the time needed for rearranging the network topology depends on the specific strategy chosen in order to reconfigure correctly (according to the updated network configuration) the connections between the sensors and the FCs and those between the FCs and the AP. In Section 2.3.2, a simple reconfiguration strategy will be pro-posed.

Given a maximum tolerable probability of decision error P_e^*, one can determine the lowest number of sensors, denoted as n_{min}, required to satisfy the desired QoS condition. For instance, considering Figure 2.6 and fixing a maximum tolerable value P_e^*, one can observe that, for decreasing numbers of sensors, at some point the actual probability of decision error P_e becomes higher than P_e^*. In other words, the probabi-lity of decision error is lower than P_e^* if *at least* n_{min} sensors are alive or, equivalently, until $n_{crit} = n - n_{min} + 1$ sensors die. Therefore, denoting as T_{net} the network lifetime, one can write:

$$P\left(T_{net} \leq t\right) = P \left\{ \begin{array}{c} \text{at least } n_{crit} \text{ sensors} \\ \text{have } T_{sensor} < t \end{array} \right\}$$

where T_{sensor} is the sensor lifetime (recall that this random variable has the same distribution for all sensors) with CDF $F(t)$. Since the lifetimes of different sensors

are supposed independent, using the repeated trials formula, one obtains

$$P\left(T_{\text{net}} \leq t\right) = \sum_{i=n_{\text{crit}}}^{n} \binom{n}{n_{\text{crit}}} \left[F(t)\right]^{i} \left[1 - F(t)\right]^{n-i}.$$

Absence of Reclustering

In the previous section, we have analyzed the network evolution in an ideal scenario where the topology is dynamically reconfigured in response to a sensor death (e.g., because of the depletion of its battery or hardware failure). However, it might happen that the initial clustered configuration is fixed, i.e., the connections between sensors, FCs, and AP cannot be modified after a sensor death. In this case, the following question is relevant: is there an optimum initial topology which leads to longest network lifetime? In order to answer this question, we will analyze the network evolution in scenarios where there is no reclustering. The network is still considered dead when the QoS condition (2.15) is no longer satisfied.

In the absence of ideal reclustering, an analytical performance evaluation is not feasible, i.e., there does not exist a closed-form expression for the CDF of the network lifetime. In fact, the CDF depends on the particular network evolution, i.e., it depends on how the sensors die among the clusters in the network. Therefore, each sequence of sensors' deaths is characterized by a specific lifetime, and one needs to resort to simulations in order to extrapolate an average statistical characterization. The simulations are performed according to the following steps.

1. The lifetimes of all n sensors are generated according to the chosen distribution and the sensors are randomly assigned to the clusters.

2. The sensors' lifetimes are ordered in an increasing manner.

3. After a sensor death, the network topology is updated.

4. The probability of decision error is computed in correspondence to the surviving topology determined at the previous point: if the QoS condition (2.15) is satisfied, then the evolution of the network continues from step 3, otherwise, step 5 applies.
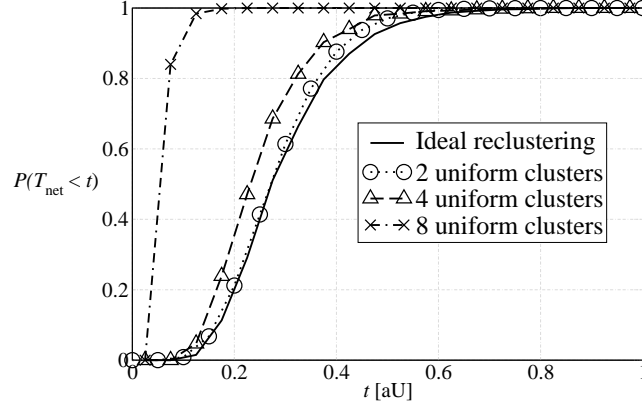
Figure 2.13: CDF of the network lifetime, as a function of time, in a scenario with $n = 32$ sensors, uniform clustering (with, respectively, 2, 4, and 8 clusters), and *absence of reclustering* (simulation results). The sensor SNR is set to 5 dB and the maximum tolerable probability of decision error is $P_e^* = 10^{-3}$. For comparison, the curve associated with ideal reclustering (analytical results) is also shown.

5. The network lifetime corresponds to the lifetime of the last dead sensor.

In Figure 2.13, the CDF of the network lifetime is shown, as a function of time, in a scenario with $n = 32$ sensors grouped, respectively, in 2, 4, and 8 clusters. The sensor SNR is set to 5 dB and the maximum tolerable probability of decision error is $P_e^* = 10^{-3}$. For comparison, the curve associated with ideal reclustering is also shown. One can observe that the larger is the number of clusters, the worse is the performance, i.e., the higher is the probability of network death. Moreover, the curve associated with 2 clusters is very close to that relative to ideal reclustering. In fact, in a scenario with only 2 clusters, the average number of sensors which die in each cluster is approximately the same and, consequently, the topology remains approximatively uniform.

In Table 2.2, the network lifetime corresponding to a CDF equal to 0.9 (i.e., an outage probability of 90%) is shown, assuming an *exponential* sensor lifetime (with $\mu = 1$ aU), for various clustering configurations and values of the maximum tolerable

Table 2.2: Sensor network lifetime corresponding to an outage probability equal to 90% in a scenario with $n = 64$ sensors and $\text{SNR}_{\text{sensor}} = 5$ dB. Three values for the maximum tolerable probability of decision error P_e^* are considered: (i) 10^{-2}, (ii) 10^{-3}, and (iii) 10^{-4}. The mean parameter of the exponential distribution is $\mu = 1$ aU. All time values in the table entries are expressed in aU.

P_e^*	Ideal reclustering	no reclustering (2 clusters)	no reclustering (4 clusters)	no reclustering (8 clusters)
10^{-2}	2.1	2.1	2.0	1.68
10^{-3}	1.3	1.3	1.2	1.012
10^{-4}	0.78	0.78	0.74	0.725

probability of decision error P_e^*. The number of sensors is $n = 64$. For comparison, the network lifetime with ideal reclustering is also shown. From the results in Table 2.2, the following observations can be carried out.

- For a small number of clusters (2 or 4), the lifetime reduction, with respect to a scenario with ideal reclustering, is negligible. This is to be expected from the results in Figure 2.13 and is due to the fact that the sensors die "more or less" uniformly in all clusters. When the number of clusters increases beyond 4, the network lifetime starts reducing appreciably. Therefore, our results show that, in the *absence of ideal reclustering*, the winning strategy to prolong network lifetime is to *form a few large clusters*.

- The impact of the QoS condition is very strong. In fact, when the QoS condition becomes more stringent (i.e., P_e^* decreases), the network lifetime shortens, since a lower number of sensor deaths is sufficient to violate this condition. On the other hand, if the QoS condition is less stringent, then a larger number of sensors have to die in order to violate it.

- The impact of the number of nodes on the network lifetime has not been di-

rectly analyzed. However, since the performance improves when the number of sensors increases (as shown in Figure 2.6), one can conclude that, for a fixed QoS condition, a network with a larger number of sensors will satisfy the QoS condition for a longer time and, therefore, the network lifetime will be prolonged. Equivalently, one can impose a stronger QoS condition (a lower value of P_e^*), still guaranteeing the same network lifetime.

2.3.2   Analytical Computation of Network Lifetime

In Section 2.3.1, we have analyzed the network performance without taking into account the *cost* of reclustering. In this section, instead, we investigate, from an analytical viewpoint, the cost of the used reclustering protocol in terms of its impact on the sensor network lifetime. In order to evaluate the cost of reclustering, one first needs to detail a reclustering protocol. We remark that we limit ourselves mainly (but not only) to scenarios with two (big) clusters, since they are associated with the minimum loss, in terms of probability of decision error at the AP, with respect to the scenario with the absence of clustering.

   The reclustering protocol which will be used can be characterized as follows.

1. When an FC senses that a sensor belonging to its cluster is dead, e.g., when it does not receive packets from this sensor, it sends a control message, referred to as "ALERT," to the AP.

2. Assuming that the AP is aware of the current network topology, when it receives an ALERT message, it decides if reclustering has to be carried out. If so, the optimized network topology is determined.

3. If no reclustering is required, the AP sends to both FCs an "OK" message to confirm the current topology. On the other hand, if reclustering has to be carried out, another message, referred to as "CHANGE" and containing the new topology information, is sent to the FCs. In the latter case, the FCs send the CHANGE message also to sensors in order to allow them to communicate with the correct FC from then on.
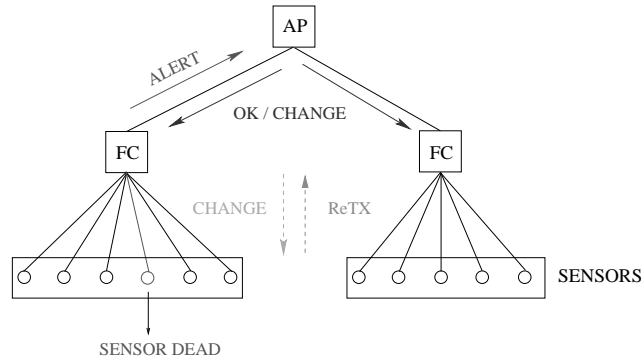
Figure 2.14: Message exchange in the proposed reclustering protocol. A network scenario with $n = 11$ sensors and two clusters (with 6 and 5 sensors, respectively) is considered. The control messages evolution follows the death of a sensor.

4. If reclustering has happened, the sensors retransmit their previous packet to the FCs according to the new topology and a new data fusion is carried out at the AP.

In Figure 2.14, the behavior of this simple protocol is pictured in an illustrative scenario with $n = 11$ sensors and two clusters (with 6 and 5 sensors, respectively). The control messages associated with solid lines are exchanged in the absence of reclustering, whereas the messages associated with dashed lines are exchanged in the presence of reclustering.

In order to derive a simple analytical framework for evaluating the sensor network lifetime, the following assumptions are expedient.

(a) The observation frequency, referred to as f_{obs}, is sufficiently low to allow regular transmissions from the sensors to the AP and, if necessary, the applicability of the reclustering protocol (this is reasonable for scenarios where the status of the observed phenomenon does not change rapidly).

(b) Transmissions between sensors and FCs and between FCs and AP are supposed instantaneous (this is reasonable, for example, if FCs and AP are connected

through wired links or very reliable wireless links).

(c) Data processing and topology reconfiguration are instantaneous (this is reasonable if the processing power at the AP is sufficiently high).

(d) There is perfect synchronization among all nodes in the network (this is a reasonable assumption if nodes are equipped with synchronization devices, e.g., global positioning system).

The proposed reclustering algorithm and the assumptions above might look too simplistic for a realistic wireless sensor network scenario. However, they allow to obtain significant insights about the cost, in terms of network lifetime, of adaptive reclustering.

We preliminary assume that the duration of a data packet transmission has no influence on the lifetime of a single sensor. A more accurate analysis, which takes properly into account the actual duration of a data transmission, will be proposed in Section 2.3.4. In this case, the network lifetime can be written as

$$D_{\text{net}} = \sum_{i=1}^{n_{\text{crit}}} T_{\text{d},i}$$

where n_{crit} has been introduced in Section 2.3.1 and $T_{\text{d},i}$ is the time interval between the $(i-1)$-th sensor death and the i-th sensor death. Obviously, $T_{\text{d},1}$ is the time interval until the death of the first sensor and can be written as

$$T_{\text{d},1} = \min_{j=1,\dots,n} \{T_j\} \tag{2.19}$$

where T_j is the lifetime of the j-th sensor. Since D_{net} is a random variable (RV), one could determine its statistics (e.g., the CDF). However, in order to concisely characterize the impact of reclustering, it is of interest to evaluate its average value, i.e.,

$$\mathbb{E}\left[D_{\text{net}}\right] = \mathbb{E}\left[\sum_{i=1}^{n_{\text{crit}}} T_{\text{d},i}\right]. \tag{2.20}$$

Absence of Reclustering

In this case, n_{crit} and $\{T_{\text{d},i}\}$ in (2.20) are independent RVs. In fact, they depend on the sensors' lifetime distribution and the particular evolution (due to the nodes' deaths) of the network topology. Therefore, the sum in (2.20) is a stochastic sum. Using the conditional expectation theorem and the fundamental theorem of probability [94], one can write

$$\mathbb{E}\left[\sum_{i=1}^{n_{\text{crit}}} T_{\text{d},i}\right] = \sum_{j=1}^{n} P(n_{\text{crit}} = j) \sum_{i=1}^{j} \mathbb{E}\left[T_{\text{d},i}\right].$$

At this point, one needs to resort to simulations to compute the probabilities $\{P(n_{\text{crit}} = j)\}$. In fact, they strongly depend on the particular network evolution before its death.

Ideal Reclustering

In Section 2.3.1, we have shown that the presence of ideal reclustering leads to an upper bound on the network lifetime, i.e., it tolerates the maximum number of sensors' deaths before the network dies. This bound can be analytically evaluated using (2.20) and replacing n_{crit} with the value $n_{\text{crit}}^{\text{R}}$ defined as follows:

$$n_{\text{crit}}^{\text{R}} = \min_{n_{\text{crit}}^* = 1,\dots,n} \{P_{\text{e}}(\text{after } n_{\text{crit}}^* \text{ sensors' deaths}) \geq P_{\text{e}}^*\}.$$

The value of $n_{\text{crit}}^{\text{R}}$ can be determined by numerical inversion of the QoS condition. Therefore, an upper bound for the network lifetime can be expressed as

$$\text{UB}_{D_{\text{net}}} \triangleq \mathbb{E}\left[D_{\text{net}}|n_{\text{crit}} = n_{\text{crit}}^{\text{R}}\right] = \sum_{i=1}^{n_{\text{crit}}^{\text{R}}} \mathbb{E}\left[T_{\text{d},i}\right]. \tag{2.21}$$

In this case, one can observe that the sum in (2.21) is deterministic and, therefore, can be analytically evaluated through the computation of $\{\mathbb{E}\left[T_{\text{d},i}\right]\}$. In [112], it is shown that this upper bound is equal to

$$\text{UB}_{D_{\text{net}}} = \frac{\mu}{n} + \sum_{i=2}^{n_{\text{crit}}^{\text{R}}} \mu \frac{n-i}{(n-i+1)^2}. \tag{2.22}$$

Similarly, we can derive a lower bound on the network lifetime. This bound, for a fixed number of sensors, is obtained when all sensors' deaths occur in the same cluster. In this way, for a fixed topology, the highest possible probability of decision error is obtained at each instant and, consequently, the corresponding network lifetime is the shortest possible. This bound can be expressed as

$$\text{LB}_{D_\text{net}} \triangleq \mathbb{E}\left[D_\text{net}|n_\text{crit} = n_\text{crit}^\text{LB}\right] = \frac{\mu}{n} + \sum_{i=2}^{n_\text{crit}^\text{LB}} \mu \frac{n-i}{(n-i+1)^2}. \qquad (2.23)$$

Expression (2.23) for LB_{D_net} is derived from (2.22) by replacing n_crit^R with n_crit^LB, which is obtained through simulations, since it depends on the network evolution. The value of LB_{D_net} is smaller than that of UB_{D_net}, since $n_\text{crit}^\text{R} > n_\text{crit}^\text{LB}$. As previously mentioned, we consider an initial topology with two big clusters. In fact, this scenario allows to obtain the lowest probability of decision error at each instant, because the network topology is less unbalanced than in scenarios with a higher number of clusters, e.g., 8. Therefore, evolution of the lower bound (2.23) in correspondence to a scenario with two clusters leads to the tightest possible lower bound with respect to a scenario with no reclustering.

Finally, one needs to evaluate the extra time required by the application of the reclustering procedure. We will refer to this quantity as T_R. Under the given assumptions and since the probability that reclustering has happened is equal to 1/2 (the derivation of this probability is summarized in [112]), T_R can be expressed as

$$T_\text{R} = (n_\text{crit}^\text{R} - 1)T_\text{RECL}$$

where T_RECL represents the time required by a single reclustering operation. The duration of this time interval cannot be a priori specified, since it depends on the dimensions of the OK, CHANGE, and ALERT messages, the data-rate, and other network parameters. It is reasonable to assume that the longer is the average sensor lifetime μ, the shorter should be (proportionally) T_RECL. In other words, one could assume $T_\text{RECL} = c \cdot \mu$, where c is small if μ is large and vice versa. In general, c can be chosen to model accurately the situation of interest.

Finally, one can define a *time penalty* as the ratio between the time necessary for the application of the reclustering protocol and the total time, given by the sum of

reclustering and "useful" times (i.e., the time spent for data transmission). It follows that:

$$
\begin{aligned}
P^{\text{time}} &= \frac{T_{\text{R}}}{T_{\text{R}} + \mathbb{E}\left[D_{\text{net}}\right]} \\
&= \frac{(n_{\text{crit}}^{\text{R}} - 1)T_{\text{RECL}}}{(n_{\text{crit}}^{\text{R}} - 1)T_{\text{RECL}} + \dfrac{\mu}{n} + \sum_{i=2}^{n_{\text{crit}}^{\text{R}}} \mu \dfrac{n-i}{(n-i+1)^2}}.
\end{aligned}
\tag{2.24}
$$

After a few mathematical passages, from it follows that

$$
P^{\text{time}} \gtrsim \frac{(n - k^* - 1)c}{(n - k^* - 1)c + \frac{1}{n} + \ln(n-2) - \ln(k^* - 1)}
\tag{2.25}
$$

where we have used the fact that $\sum_{i=1}^{m} 1/i \simeq \ln m + 0.577$ [113].

From (2.25) and owing to the fact that k^* is approximately constant, one can analytically show that

$$
\lim_{n \to \infty} P^{\text{time}} \simeq 1 \qquad \forall c.
$$

In other words, if the number of sensors is large, for a fixed value of c the proposed reclustering algorithm does not guarantee a limited time penalty. Similarly, one can show that

$$
\lim_{c \to 0} P^{\text{time}} \simeq 0 \qquad \forall n.
$$

In other words, for a fixed number of nodes the reclustering protocol is effective, using the algorithm proposed in Section 2.3.2, *provided that* the duration of a single reclustering operation is sufficiently short (e.g., very small control packets are used).

2.3.3   Numerical Results

In Figure 2.15, numerical results based on the application of the analytical framework derived in Sections 2.3.2 and 2.3.2 are shown. In particular, (a) the average network lifetime $\mathbb{E}\left[D_{\text{net}}\right]$ and (b) the critical number of deaths n_{crit} are shown as functions of the number of sensors n. The average network lifetime in a scenario with the no reclustering (for various numbers of clusters) is compared with the upper and lower bounds derived in Section 2.3.2. The QoS condition is associated with $P_{\text{e}}^* = 10^{-3}$

(a)   (b)
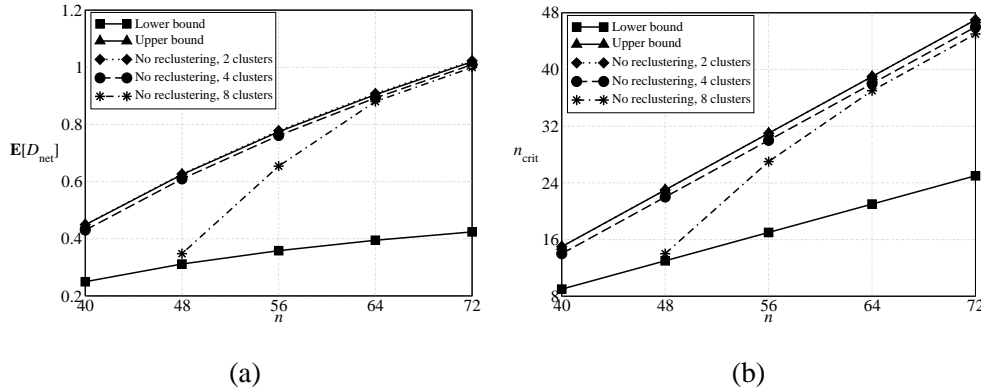
Figure 2.15: Sensor network performance using the proposed reclustering algorithm: (a) network lifetime and (b) critical number of deaths, as functions of the number of sensors. The performance in the absence of reclustering (with 2, 4, and 8 clusters, respectively) is compared with the proposed upper bound $UB_{D_{net}}$ and lower bound $LB_{D_{net}}$. The QoS condition is $P_e^* = 10^{-3}$ and the sensor SNR is set to 5 dB. The average sensor lifetime is $\mu = 1$.

and the sensor SNR is set to 5 dB. In order to compare these results with those in Section 2.3.1, the distribution of the sensors' lifetime is assumed to be exponential with $\mu = 1$ aU. From the results in Figure 2.15 (a), one can observe that, when the number of sensors increases, also the network lifetime becomes longer, since a larger number of sensors' deaths have to occur in order to violate the QoS condition. This is confirmed in Figure 2.15 (b), where the critical number of sensors' deaths is shown as a function of the number of sensors. Moreover, as expected, the sensor network lifetime in the absence of reclustering is shorter than in the presence of ideal reclustering (with the proposed reclustering protocol), since the network topology becomes more and more non-uniform and, therefore, the probability of decision error becomes higher and higher. As previously shown in Figure 2.13, when the initial number of clusters is equal to two, the network lifetime with no reclustering is very close to that corresponding to the application of the reclustering protocol. This is due to the fact that the sensors' deaths are, on average, equally distributed among the two clusters,

i.e., there is a sort of "natural" reclustering. Finally, one can observe that when the number of clusters in the initial topology increases (e.g., is equal to 8) the network lifetime drastically reduces for *low* values of the number of sensors, since it is more difficult to satisfy the QoS condition. However, it is interesting to observe that for sufficiently large values of n, the lifetime penalty incurred by the presence of a large number of clusters is negligible, suggesting that there may exist a minimum cluster dimension which guarantees acceptable performance. This is probably due to the fact that when the number of sensors is sufficiently large, the cluster dimension is also sufficiently large and, consequently, its lifetime is longer. Therefore, the lifetime of the entire sensor network is longer, since the network topology is less unbalanced.

2.3.4 Energy Budget

The analysis of the reclustering cost provided in Section 2.3.2 is ideal, since it does not consider the energy spent by the nodes in the network. Although this assumption is reasonable for the FCs and the AP,[3] this is not realistic for remote nodes (sensors) which need to rely on a limited battery energy. Moreover, there exists a delay associated with a packet transmission. In this section, the realistic network energy consumption is evaluated in the presence of ideal reclustering, using the reclustering protocol proposed in Section 2.3.2. In order to analyze this energy consumption, we will refer to a commercial wireless sensor network with a communication protocol based on the IEEE 802.15.4 standard (also considered in Section 2.3.6) [57]. In particular, while the first analysis does not take into account the energy of the sensor battery, we then show the impact of a limited battery energy at the sensors.

Analysis with Infinite Energy Battery at the Sensors

The energetic cost, for a single sensor, of the application of our reclustering algorithm can be written as

$$C_{\text{tot}}^{\text{en}} = P_{\text{t}} C_{\text{tot}}^{\text{time}} \tag{2.26}$$

---

[3]In fact, they may be placed by the network designer so that they can be power-supplied.

where $C_{\text{tot}}^{\text{en}}$ is the total cost in terms of energy spent by a sensor, P_{t} is the transmit power at each sensor, and $C_{\text{tot}}^{\text{time}}$ is the total time cost associated with packet transmission. After a few manipulations, the total energetic cost can be written as [112]

$$C_{\text{tot}}^{\text{en}} = P_{\text{t}} \left\{ \underbrace{\frac{1}{2} \left[\frac{L_{\text{cont}} + L_{\text{data}}}{R_{\text{b}}} \right] (n_{\text{crit}}^{\text{R}} - 1)}_{\substack{\text{Cost for transmission of} \\ \text{control packets: } C_{\text{R}}^{\text{time}}}} + \underbrace{\frac{L_{\text{data}}}{R_{\text{b}}} f_{\text{obs}} \sum_{i=1}^{n_{\text{crit}}^{\text{R}}} \mathbb{E}\left[T_{\text{d},i}\right]}_{\substack{\text{Cost for transmission} \\ \text{of data packets: } C_{\text{data}}^{\text{time}}}} \right\} \qquad (2.27)$$

where R_{b} is the data-rate (dimension: [b/s]), L_{cont} and L_{data} are, respectively, the length of a control packet and data packet (dimension: [b/pck]), and f_{obs} is the observation frequency. Expression (2.27) for the energetic cost represents the total energy spent by any of the $n - n_{\text{crit}}^{\text{R}}$ surviving sensors after the network death. Obviously, this energetic cost represents a worst case, since there are $n_{\text{crit}}^{\text{R}}$ nodes (i.e., those which die while the network is still alive) which spend a lower amount of energy in their shorter lifetimes. An average cost per sensor can be easily computed using the same approach proposed above. In [112], the following expression for the average energy cost is derived:

$$\begin{aligned} \overline{C}_{\text{tot}}^{\text{en}} &= P_{\text{t}}(\overline{C}_{\text{R}}^{\text{time}} + \overline{C}_{\text{data}}^{\text{time}}) \\ &= P_{\text{t}} \left\{ \frac{(n_{\text{crit}}^{\text{R}} - 1)(L_{\text{data}} + L_{\text{cont}})}{4R_{\text{b}}} + \frac{L_{\text{data}} f_{\text{obs}}}{R_{\text{b}} n} \sum_{i=1}^{n_{\text{crit}}^{\text{R}}} \left((n - n_{\text{crit}}^{\text{R}}) \mathbb{E}\left[T_{\text{d},i}\right] + \sum_{j=1}^{i} \mathbb{E}\left[T_{\text{d},j}\right] \right) \right\}. \end{aligned}$$
$$(2.28)$$

Similarly to (2.24), we define the following *energy penalties*:

$$P^{\text{en}-1} \triangleq \frac{C_{\text{R}}^{\text{en}}}{C_{\text{tot}}^{\text{en}}} = \frac{C_{\text{R}}^{\text{time}}}{C_{\text{R}}^{\text{time}} + C_{\text{data}}^{\text{time}}} \qquad (2.29)$$

$$P^{\text{en}-2} \triangleq \frac{\overline{C}_{\text{R}}^{\text{en}}}{\overline{C}_{\text{tot}}^{\text{en}}} = \frac{\overline{C}_{\text{R}}^{\text{time}}}{\overline{C}_{\text{R}}^{\text{time}} + \overline{C}_{\text{data}}^{\text{time}}} \qquad (2.30)$$

where $P^{\text{en}-1}$ is the *worst-case* penalty (associated with a sensor which survives until the end) and $P^{\text{en}-2}$ is the *average-case* penalty (associated with the average energetic
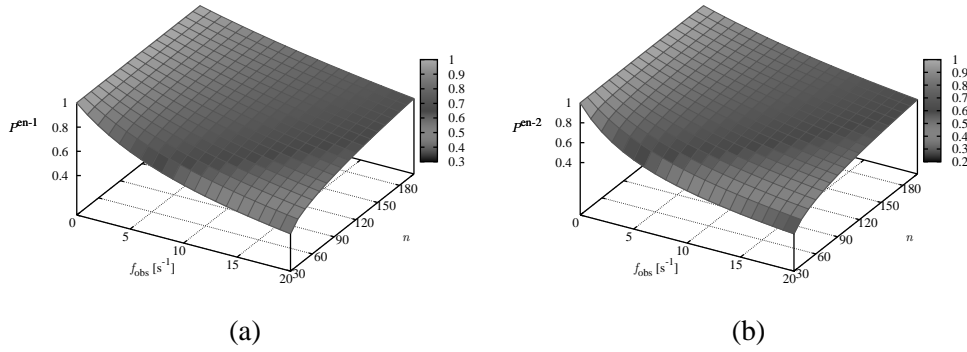
Figure 2.16: Energy penalty, associated with the reclustering protocol, as a function of both the observation frequency f_{obs} and the number of sensors n. Two possible cases are considered: (a) *maximum* penalty (associated with a sensor which survives until the end) and (b) *average* penalty (among all the sensors in the network).

costs among all sensors in the network). As mentioned before, the energy penalties (2.29) and (2.30) take into account, with respect to (2.24), realistic network parameters, such as L_{data}, f_{obs}, R_b, and P_t.

In Figure 2.16, the energy penalty is shown, as a function of the number of sensors n and the observation frequency f_{obs}, in the two cases previously highlighted: (a) *worst-case* energy consumption (obtained by using expression (2.29)) and (b) *average-case* energy consumption (obtained by using expression (2.30)). In order to compare the results in Figure 2.16 with the results given in the previous sections, we have set $P_e^* = 10^{-3}$ and $SNR_{sensor} = 5$ dB. Realistic values for the network parameters, provided by the Zigbee standard, correspond to $P_t = 1$ mW, $R_b = 250$ Kb/s, $L_{data} = 1024$ b/pck, and $L_{cont} = 80$ b/pck.[4] One can note that for low values of the observation frequency (*rare observations*), the performance worsens since the network

---

[4]In our analysis, we use the maximum possible data-rate allowed by the Zigbee standard, i.e., $R_b = 250$ Kb/s. However, our experimental results show that only a maximum value $R_b = 25$ Kb/s can be achieved by practical sensor networks [114]. Moreover, the length of data packets is the maximum allowed by the standard.

spends more time in reclustering than in transmitting useful data. For a fixed value of the number of sensors n, the following limits hold:

$$\lim_{f_{\text{obs}}\to 0} P^{\text{en}-1} = \frac{C_{\text{R}}^{\text{en}}}{C_{\text{R}}^{\text{en}}} = 1 \qquad \lim_{f_{\text{obs}}\to 0} P^{\text{en}-2} = \frac{\overline{C}_{\text{R}}^{\text{en}}}{\overline{C}_{\text{R}}^{\text{en}}} = 1.$$

Besides, one can observe that for increasing values of the observation frequency (*frequent observations*), the performance is better. In fact, for a fixed number of sensors, there is a larger number of data transmissions from the sensors to the AP and the value of D_{R}^{en} becomes increasingly negligible with respect to the value of $D_{\text{data}}^{\text{en}}$. Analytically, one can write

$$\lim_{f_{\text{obs}}\to\infty} P^{\text{en}-1} = \frac{1}{C_{\text{data}}^{\text{en}}} = 0 \qquad \lim_{f_{\text{obs}}\to\infty} P^{\text{en}-2} = \frac{1}{\overline{C}_{\text{data}}^{\text{en}}} = 0.$$

Note that a high value of the observation frequency might not be admissible. In fact, in Section 2.3.2 we have supposed that the inverse of the observation frequency is much smaller than the time necessary to complete a transmission to the AP and, eventually, the reclustering protocol (hypothesis (a) in Section 2.3.2).

Analysis with Energy-Limited Battery at the Sensors

In the previous derivations, the proposed framework and the presented results have used arbitrary time units. However, it is of interest to map these arbitrary time units into realistic units. In order to do so, we assume that a node is equipped with a limited-energy battery with initial energy E_{battery} (dimension: [J]). When a sensor battery energy exhausts, the sensor dies and, consequently, the network is closer to breaking the QoS condition. The average sensor lifetime (dimension: [s]) can be expressed as

$$\mathbb{E}\left[T_{\text{sensor}}\right] = \frac{E_{\text{battery}}}{\overline{P}}$$

where $\overline{P}$ is the average power depleted at the node (dimension: [W]). In a realistic wireless sensor network (e.g., Zigbee wireless sensor networks [57]), four *states* are admissible at the node: (1) *transmission*, (2) *reception*, (3) *idle*, and (4) *sleep*. In this

case, the average power depleted at the node is given by

$$\overline{P} = \sum_{i=1}^{4} P_i p_i \tag{2.31}$$

where P_i and p_i ($i = 1, 2, 3, 4$) are, respectively, the power consumption in the i-th state and the probability that the sensor is in the i-th state—note that $P_1 = P_t$. Typically, in a Zigbee wireless sensor network $P_4 \ll 1$ and $p_2 \ll p_3, p_1$ [115]. Therefore, the average depleted power in (2.31) can be written as

$$\overline{P} \simeq P_1 p_1 + P_2 p_2$$

where $p_2 = 1 - p_1$ and $P_1 = P_2 = P_t$ [115]. Therefore, the average consumed power in (2.31) becomes

$$\overline{P} = P_t$$

and it follows that

$$\mathbb{E}\left[T_{\text{sensor}}\right] = \frac{E_{\text{battery}}}{P_t}. \tag{2.32}$$

Using the value of $\mathbb{E}\left[T_{\text{sensor}}\right]$ given in (2.32) for the computation of $C_{\text{tot}}^{\text{time}}$ according to the framework derived in Section 2.3.4, the lifetime of a realistic Zigbee wireless sensor network, with the parameters used to derive the results in Figure 2.16, can be obtained. The sensor network lifetime values, associated with different battery energies at the sensors (typical for practical applications), are summarized in Table 2.3.4. In particular, a scenario with $n = 64$ sensors, $P_t = 1$ mW, and $f_{\text{obs}} = 20 \, s^{-1}$ is considered. One can observe that the theoretical results given in Section 2.3.3 are confirmed also in a more realistic Zigbee wireless sensor network. However, note that for $n = 64$ sensors the network lifetime in the ideal scenario is shorter than $\mathbb{E}\left[T_{\text{sensor}}\right]$, whereas it is longer in a realistic scenario. This behavior is due to the fact that our theoretical framework does not consider the delay associated with packet transmissions, as considered, instead, in the performance analysis for a Zigbee network.

2.3.5   Noisy Communication Links

The analysis of the sensor network lifetime proposed in Section 2.3.2 is quite general and, in particular, no assumption has been made on the communication links.

Table 2.3: Sensor network lifetime for a realistic Zigbee wireless sensor network in a scenario with $n = 64$ sensors, $P_t = 1$ mW, and $f_{obs} = 20 \ s^{-1}$. The Zigbee parameters are the same considered in Figure 2.16. Different values of the battery energy at a sensor are considered.

Battery energy $E_{battery}$ [kJ]	Average sensor lifetime $\mathbb{E}\left[T_{sensor}\right]$ [days]	Sensor network lifetime C_{tot}^{time} [days]
12.96 (400 mAh, 9 V)	150	196
19.44 (600 mAh, 9 V)	224	294
31.68	365	480
32.4 (1 Ah, 9 V)	375	491

However, the results presented in Section 2.3.3 are obtained under the assumption of *ideal* communication links. In a scenario with noisy communication links, two main differences, with respect to a scenario with ideal communication links, can be observed:

- for a given value of the sensor SNR, the presence of noisy communication links leads to a performance loss (i.e., higher probability of decision error);

- a probability of decision error floor can be visualized for high values of the sensor SNR.

These differences between the scenarios with ideal communication links and those with noisy communication links imply that the network lifetime will be shorter, since the QoS condition will be satisfied for a shorter time. Moreover, the presence of a probability of decision error floor implies that, for a given value of the sensor SNR, the QoS condition might never be satisfied. These considerations suggest that the QoS condition and the operating sensor SNR, for a given value of the number of sensors n, have to be properly chosen.
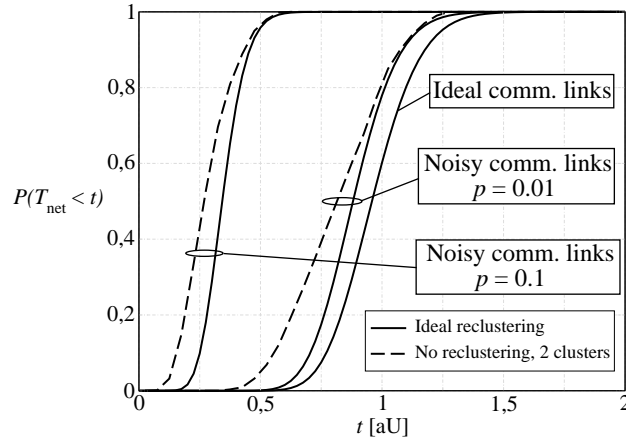
Figure 2.17: CDF of the network lifetime, as a function of time, in a scenario with $n = 64$ sensors, uniform clustering, and noisy communication links. Two possible values for the cross-over probability are considered: (i) $p = 0.1$ and (ii) $p = 0.001$. The sensor SNR is set to 5 dB and the maximum tolerable probability of decision error is $P_e^* = 10^{-3}$.

In Figure 2.17, the CDF of the network lifetime is shown, as a function of time,[5] in a scenario with $n = 64$ sensors, uniform clustering, and noisy communication links. Two possible values for the cross-over probability are considered: (i) $p = 0.1$ and (ii) $p = 0.001$. For comparison, the curve associated with ideal communication links is also shown. The sensor SNR is set to 5 dB and the maximum tolerable probability of decision error is $P_e^* = 10^{-3}$. One can observe that the higher is the noise intensity in the communication links, the higher is the CDF of the network lifetime. In fact, in this case the transfer of information from the sensors to the AP is less reliable and, consequently, the probability of decision error becomes higher and higher and the QoS condition can be guaranteed for a shorter time. As in a scenario with ideal communication links, the presence of reclustering prolongs the network lifetime with

---

[5]We recall that the time is measured, here, in arbitrary units. For more realistic scenarios, see the considerations at the end of Section 2.3.4.

respect to a scenario with no reclustering. Obviously, for a given reclustering strategy a scenario with ideal communication links corresponds to a longer network lifetime, since the probability of decision error is the lowest possible.

2.3.6   Throughput and Delay with Varying Sensor Network Lifetime

In this section, we evaluate the performance of a realistic Zigbee wireless sensor network subject to nodes' failures. In order to carry out this analysis, we resort, as in Section 2.2.5, to simulations using Opnet Modeler 11.5 [105] and a built-in model for IEEE 802.15.4 networks, provided by the NIST [106]. In this section we analyze the network performance (in terms of number of transmitted packets, throughput, and delay) in scenarios with no clustering (and, therefore, no reclustering). The goal of this section is to show the impact of different QoS conditions (given in terms of the required percentage of nodes' deaths which make the network die) on different network performance indicators (e.g., throughput and delay). For the performance in the presence of relaying see [116]. As discussed in Section 2.3.1, the performance of sensor networks with no clustering can be considered, from a network lifetime viewpoint, as a lower bound, since the probability of decision error is lower than in scenarios with clustering. In the simulations, the following parameters are considered: $R_b = 250$ Kb/s, $L_{data} = 994$ b/pck, and $g = 0.236$ s, where g is the packet interarrival time at the sensors. Moreover, no transmission of acknowledgement packets is considered from the AP to the remote nodes. In all presented results, four QoS conditions will be considered: (i) network death corresponds to 100% of sensors' deaths (i.e., the network survives until there is a single sensor alive), (ii) network death corresponds to 70% of sensors' deaths, (iii) network death corresponds to 50% of sensors' deaths, and (iv) network death corresponds to 20% of sensors' deaths.

In Figure 2.18, the packet delivery fraction is shown, as a function of the number of sensors n, for two possible distributions of a single sensor lifetime: (a) exponential with $\mu = 300$ s (solid lines) and (b) uniform with $t_{max} = 600$ s (dashed lines). First, one can observe that the more stringent is the QoS condition, the lower is the throughput. In fact, a smaller number of transmissions are possible (since the network lifetime is shorter) and a larger number of collisions happen, because there is a large
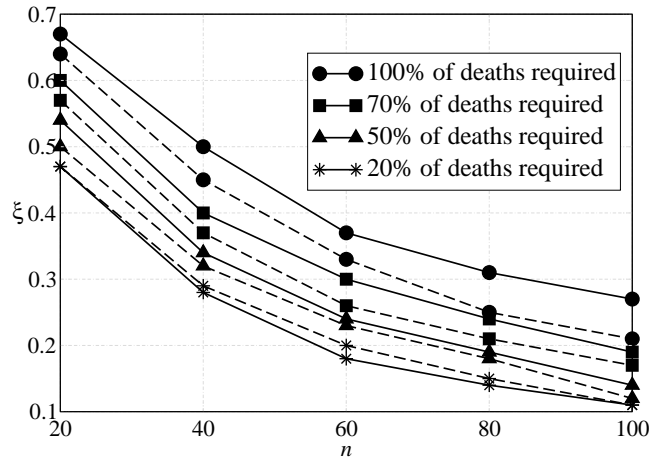
Figure 2.18: Packet delivery fraction, as a function of the number of sensors n, in a Zigbee wireless sensor network with nodes' failures. Two possible distributions for a single sensor lifetime are considered: (a) exponential with $\mu = 300$ s (solid lines) and (b) uniform with $t_{max} = 600$ s (dashed lines).

number of sensors which try to transmit to the AP and a larger number of packets are lost. Moreover, a scenario with uniform distribution of the sensors' lifetime has a lower throughput with respect to a scenario with exponential distribution, since more packets are lost due to the collisions.

In Figure 2.19, the average MAC delay[6] over all the received packets D is shown, as a function of the number of sensors n, for two possible distributions of a single sensor lifetime: (a) exponential with $\mu = 300$ s (solid lines) and (b) uniform with $t_{max} = 600$ s (dashed lines). Similarly to what happens for the throughput in Figure 2.18, a larger number of collisions also causes a higher delay in receiving the packets. Therefore, scenarios with a uniform distribution of the sensors' lifetimes are characterized by a higher delay with respect to scenarios with an exponential distribution. In this case as well, however, the more stringent is the QoS condition, the higher

---

[6]The average MAC delay corresponds to the delay averaged over all packets which are correctly received at the MAC level during the Opnet simulations.
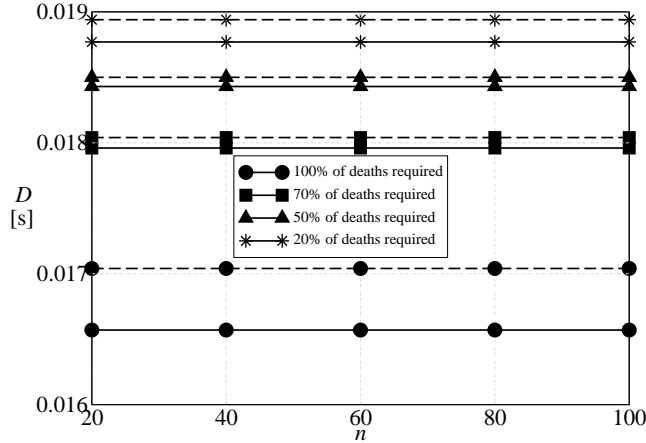
Figure 2.19: Average MAC delay D, as a function of the number of sensors n, in a Zigbee wireless sensor network with nodes' failures. Two possible distributions for a single sensor lifetime are considered: (a) exponential with $\mu = 300$ s (solid lines) and (b) uniform with $t_{\max} = 600$ s (dashed lines).

is the average MAC delay. Finally, the average MAC delay does not depend on the number of sensors, for a fixed QoS condition, since the number of surviving sensors is (almost) the same and, therefore, the average delay in the packet transmissions is constant.

2.4   Impact of Different SNRs at the Sensors

Consider now a generic scenario with different SNRs at the sensors. For the sake of simplicity, we consider a scenario with no clustering, i.e., direct communications between the sensors and the AP. In this case, a decision based on the *majority-like* fusion rule might not be the best choice. In fact, if a sensor is very noisy (i.e., its observation SNR is very small), its decision should be taken into account with a low level of reliability in the fusion process at the AP. Therefore, it would be reasonable to assign each sensor a weight proportional to its own SNR—this approach is similar to

that proposed in [31], where the weights are assigned according to the link qualities. The AP could then make a final decision taking into account the weights assigned to the sensors. Note that the improvement, in terms of probability of decision error, comes at the price of a non-optimal network energy efficiency, since all sensors, even those with low SNR, have to send their decisions to the AP and waste the same amount of energy.

In the following, we consider a system where the AP takes into account the n local sensor decisions with the same weight, i.e., without considering their SNRs, and adopts a majority-like decision rule. In order to take into consideration the sensor SNR profile, the threshold for local decision at each sensor is properly optimized, as explained in detail in Section 2.4.1.

We now derive analytical expressions for the probability of decision error, distinguishing between a scenario with *ideal* communication links and a scenario with *noisy* communication links. In [117], the reader might found an analytical expression for the probability of decision error also in the case when no quantization is carried out at the sensors, i.e., when sensors transmit their local likelihood values.

2.4.1   Ideal Communication Links

Probability of Decision Error

Consider the first conditional probability at the right-hand side of (2.5) and define the threshold value k in the majority-like decision rule. There is an error, i.e., $\widehat{H} = H_1$ given that $H = H_0$, if $i \geq k$ sensors decide for H_1 when H_0 has happened. In this case, there can be $\binom{n}{i}$ combinations of sensors deciding for H_1. We denote as $\Omega_i(j)$ the j-th possible combination $(j = 1, \ldots, \binom{n}{i})$ in a scenario where i sensors are in error.[7] Therefore, the conditional probability of interest can be expressed as follows:

$$P(\widehat{H} = H_1 | H_0) = \sum_{i=k}^{n} \sum_{j=1}^{\binom{n}{i}} \left\{ \prod_{\ell=1}^{i} P\left(u_{\ell}^{(\Omega_i(j))} = H_1 | H_0\right) \prod_{m=i+1}^{n} P\left(u_m^{(\Omega_i(j))} = H_0 | H_0\right) \right\}$$
(2.33)

---

[7]Note that $\Omega_i(j)$ depends also on n. However, for the sake of notational simplicity, this dependence is not explicitly indicated. The context should eliminate any ambiguity.

where $P(u_\ell^{(\Omega_i(j))} = H_1|H_0)$ is the probability that at the ℓ-th sensor, in the $\Omega_i(j)$-th combination (out of the $\binom{n}{i}$ possible ones), a wrong decision is made when H_0 has happened.

Similarly, the second conditional probability at the right-hand side of (2.5) can be expressed as

$$P(\widehat{H} = H_0|H_1) = \sum_{i=0}^{k-1} \sum_{j=1}^{\binom{n}{i}} \left\{ \prod_{\ell=1}^{i} P\left(u_\ell^{(\Omega_i(j))} = H_1|H_1\right) \prod_{m=i+1}^{n} P(u_m^{(\Omega_i(j))} = H_0|H_1) \right\}$$
(2.34)

where $P(u_\ell^{(\Omega_i(j))} = H_1|H_1)$ is the probability that at the ℓ-th sensor, in the $\Omega_i(j)$-th combination, a correct decision is made when H_1 has happened.

Decision Threshold Selection at the Sensors

In the literature, it is shown that using the same threshold at all sensors is an asymptotically optimal solution *if and only if* the SNR at the sensors is constant [118]. In the currently considered scenario (with different SNRs at the sensors), it is not reasonable to use the same threshold at all sensors. Therefore, one needs to choose another criterion for local decisions at the sensors.

In this section, we consider a *locally optimal* decision scheme.[8] In other words, each sensor makes a binary decision which minimizes, for the corresponding SNR, its probability of (local) error—this corresponds to a *person-by-person optimization* (PBPO) approach to distributed detection [119]. The optimal value for the threshold τ_i is such that

$$p(\tau_i|H_1)P(H_1) \quad = \quad p(\tau_i|H_0)P(H_0).$$
(2.35)

In general, the computation of the probability of decision error, based on the evaluation of (2.33) and (2.34), depends on (i) the chosen value for k, (ii) the sequence of the detected phenomenon amplitudes $\{s_i\}$ at the sensors, (iii) the sequence of noise variances $\{\sigma_i\}$, and (iv) the sequence of thresholds $\{\tau_i\}$. Recalling the Gaussian model

---

[8]We are implicitly assuming that each sensor estimates its own observation SNR.

for the observable in (2.1), one can obtain [117]

$$
\begin{aligned}
P(u_\ell = H_1 | H) &= 1 - Q\left(\frac{\tau_\ell - s_\ell \cdot H}{\sigma_\ell}\right) \\
&= 1 - Q\left(\frac{1}{2}\sqrt{\text{SNR}_{\text{sensor}}^{(\ell)}} + \frac{1}{\sqrt{\text{SNR}_{\text{sensor}}^{(\ell)}}}\ln\frac{p_0}{1-p_0} - \sqrt{\text{SNR}_{\text{sensor}}^{(\ell)}}H\right).
\end{aligned}
$$

As expected, the probability of decision error does not depend on the sequences $\{s_i\}$ and $\{\sigma_i\}$ separately but, rather, only on the sequence of ratios $\{s_i/\sigma_i\}$, i.e., on the sequence of sensor SNRs. In other words, the probability of decision error depends on the sensor *SNR profile* $\{\text{SNR}_{\text{sensor}}^{(i)}\}$. Therefore, evaluating the system performance of the sensor network as a function of the sensor SNR profile is a meaningful problem.

2.4.2 Noisy Communication Links

Let us denote by p the cross-over probability of the BSCs (the same for all noisy communication links). In this case, the decision made at the ℓ-th sensor, i.e., u_ℓ, might be "flipped," with probability p, by the communication link. In particular, the component conditional probabilities in (2.5) depend on p. For instance, the conditional probability (2.33) has to be modified by replacing the decisions made locally by the sensors with the corresponding *received* decisions:

$$
\begin{aligned}
P(\widehat{H} = H_1 | H_0) &= \sum_{i=k}^{n}\sum_{j=1}^{\binom{n}{i}}\left\{\prod_{\ell=1}^{i}P\left(u_\ell^{(\Omega_i(j))-\text{rec}} = H_1 | H_0\right)\right. \\
&\quad \left. \cdot \prod_{m=i+1}^{n}P\left(u_m^{(\Omega_i(j))-\text{rec}} = H_0 | H_0\right)\right\} \quad (2.36)
\end{aligned}
$$

where $u_\ell^{(\Omega_i(j))-\text{rec}}$ and $u_m^{(\Omega_i(j))-\text{rec}}$ are the received versions of the local decisions $u_\ell^{(\Omega_i(j))}$ and $u_m^{(\Omega_i(j))}$, respectively. The conditional probability (2.34) has to be modified similarly. A generic term in (2.36) can then be expressed as follows:

$$
P(u_\ell^{\text{rec}} = H_1 | H_0) = (1-p)Q\left(\frac{\tau_l}{\sigma_l}\right) + p\left[1 - Q\left(\frac{\tau_l}{\sigma_l}\right)\right]. \quad (2.37)
$$
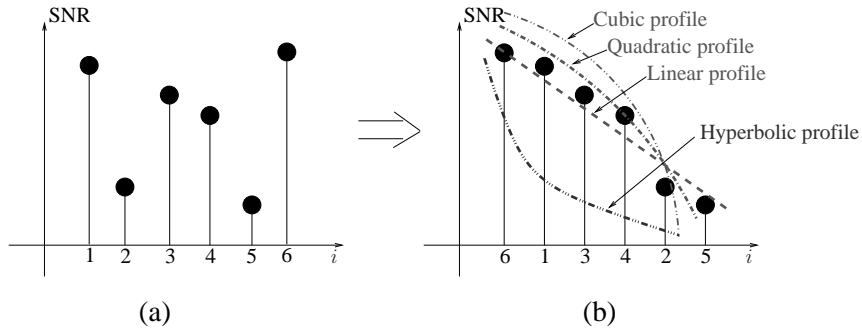
Figure 2.20: Illustrative sensor SNR profile: (a) realistic and (b) reordered with non-increasing values of the SNRs. In particular, in (b) four possible interpolating profiles (linear, quadratic, cubic, and hyperbolic) are shown.

Since we are considering locally optimal selection of the decision thresholds at the sensors, there is no difference (in terms of the decision strategy at the sensors) between a scenario with ideal communication links and a scenario with noisy communication links. Therefore, the derivation considered in Section 2.4.1 for sensor threshold selection holds in this case as well.

2.4.3   Sensor SNR Profiles

As observed in Section 2.4.1, the probability of decision error ultimately depends on the *sensor SNR profile* $\{\mathrm{SNR}_{\mathrm{sensor}}^{(i)}\}$. A generic example of sensor SNR profile is shown in Figure 2.20 (a): the sensor SNRs are generally not monotonically ordered. However, since it is always possible to reorder the sensor SNRs from highest to lowest, as shown in Figure 2.20 (b), without loss of generality, one can restrict his/her attention to a scenario where the sensor SNR profile is *non-increasing*.

Based on the observation in the previous paragraph, in order to characterize non-increasing sensor SNR profiles we consider four possible cases (the SNRs are ex-

pressed in dB):

$$\text{Linear profile:} \quad \text{SNR}_i = \text{SNR}_0 - c \cdot i$$

$$\text{Quadratic profile:} \quad \text{SNR}_i = \text{SNR}_0 - c \cdot i^2$$

$$\text{Cubic profile:} \quad \text{SNR}_i = \text{SNR}_0 - c \cdot i^3 \tag{2.38}$$

$$\text{Hyperbolic profile:} \quad \text{SNR}_i = \frac{\text{SNR}_0}{1 + c \cdot i}$$

where: $i = 0, \ldots, n-1$; n is the number of sensors; SNR_0 is the highest sensor SNR; and c is a suitable constant which uniquely characterizes the sensor SNR profile *slope*. For this reason, we denote c as *slope coefficient*. A large value of c corresponds to a scenario where the sensor SNRs decrease rapidly (i.e., the corresponding realistic non-ordered sensor SNR profile is highly varying), whereas a small value of c corresponds to a scenario where the sensor SNRs are similar (i.e., the corresponding realistic non-ordered sensor SNR profile is almost constant). If $c = 0$, all profiles degenerates to a constant profile, i.e., $\text{SNR}_i = \text{SNR}_0$, $\forall i$. In Figure 2.20 (b), illustrative graphical examples of the four profiles are shown. In the following, we will restrict our attention to scenarios with convex SNR profiles (linear, quadratic, and cubic), since concave profiles (e.g., hyperbolic) can be shown to lead to worse performance [117]. As one can see, by suitably setting the values of SNR_0 and c, a large number of realistic sensor SNR profiles can be characterized. This underlines the applicability of our framework. In Section 2.4.5, we will propose a simple experiment to characterize a realistic sensor SNR profile.

In (2.38), we have assumed that the maximum SNR and the slope coefficient c are the same for all profiles. However, in this case the winning profile is always the linear, since the sensor SNR at any position is higher than the corresponding one in any other profile. In order to obtain a "fair" comparison between the various profiles, one can impose that all the SNR profiles have the same average value, denoted as $\overline{\text{SNR}}$.

- By imposing that the slope coefficient c is the same for all profiles, after a few manipulations one obtains that the maximum SNRs in the various cases need

to be set as follows:

$$SNR_{0,l} = \overline{SNR} + c\,\frac{n-1}{2}$$

$$SNR_{0,q} = \overline{SNR} + c\,\frac{(n-1)(2n-1)}{6} \qquad (2.39)$$

$$SNR_{0,c} = \overline{SNR} + c\,\frac{n(n-1)^2}{4}.$$

- Specularly, imposing that the maximum SNR is the same for all the sensors, the slope coefficient in the four considered cases need to be set in the following way:

$$c_l = (SNR_0 - \overline{SNR})\,\frac{2}{n-1}$$

$$c_q = (SNR_0 - \overline{SNR})\,\frac{6}{(n-1)(2n-1)} \qquad (2.40)$$

$$c_c = (SNR_0 - \overline{SNR})\,\frac{4}{n(n-1)^2}.$$

Finally, one should observe that in (2.40) it must hold that $SNR_0 - \overline{SNR} \geq 0$.

We point out that throughout this section we make the implicit assumption that the SNR profiles are perfectly known and available at the AP. This is expedient for performance analysis. However, in a realistic scenario, the mechanisms to collect SNR values from the resource-constrained sensors may not be very accurate, and relying too much on it may not be helpful. Collecting the values accurately is a challenging problem, which needs further investigation. For example, the SNR values could be collected during a *training phase*, when each sensor computes its local SNR and send it to the AP. In Section 2.4.5, we propose a simple experimental validation of our theoretical assumptions.

2.4.4   Numerical Results

Ideal Communication Links

Let us first consider a sensor network with ideal communication links from the sensors to the AP. Moreover, the a priori probabilities of the phenomenon are such that
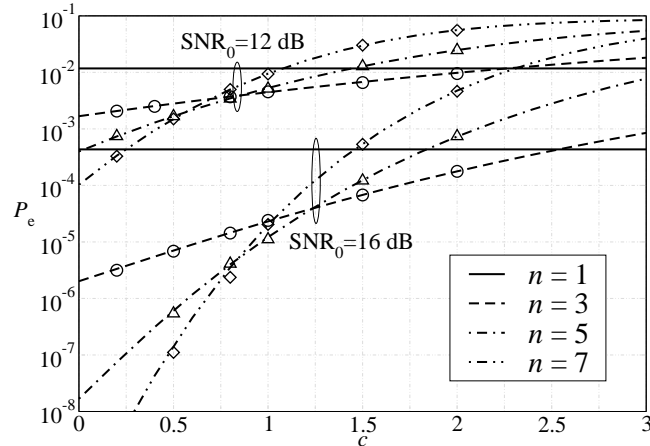
Figure 2.21: Probability of decision error, as a function of the coefficient c, with SNR_0 equal to 12 dB and 16 dB, respectively. Various values of the number of sensors n are considered, in a scenario with *linear* sensor SNR profile. The lines correspond to analytical results, whereas the symbols are associated with simulation results.

$P(H_0) = 10P(H_1)$: this is meaningful for situations where a phenomenon is rare (e.g., the phenomenon under observation is an unusually high humidity level).

The following question is meaningful: for a given value of SNR_0, what are the conditions under which the use of a limited number of sensors (lower, for instance, than n) is the winning strategy? In order to answer this question, in Figure 2.21 the probability of decision error is shown, as a function of the coefficient c, in a scenario with linear SNR profile. The lines correspond to analytical results, whereas the symbols are associated with Monte Carlo simulation results. Two possible values for the highest sensor SNR, i.e., SNR_0, are considered: 12 dB and 16 dB, respectively. For each value of the sensor SNR, various numbers of sensors are considered. Obviously, the curves corresponding to scenarios with only $n = 1$ sensor are constant with respect to c. The impacts of the parameters c and SNR_0 can be characterized as follows.

- For *small* values of c, i.e., in a scenario with almost constant SNR profile, the

best performance is obtained using *all sensors*, regardless of the value of SNR_0. For *large* values of c (i.e., irregular sensor SNR profile before monotonic reordering), the best performance is obtained using only the sensors with *highest SNRs*. Note that the best asymptotic performance ($c \to \infty$) is obtained using only *the* sensor with highest SNR (SNR_0): however, the probability of decision error might be intolerably high.

- For low values of SNR_0, the impact of c is "mild," whereas for high values of SNR_0 the impact of c is relatively stronger. This behavior can be interpreted as follows. If *at least* one sensor is highly accurate, i.e., SNR_0 is high, then in order to optimize the network performance the right subset of sensors should be carefully chosen. In other words, the higher is the sensitivity of at least one sensor in observing the phenomenon, the more accurate the selection of a suitable subset of sensors has to be carried out.

As one can observe from Figure 2.21, for a given value of c, the best performance is obtained selecting a specific number of sensors—those with highest SNRs, starting from the one with SNR_0. In order to characterize this behavior in more detail, in Figure 2.22 the optimal value of the number of sensors to be selected is shown, as a function of c, for various values of SNR_0. The results in Figure 2.22 show that (i) the optimal number of sensors is a decreasing function of c, and (ii) the lower is SNR_0, the faster the optimal number of sensors decreases for increasing values of c. A careful reader might wonder, at this point, why the optimal number of sensors does not reduce by one in correspondence with each vertical (decreasing) step. This behavior is due to the fact that the decision threshold τ_i at the $i-$th sensor is computed according to (2.35), which represents a *locally optimal* threshold selection strategy. Therefore, one can conclude that such a threshold selection strategy is not *globally optimal* (from the entire distributed decision process), as already observed in [120]. The individuation of globally optimal decision thresholds at the sensors in a scenario with non-constant sensor SNR profile is currently under investigation.
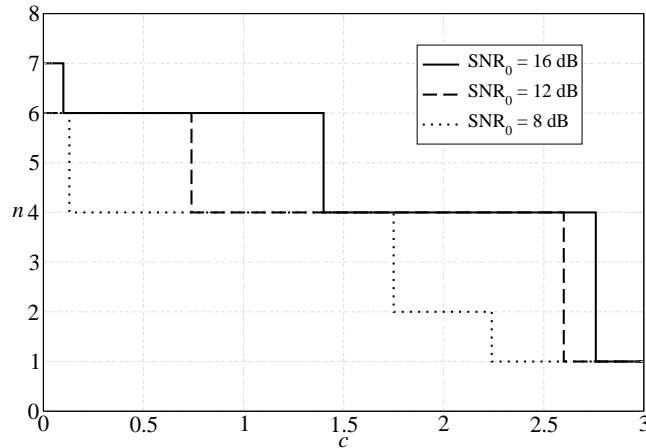
Figure 2.22: "Optimal" number of sensors (for minimizing the probability of decision error) as a function of the coefficient c, in a scenario with *linear* sensor SNR profile and $P(H_0) = 10 P(H_1)$. Three values for SNR_0 are considered.

Noisy Communication Links

While in the previous section we have considered a scenario with *ideal* communication links, we now extend the previous analysis in order to evaluate the impact of the sensor SNR profile in the presence of noisy communication links. More precisely, in a simple network scenario with $n = 3$ sensors, we compare directly the performance with linear, quadratic, and cubic sensor SNR profiles. We do not consider the hyperbolic profile, since we have shown in Section 2.4.4 that the overall performance with this profile is worse than that with the other profiles—in fact, in the presence of a hyperbolic profile the average sensor SNR has to be very high in order to obtain an acceptable performance level. We evaluate the probability of decision error in a scenario with *all noisy* communication links (considering two values for the cross-over probability p, equal to 10^{-3} and 10^{-1}, respectively) and, for comparison, in a scenario with all ideal links.

In Figure 2.23, the probability of decision error is shown, as a function of the slope coefficient c, in various scenarios with $SNR_0 = 16$ dB and $P(H_0) = 10 P(H_1)$.
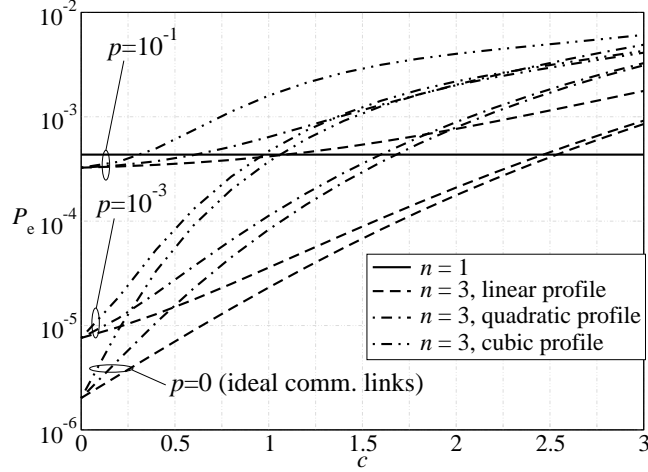
Figure 2.23: Probability of decision error, as a function of the coefficient c, in a scenario with $n = 3$ sensors. The common value of the maximum sensor SNR is $SNR_0 = 16$ dB. Three possible scenarios are considered: (i) all ideal links ($p = 0$), and all noisy links with (ii) $p = 10^{-3}$ and (iii) $p = 10^{-1}$, respectively. For comparison, the performance with $n = 1$ sensor is also shown (horizontal solid line).

In Figure 2.24, the same sensor network scenario is considered, but the *average* sensor SNR is kept constant to $\overline{SNR} = 16$ dB—for each value of c, the corresponding value of SNR_0 is determined according to (2.39). On the basis of the results shown in Figure 2.23 and Figure 2.24, it is possible to characterize, performance-wise, the interaction between the sensor SNR profile and the communication noise as follows.

- In a scenario with *common* value of SNR_0, the impact of the sensor SNR profile is very similar in scenarios with ideal communication links and with noisy communication links. For the same value of c, the probability of decision error increases if the profile changes from linear to cubic. Obviously, for $c = 0$ the performance with the three profiles coincides. Moreover, asymptotically (for large values of c) the probability of decision error is the same regardless of the profile. Therefore, it is possible to identify a critical value of c beyond which
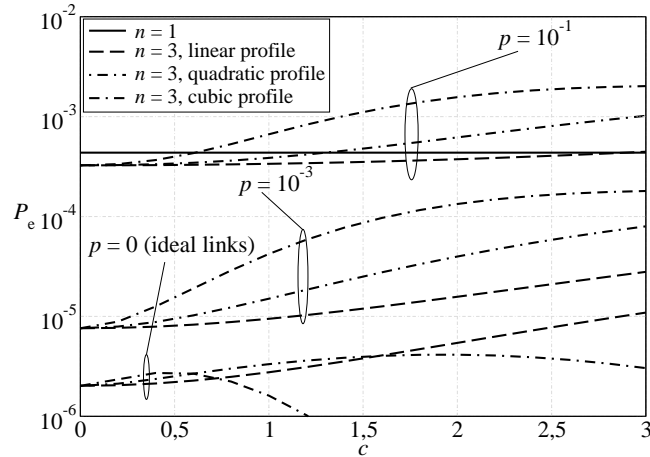
Figure 2.24: Probability of decision error, as a function of the coefficient c, for the same scenario of Figure 2.23 and a common *average* value of the sensor SNR equal to $\overline{\mathrm{SNR}} = 16$ dB.

the impact of the sensor SNR profile is the highest.

The impact of the noise is strong for small values of c, whereas it becomes negligible for large values of c. In fact, for any given profile, the curves associated with ideal links and those associated with noisy links tend to coincide for increasing values of c. In other words, the less regular is the sensor SNR profile (i.e., the larger is c), the milder is the impact of the noise in the communication links. On the other hand, if the sensor SNR is very similar across the sensors, then the noise in the communication links has a severe impact of the network performance. This latter scenario is analyzed in detail in [21].

• In a scenario with a common value of $\overline{\mathrm{SNR}}$, rather than a common maximum sensor SNR, the $P_{\mathrm{e}} - c$ curves do not tend to coincide for large values of the slope coefficient c. In other words, the impact of value of c in a scenario with common $\overline{\mathrm{SNR}}$ is stronger than in a scenario with common SNR_0. On the other hand, for small values of the slope coefficient c, the performance in a scenario with common $\overline{\mathrm{SNR}}$ is similar to that in a scenario with common SNR_0.

From the results in Figure 2.24, one can also make another observation. In the presence of ideal communication links, for increasing values of c the best performance is obtained by quadratic and cubic profiles. On the opposite, in the presence of noisy communication links, for increasing values of c the best performance is given by a linear sensor SNR profile.

2.4.5   Experimental Validation

In this section, we show experimental results relative to the SNRs measured at the sensors, in order to validate the theoretical models proposed in this section. In particular, we evaluate the *Received Signal Strength Indication* (RSSI) in order to obtain *sensor SNR-like* profiles. Equivalently to the RSSI, one could also use the *Path Loss* indicator. In fact, the following equation (in logarithmic scale) holds:

$$P_t = \text{RSSI} + \text{PathLoss}$$

where P_t is the transmit power (dimension: [dBm]) and Path Loss is the power reduction incurred by propagation (dimension: [dB]). Since in our experiments we set $P_t = 0$ dBm, one easily obtains:

$$\text{RSSI} = -\text{PathLoss}.$$

The main idea of our experiments is the following. A mobile mote sends periodically a message, called *beacon*, whereas n remote nodes, at fixed positions with respect to the mobile mote, receive the beacon and store the received power. Finally, a vector of n power levels is obtained, and an SNR-like profile can be derived. The experimental set-up[9] is schematically shown in Figure 2.25, from (a) practical and (b) logical viewpoints, respectively. We deploy four MicaZ nodes at the vertices of a square area of 90x90 cm^2, and the remaining mobile (beacon) mote acts as the event "generator" and is denoted as *firing mote* (fm). As shown in Figure 2.25, four nodes are placed at the vertices of the network surface. The fm moves inside the network,

---

[9]Since our experiments are developed in a laboratory environment, there is furniture all around the square area where the sensors are deployed. However, we can consider the reflected signals negligible.
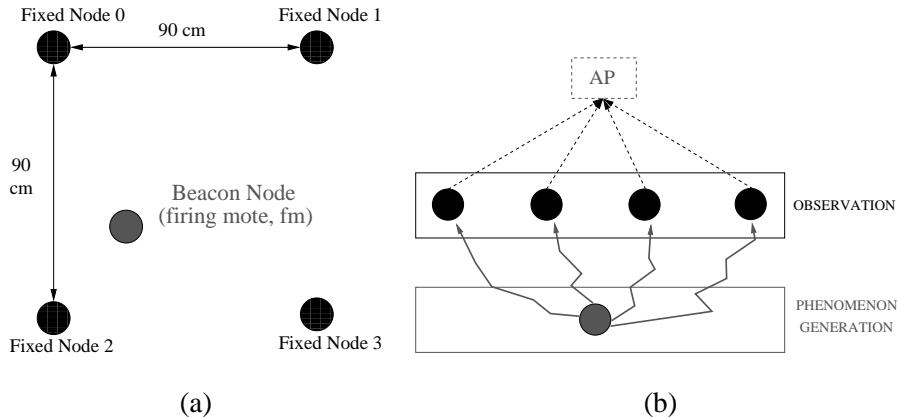
Figure 2.25: Experimental set-up: (a) practical scheme with five motes (one "firing/beacon node" and four fixed nodes), deployed over a square network surface with area equal to 90x90 cm^2, and (b) its corresponding logical scheme. The considered platforms are constituted by MicaZ motes using a communication protocol compliant with the IEEE 802.15.4 standard.

sending messages to the fixed nodes. Note that in the considered experimental set-up, the observed phenomenon corresponds to the message sent by the mobile node. In order to replicate the theoretical analysis, after receiving the message from the fm, the four fixed nodes should take a decision (e.g., based on the received power), and send their decisions to an AP. Since our goal, in this section, is to characterize the sensor SNR profile, we do not consider the communication phase from the sensors to the AP.

Two experiments have been run:

- the fm, which sends the beacon, is very close to one of the remote (fixed) nodes;

- the fm is in the middle between the network center and one of the four vertices of the square network surface, i.e., a fixed node.

In Figure 2.26, the Path Loss is shown, as a function of the remote node IDs (indicated in Figure 2.25 (a)), in two different scenarios: (a) the fm is very close to

(a)   (b)
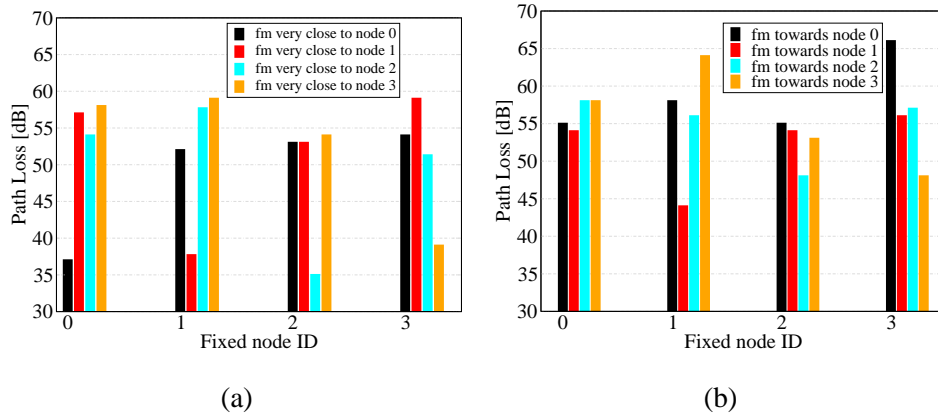
Figure 2.26: Path Loss profiles in the presence of four MicaZ motes sensing a firing
mote (fm). The fm is placed either (a) very close to one of the vertices or (b) between
the center of the area and one of the vertices.

one of the fixed nodes, and (b) the fm is in the middle between the network center
and one of the fixed nodes. As one can see from Figure 2.26 (a), the lowest Path
Loss is obtained, as expected, in correspondence to the nearest remote node. In this
case, the profile described is a *heavyside-like* function, since only the fixed node
closest to the fm senses a high RSSI (or, equivalently, a low Path Loss), while the
others do the opposite. In Figure 2.26 (b), the fm is in a more central region and,
therefore, the measured power profile is, as expected, smoother than that observed in
Figure 2.26 (a).

Rearranging the values in Figure 2.26 (b) in an increasing order, one can obtain a
decreasing profile, as described in the previous sections, of Path Loss or RSSI mea-
sures. In Figure 2.27, the *Path Loss* profile is shown, as a function of the mote ID,
for the four different cases (relative to the position of the mobile mote) considered
in Figure 2.26 (b). As one can observe, on the average, the profile is approximately
linear.
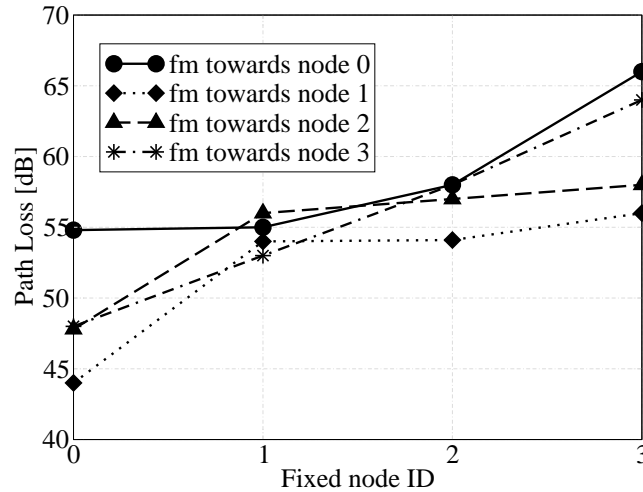
Figure 2.27: Reordered Path Loss profiles in the scenarios considered in Figure 2.26 (b).

2.5   On the Interplay Between Decoding and Fusion

2.5.1   Distributed Channel Coding and Detection/Decoding/Fusion Strategies

In Figure 2.28, a pictorial description of the considered sensor network model is shown. There are source nodes (the sensors), which observe (in a noisy manner) a spatially constant phenomenon and send their decisions to the AP, possibly using channel coding. The presence of a relay is also considered and a simple relaying strategy is proposed. The impact of multiple access interference is not investigated here: in other words, we assume orthogonal transmissions to the AP (e.g., perfect transmission scheduling between the sensors and, if present, the relay). The AP performs the following operations:

- *detection* of the observables, taking into account their statistical characterization;
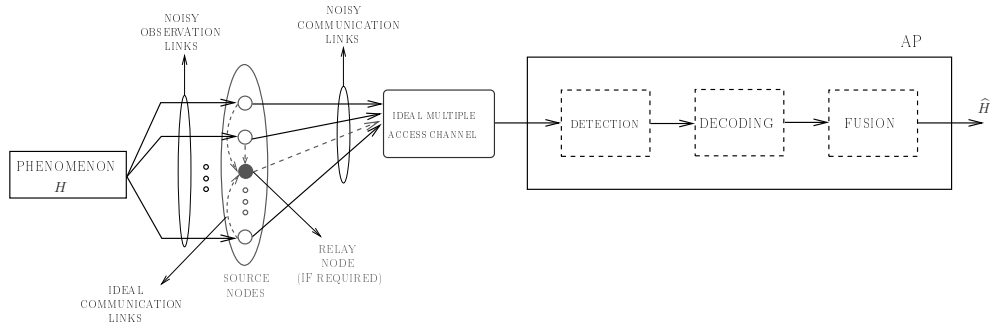
Figure 2.28: Pictorial description of the considered sensor network schemes. Solid lines are associated with *mandatory* elements (either blocks or connections), whereas dashed lines are associated with *optional* elements.

- *decoding* of the embedded error correction code (when used);

- *fusion* of the decoded data to estimate the status of the phenomenon under observation.

Note that some of the elements in Figure 2.28 are present only in specific scenarios—for instance, the relay node and the decoding block in the AP appear only in coded scenarios.

Repetition Coded Sensor Network

A sensor network with multiple observations (*M* consecutive and independent observations of the same phenomenon) can be interpreted as a system embedding a *repetition code* (with code rate $1/M$) at each sensor. In this case, redundant information is not sent by a relay, but from the sensors themselves through *M* consecutive transmission acts per sensor.

Systematic Block Coded Sensor Network

In order to embed a *systematic* block channel code into a sensor network, we propose a simple relaying strategy. More precisely, we assume that each sensor transmits

its (uncoded) decision to the AP and, owing to the broadcast nature of the wireless medium, also to the relay. Upon reception of the decisions from the sources, the relay, by using a systematic block code, generates parity bits and sends them to the AP. For example, a $(n_{cod}, n) = (7, 4)$ systematic Hamming code [121, p. 562] can be embedded into a sensor network with $n = 4$ sensors and one relay, which generates $n_{cod} - n = 3$ bits according to the parity-check equations of the Hamming code. Assuming (as mentioned) that each sensor can reach both the AP and the relay in a single transmission act, the total number of transmission acts in the proposed sensor network is n_{cod}. The equivalent code rate of this distributed coded scheme is $R_c = n/n_{cod} = 4/7$. Note, however, that the connections between the sensors and the relay have to be *ideal* (i.e., with no communication noise) in order for the proposed schemes to be applicable. This assumption is reasonable provided that, for example, the relay is relatively closer to the sensors than the AP is. In Section 2.5.4, we will comment on the impact of the noise in the communication links from the sensors to the relay.

With a slight abuse of notation, in the following we will denote a scenario as "coded" only if a block channel code is embedded into the network structure, in order to distinguish it from a scenario with multiple observations (i.e., repetition coded).

Communication Schemes

In a coded scenario with binary phase shift keying (BPSK) and Rayleigh faded links, the observable at the output of the communication channel can be expressed as

$$r_i = f_i(2c_i - 1)\sqrt{E_c} + w_i \qquad i = 1, \ldots, n_{cod} \tag{2.41}$$

where $c_i \in \{0, 1\}$ is the symbol transmitted from either a sensor (c_i is an information bit, $i = 1, \ldots, n$) or the relay (c_i is a parity bit, $i = n + 1, \ldots, n_{cod}$), $\{w_i\}$ are statistically independent AWGN samples with the same distribution $\mathcal{N}(0, N_0/2)$, N_0 being the single-sided noise power spectral density, $E_c \triangleq R_c E_b$ is the energy per coded bit, E_b being the energy per information bit, and f_i is a random variable with Rayleigh distribution—perfectly coherent demodulation is considered. Under the assumptions

of independence between consecutive fading samples (e.g., through the use of channel interleaving) and that $\mathbb{E}[|f_i|^2] = 1$, the BER at the output of the detector at the AP is [122]

$$p^{\text{Rayleigh}} = \frac{1}{2}\left[1 - \sqrt{\frac{R_c \gamma_b}{1 + R_c \gamma_b}}\right] \qquad (2.42)$$

$\gamma_b \triangleq E_b/N_0$ is the SNR at the AP. A scenario with AWGN communication links can be modeled using (2.41), by imposing $f_i = 1$ ($i = 1, \ldots, n_{\text{cod}}$). In this case, the bit error rate (BER) at the output of the detector at the AP can be written as [122]

$$p^{\text{AWGN}} = Q\left(\sqrt{2R_c \gamma_b}\right). \qquad (2.43)$$

In general, one can denote as p the BER at the output of the detector, where p has a specific expression (either (2.43) or (2.42)), depending on the communication channel and the detection strategy. For simplicity, we assume that p is the same for all sensor-AP links.

In all above communication schemes, the probability of decision error at the AP can be evaluated by computing the conditional probabilities $P(\widehat{H} = H_i | H = H_j)$ in (2.5) ($i, j = 0, 1$, $i \neq j$). These values depend on the presence/absence of channel coding and on the detection/decoding/fusion strategy at the AP, as will be described in the following sections, distinguishing on the basis of the observations at the sensors.

2.5.2   Ideal Observations at the Sensors

In order to obtain performance benchmarks, we first consider scenarios where the spatially constant phenomenon H is detected by the sensors ideally. In this case, we distinguish between AP structures where the decoding and fusion operations are either separate or joint.

Separate Decoding and Fusion

When the decoding and fusion operations are separate, assuming majority-like fusion the conditional probabilities at the right-hand side of (2.5) can be computed as

follows:

$$P(\widehat{H} = H_1 | H = H_0) \;=\; \sum_{i=k}^{n} \binom{n}{i} (p_{\mathrm{ch}}^{\mathrm{ideal}})^i (1 - p_{\mathrm{ch}}^{\mathrm{ideal}})^{n-i} \tag{2.44}$$

$$P(\widehat{H} = H_0 | H = H_1) \;=\; \sum_{i=0}^{k-1} \binom{n}{i} (1 - p_{\mathrm{ch}}^{\mathrm{ideal}})^i (p_{\mathrm{ch}}^{\mathrm{ideal}})^{n-i} \tag{2.45}$$

where the repeated trials formula has been used [94], k (i.e., the majority decision threshold) is $\lfloor \frac{n}{2} \rfloor + 1$, and the probability $p_{\mathrm{ch}}^{\mathrm{ideal}}$ depends on the noisy communication link model and the specific distributed channel coding strategy. Note that the upper index of the sum in (2.44) is n (and not n_{cod}) also in coded scenarios, since the information from the relay (i.e., the parity bits) is not used in the *fusion* process (only the systematic bits are used). The parity bits are used only in the *detection/decoding* process.

Since the local sensors' decisions are error-free, $p_{\mathrm{ch}}^{\mathrm{ideal}}$ and $1 - p_{\mathrm{ch}}^{\mathrm{ideal}}$ in (2.44) and (2.45) correspond to the probabilities of error and correct decision at the detector output, respectively. In an "uncoded scenario" (i.e., $n_{\mathrm{cod}} = n$), it holds that $p_{\mathrm{ch}}^{\mathrm{ideal}} = p$. In a scenario with multiple observations, the AP preliminary decides for the phenomenon status at each sensor through a majority fusion rule over the M consecutive decisions sent by that sensor. In this case, $p_{\mathrm{ch}}^{\mathrm{ideal}}$ can be expressed, similarly to (2.44), as

$$p_{\mathrm{ch}}^{\mathrm{ideal}} = \sum_{i=k_{\mathrm{NC}}}^{M} \binom{M}{i} p^i (1 - p)^{M-i} \tag{2.46}$$

where $k_{\mathrm{NC}} \triangleq \lfloor \frac{M}{2} \rfloor + 1$. In a coded scenario and for sufficiently small values of p, the following approximation holds [121]:

$$p_{\mathrm{ch}}^{\mathrm{ideal}} \simeq \binom{n_{\mathrm{cod}} - 1}{t} p^{t+1}$$

where $t = (d_{\min} - 1)/2$ is the number of errors which can be corrected by a code with minimum distance $d_{\min}$ [121, 123]. We point out that, provided that $1/M = n/n_{\mathrm{cod}}$, the comparison between coded schemes and schemes with multiple observations is consistent from an energetic viewpoint.

Joint Decoding and Fusion

In a scenario with multiple (M) independent observations at the sensors, joining the decoding and fusion operations consists in adopting a majority fusion rule over all the $n \times M$ bits sent from the sensors to the AP. In this case, the probability of decision error becomes

$$P_{\text{e}}^{\text{mult.obs.}} = \frac{1}{2} \left[\sum_{i=k_{\text{M}}}^{n \times M} \binom{n \times M}{i} p^i (1-p)^{n \times M - i} + \sum_{i=0}^{k_{\text{M}}-1} \binom{n \times M}{i} (1-p)^i p^{n \times M - i} \right]$$

(2.47)

where $k_{\text{M}} \triangleq \lfloor \frac{n \times M}{2} \rfloor + 1$ is the majority decision threshold.

In a coded scenario, the receiver with joint decoding and fusion can be designed as follows. Since the considered sensor networks embed *systematic* codes, we denote as $[u_1^{(j)}, \ldots, u_n^{(j)}, b_1^{(j)}, \ldots, b_{n_{\text{cod}}-n}^{(j)}]$ ($j = 0, 1$) the entire sequence of bits transmitted by the sensors ($u_i^{(j)}$ from sensor i) and the relay ($\{b_i\}_{i=1}^{n_{\text{cod}}-n}$ from the relay) in correspondence to the phenomenon status H_j. Note that in the current case with a spatially constant binary phenomenon and ideal observations at the sensors, $(u_1, \ldots, u_n)$ is either $(0, \ldots, 0)$ or $(1, \ldots, 1)$. In other words, in the presence of *ideal* observations, only two codewords, denoted as $\boldsymbol{c}^{(0)}$ and $\boldsymbol{c}^{(1)}$, are allowed—this does not hold with noisy observations, as will be shown in Section 2.5.3. In particular, $\boldsymbol{c}^{(0)} = (0, \ldots, 0)$. In all cases considered in this section, it will also hold that $\boldsymbol{c}^{(1)} = (1, \ldots, 1)$.

Given that decoding and fusion are joint, two possible detection strategies at the AP can be devised:

- hard-output detection is followed by (hard-input) joint decoding/fusion;

- detection, decoding, and fusion are all joined together.

In the former case, the maximum a posteriori probability (MAP) joint decoding/fusion strategy can be formalized as

$$\widehat{H} = \underset{j=0,1}{\text{argmax}}\, P\left(\boldsymbol{c}^{(j)} | \boldsymbol{c}_{\text{rx}}\right) = \underset{j=0,1}{\text{argmax}}\, P\left(\boldsymbol{c}_{\text{rx}} | \boldsymbol{c}^{(j)}\right) P(\boldsymbol{c}^{(j)})$$

(2.48)

where $\boldsymbol{c}_{\text{rx}}$ is the codeword at the output of the detector at the AP. Since only two codewords $\boldsymbol{c}^{(0)}$ and $\boldsymbol{c}^{(1)}$ are used, the a priori probability of the sequence $\boldsymbol{c}^{(j)}$ is equal

to the a priori probability of the phenomenon status H_j, i.e., $P(\boldsymbol{c}^{(j)}) = p_j = 1/2$. Owing to the independence of the communication channels (conditionally on the transmitted bits), the MAP decoding/fusion strategy in (2.48) can be rewritten as

$$\widehat{H} = \underset{j=0,1}{\operatorname{argmax}} \, p_j \prod_{i=1}^{n_{\text{cod}}} P\left(c_{i,\text{rx}} | c_i^{(j)}\right). \tag{2.49}$$

After a few manipulations, the MAP decoding/fusion strategy in (2.49) can be finally formulated as

$$\left(\frac{1-p}{p}\right)^{2\vartheta(1,\boldsymbol{c}_{\text{rx}})-n_{\text{cod}}} \underset{H_1}{\overset{H_0}{\gtrless}} 1. \tag{2.50}$$

where $\vartheta(1,\boldsymbol{c}_{\text{rx}})$ is the number of 0's in $\boldsymbol{c}_{\text{rx}}$.

At this point, one can evaluate the probability of decision error in (2.5). In particular, the terms $\left\{P(\widehat{H} = H_i | H = H_j)\right\}$ ($i, j = 0, 1, i \neq j$) can be computed from the decision rule (2.50). After a few manipulations, one obtains:

$$P_{\text{e}} = \frac{1}{2}\left[\sum_{k=k^*}^{n_{\text{cod}}} \binom{n_{\text{cod}}}{k} p^k (1-p)^{n_{\text{cod}}-k} + \sum_{k=0}^{k^*-1} \binom{n_{\text{cod}}}{k} (1-p)^k p^{n_{\text{cod}}-k}\right]$$

where we have used the fact that $\vartheta(1,\boldsymbol{c}_{\text{rx}})$ is a binomial random variable with parameters n_{cod} and p, $\boldsymbol{c}^{(1)} = \boldsymbol{1}$, and k^* is defined as follows:

$$k^* = \min\{1,\ldots,n_{\text{cod}}\}$$
$$\text{s.t.} \; \left(\frac{1-p}{p}\right)^{2k^*-n_{\text{cod}}} > 1.$$

In the case with joint detection/decoding/fusion, we first consider a scenario with Rayleigh faded links, and we denote by $\boldsymbol{f} = [f_1,\ldots,f_{n_{\text{cod}}}]$ the fading samples and by $\boldsymbol{r} = [r_1,\ldots,r_{n_{\text{cod}}}]$ the observables at the output of the communication links. Under the assumption of perfect channel state information at the AP, the MAP detection/decoding/fusion strategy can be formulated as[10] [123]

$$\widehat{H} = \underset{j=0,1}{\operatorname{argmax}} \, p\left(\boldsymbol{r}|\boldsymbol{c}^{(j)},\boldsymbol{f}\right) P\left(\boldsymbol{c}^{(j)}|\boldsymbol{f}\right) = \underset{j=0,1}{\operatorname{argmax}} \, p_j \prod_{i=1}^{n_{\text{cod}}} p\left(r_i|c_i^{(j)},f_i\right) \tag{2.51}$$

---

[10]In (2.51) and in the remainder of this section, the uppercase P is used to denote the probability of an event, whereas the lowercase p is used to denote the conditional probability density function (PDF) of a random variable.

where we have used the facts that the observables are conditionally independent given $\{c_i^{(j)}\}$ and the coded bit $c_i^{(j)}$ is independent of the fading sample f_i. Discarding $p_j = 1/2$, from (2.51) one can derive, after a few manipulations, the following decision rule:

$$\sum_{i=1}^{n_{\text{cod}}} r_i f_i c_i^{(1)} \underset{H_0}{\overset{H_1}{\gtrless}} 0. \tag{2.52}$$

On the basis of (2.52) and recalling that a linear combination of Gaussian random variables is still a Gaussian random variable [94], after a few manipulations the probability of decision error at the AP (2.5) becomes

$$P_{\text{e}} = \frac{1}{2}\left[Q\left(2\frac{\sqrt{R_{\text{c}}E_{\text{b}}}\sum_{i=1}^{n_{\text{cod}}} f_i c_i^{(1)}}{\sqrt{N_0 \sum_{i=1}^{n_{\text{cod}}} f_i^2 (c_i^{(1)})^2}} \right) + \Phi\left(-2\frac{\sqrt{R_{\text{c}}E_{\text{b}}}\sum_{i=1}^{n_{\text{cod}}} f_i(2c_i^{(1)}-1)c_i^{(1)}}{\sqrt{N_0 \sum_{i=1}^{n_{\text{cod}}} f_i^2 (c_i^{(1)})^2}} \right) \right]$$
$$\tag{2.53}$$

where $\Phi(x) \triangleq 1 - Q(x)$. Observe that (2.53) depends on the particular sequence of fading samples $\{f_i\}$.

An expression for the probability of decision error in the case with AWGN links can be directly obtained from (2.53) by imposing $f_i = 1$ $(i = 1, \ldots, n_{\text{cod}})$. In particular, in the presence of a code with $c^{(1)} = 1$ (recall that, in all cases, $c^{(0)} = 0$) it can be shown that

$$P_{\text{e}} = Q\left(\sqrt{2n_{\text{cod}}R_{\text{c}}\gamma_{\text{b}}} \right) = Q\left(\sqrt{2n\gamma_{\text{b}}} \right).$$

2.5.3 Noisy Observations at the Sensors

We now extend the derivation presented in Section 2.5.2 to encompass the presence of observation noise.

Separate Decoding and Fusion

In the case with separate decoding and fusion, only the expressions of the probabilities $p_{\text{ch}}^{\text{ideal}}$ in (2.44) and (2.45) need to be modified. In particular, by using the total

probability theorem [94], one can write

$$
\begin{aligned}
p_{\text{ch}}^{\text{noisy}} &= P(c_{i,\text{rx}} = 1|H_\ell) && i = 1,\dots,n \\
&= p_{\text{ch}}^{\text{ideal}}[1 - Q(\tau - s \cdot \ell)] + (1 - p_{\text{ch}}^{\text{ideal}})Q(\tau - s \cdot \ell)
\end{aligned}
$$

where the sensors' decisions $\{c_i^{(\ell)}\}$ are done as outlined in Section 2.2.1 and $p_{\text{ch}}^{\text{ideal}}$ is the final BER, which depends on the presence/absence of distributed channel coding, as shown in Section 2.5.2.

In a scenario with M observations at each sensor, expression (2.46) for $p_{\text{ch}}^{\text{ideal}}$ has to be similarly modified. In particular, one obtains:

$$
p_{\text{ch}}^{\text{noisy}} = \sum_{i=k_{\text{NC}}}^{M} \binom{M}{i} [g(p,\ell)]^i [1 - g(p,\ell)]^{M-i} \tag{2.54}
$$

where $g(p,\ell) \triangleq p[1 - Q(\tau - s \cdot \ell)] + (1 - p)Q(\tau - s \cdot \ell)$.

Joint Decoding and Fusion

In the case with hard-output detection followed by joint decoding/fusion, expression (2.48) for the phenomenon estimate in a scenario with multiple observations at the sensors has to be modified, similarly to (2.54), as follows:

$$
\begin{aligned}
P_{\text{e,noisy}}^{\text{mult.obs.}} &= \frac{1}{2}\sum_{i=k_{\text{M}}}^{n \times M} \binom{n \times M}{i} [g(p,1)]^i [1 - g(p,1)]^{n \times M - i} \\
&\quad + \frac{1}{2}\sum_{i=0}^{k_{\text{M}}-1} \binom{n \times M}{i} [1 - g(p,0)]^i [g(p,0)]^{n \times M - i}.
\end{aligned}
$$

We now derive the MAP decoding/fusion strategy for the coded scenarios in the presence of noisy observations at the sensors. In the case with hard-output detection followed by (hard-input) joint decoding/fusion, in order to take into account the observation noise statistics expression (2.48) has to be modified as follows:

$$
\widehat{H} = \operatorname*{argmax}_{j=0,1} P(H_j|\boldsymbol{c}_{\text{rx}}) = \operatorname*{argmax}_{j=0,1} \prod_{i=1}^{n_{\text{cod}}} P(c_{i,\text{rx}}|H_j) \tag{2.55}
$$

where the irrelevant term $P(H_j) = p_j = 1/2$ has been discarded and the probability $P(c_{i,\text{rx}}|H_j)$ can be written, after a few manipulations, as

$$P(c_{i,\text{rx}}|H_j) = \begin{cases} (1-p)[1-Q(\tau - s \cdot j)] + pQ(\tau - s \cdot j) & \text{if } c_{i,\text{rx}} = 0 \\ p[1-Q(\tau - s \cdot j)] + (1-p)Q(\tau - s \cdot j) & \text{if } c_{i,\text{rx}} = 1. \end{cases}$$

In a coded scenario with joint detection/decoding/fusion, the MAP estimation strategy (2.51) has to be modified as follows:

$$\widehat{H} = \underset{j=0,1}{\operatorname{argmax}} \prod_{i=1}^{n_{\text{cod}}} P(r_i|H_j, f_i)$$

which can be rewritten, after a few manipulations, as

$$\frac{\prod_{i=1}^{n_{\text{cod}}} \Upsilon(0, r_i, f_i)}{\prod_{i=1}^{n_{\text{cod}}} \Upsilon(1, r_i, f_i)} \underset{H_1}{\overset{H_0}{\underset{<}{>}}} 1$$

where

$$\Upsilon(m, r_i, f_i) \triangleq \Phi(\tau - m \cdot s) \exp\left(-2\frac{r_i f_i \sqrt{E_c}}{N_0}\right) + [1 - \Phi(\tau - m \cdot s)] \exp\left(2\frac{r_i f_i \sqrt{E_c}}{N_0}\right).$$

2.5.4   Impact of Noisy Communication Links Towards the Relay

The previous derivations in coded scenarios are based on the assumption of ideal communication links between the sensors and the relay. In this section, we briefly discuss on the impact of *noisy* communication links between the sensors and the relay. No analytical derivation nor numerical results will be presented. The considerations which will be carried out are simply meant to give some guidelines on the benefits brought by the distributed use of properly designed block error correction codes.

We first consider the case with *ideal* observations at the sensors. In Figure 2.29, we give a pictorial description of how the communication noise influences data transmission to the relay. As previously seen, two possible codewords are selected at the sensors and relay, namely $c^{(0)}$ and $c^{(1)}$, which are shown, in Figure 2.29, as a filled circle and an empty circle, respectively.
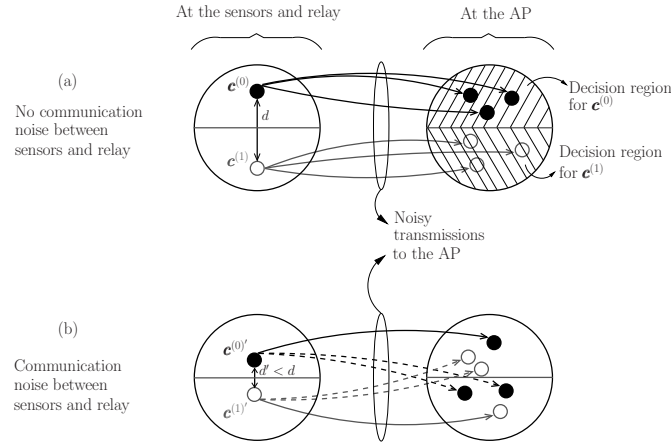
Figure 2.29: Codebook perspective on the considered distributed detection schemes: (a) ideal commnunication links between sensors and relay and (b) noisy communication links. In each case, on the left the two possible codewords at sensors and relay are shown, whereas on the right possible received words at the AP are shown.

- In the scenario with no communication noise between the sensors and the relay (case (a)), we denote the Hamming distance between the two codewords as d. If $\boldsymbol{c}^{(0)} = \boldsymbol{0}$ and $\boldsymbol{c}^{(1)} = \boldsymbol{1}$, then $d = n_{\text{cod}}$. The presence of noisy communication links from the sensors and the relay to the AP is such that the word $\boldsymbol{c}_{\text{rx}}$ (one of the $2^{n_{\text{cod}}}$ possible binary sequences of length n_{cod}) received at the AP may be different from the codeword transmitted by the sensors and the relay. In particular, $\boldsymbol{c}_{\text{rx}}$ may not even be a codeword. Decoding and fusion at the AP corresponds to associating the received word to one of the information sequences $\boldsymbol{0}$ or $\boldsymbol{1}$. It is intuitive that the larger is d, the more robust is the system against communication noise in the links to the AP.

- In the presence of communication noise between the sensors and the relay (case b), the latter may receive a sequence of bits which differs from that sent by the sensors. Therefore, the parity bits generated by the relay may lead to the association of H_0 and H_1 to two codewords $\boldsymbol{c}^{(0)'}$ and $\boldsymbol{c}^{(1)'}$ which are at a distance

$d' < d$. As a consequence of this decreased distance, the system performance will be worse than in the previous scenario, since the probability of associating (through decoding and fusion) the received word to the wrong phenomenon status will increase. This can be understood from the codebook scenario at the AP, where the received word at the AP might belong to the portion of the signal space which is associated (by decoding and fusion) to the wrong phenomenon status.

The presence of *noisy* observations may lead to the association of the phenomenon statuses H_0 and H_1 to two codewords $c^{(0)''}$ and $c^{(1)''}$ at a distance smaller than d. In particular, in the presence of both (i) observation noise and (ii) communication noise from the sensors to the relay, when the intensities of these two noises are sufficiently small, their negative effects tend to add, so that the distance d'' between $c^{(0)''}$ and $c^{(1)''}$ might be even smaller than d'.

Obviously, an open problem is to quantify precisely the decrease of the error correction capability t of the code in the presence of noisy communication links between the sensors and the relay. In fact, the parameter t depends on the particular structure (codebook) of the considered error correction code. An interesting research direction is the design of robust (fault tolerant) error correcting codes for the proposed distributed detection schemes.

2.5.5   Numerical Results

We resort to Monte Carlo simulations to evaluate the probability of decision error with the devised MAP detection/decoding/fusion strategies presented in Section 2.5.2 and Section 2.5.3.

In order to make the detection/decoding process at the input of the AP more effective, *soft-input* decoding/fusion (either separate or joint), rather than hard-input decoding/fusion, can be considered. In Figure 2.30, the probability of decision error is shown, as a function of the SNR at the AP, in a scenario with $n = 16$ sensors, AWGN communication links (similar results can be obtained in scenarios with Rayleigh faded communication links), and *error-free* observations at the sensors. Six coding

Figure 2.30: Probability of decision error, as a function of the SNR at the AP, in a scenario with $n = 16$ sensors, AWGN communication links, and *error-free* phenomenon observations. Various coding strategies are considered.

strategies are considered: (i) uncoded, (ii) (31,16) BCH [123, p. 438] (the corresponding BCH code has $t = 3$)[11] coded with hard-input and separate decoding/fusion, (iii) (31,16) BCH coded with soft-input and joint decoding/fusion, (iv) with $M = 2$ observations and joint decoding/fusion, (v) with $M = 3$ observations and separate decoding/fusion, and (vi) with $M = 3$ observations and joint decoding/fusion. One can observe that the probability of decision error in coded scenarios shows a "waterfall" behavior, which is due to the concatenation of the decoding and fusion operations. However, the improvement brought by the presence of distributed channel coding, with respect to schemes with multiple observations, becomes apparent at very low probabilities of decision error, which may not be of practical interest One can observe that the coded network with soft-input and joint decoding/fusion at the AP has a performance significantly better than that associated with the schemes with hard-input and separate decoding/fusion. This is to be expected, since in a scenario with

_____

[11]We remark that the BCH is one of the block channel codes that it is possible to consider. However, the same results would be asymptotically obtained with any code with $t = 3$.
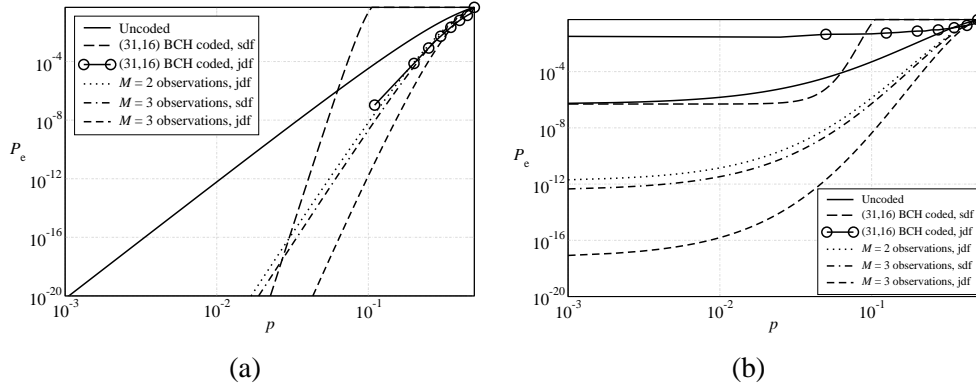
Figure 2.31: Probability of decision error, as a function of the BER p at the output of he detector, in a scenario with $n = 16$ sensors and *noisy* phenomenon observations. Two values for the observation SNR are considered: (a) 20 dB and (b) 10 dB. Various sensor network architectures are considered.

soft-input decoding no information is lost upon reception of the observables from the communication links. Note, however, that in this case as well the proposed coded scheme outperforms a scheme with multiple observations only at very low values of the probability of decision error.

In Figure 2.31, the probability of decision error is shown, as a function of the BER p at the output of the AP detector, in a scenario with $n = 16$ sensors and *noisy* phenomenon observations. Two values for the observation SNR are considered: (a) 20 dB and (b) 10 dB. The performance is evaluated with six sensor network architectures: (i) uncoded, (ii) (31,16) BCH coded with separate decoding/fusion, (iii) (31,16) BCH coded with joint decoding/fusion, (iv) with $M = 2$ observations and joint decoding/fusion, (v) with $M = 3$ observations and separate decoding/fusion, and (vi) with $M = 3$ observations and joint decoding/fusion. In the case with high observation SNR (e.g., in Figure 2.31 (a)), the phenomenon observations at the sensors are practically error-free and, therefore, the network performance is similar to that in Figure 2.30. When the observation SNR decreases (e.g., in Figure 2.31 (b)), instead, the proposed detection/decoding/fusion strategies are not effective, since the quality of the sensors'

observations heavily affects the system performance, and this is more pronounced in the presence of joint decoding/fusion. One can observe that the probability of decision error curve reaches a floor, due to the observation noise (which is independent of the communication noise). As before, the schemes with multiple observations at the sensors outperform those with block channel coding.

Finally, we investigate the performance of the proposed distributed schemes in *large scale* sensor networks, by using an LDPC code and the sum-product (SP) decoding algorithm. In particular, we consider a (3,6) regular and systematic LDPC code: the systematic bits of the codeword correspond to the n decisions sent by the sensors, whereas the $n_{\text{cod}} - n$ parity bits are generated by the relay node. The LDPC code is constructed in a *random* fashion, according to an algorithm, which exploits an idea similar to the progressive edge growth (PEG) algorithm presented in [124]. In Figure 2.32, the probability of decision error is shown, as a function of the SNR at the AP, in a scenario with $n = 100$ sensors, AWGN communication links, and *noisy* phenomenon observations. Three sensor network architectures are considered: (i) LDPC coded with standard SP decoding [1, 125], (ii) LDPC coded with *enhanced* (as described in the following) channel log-likelihood ratios (LLRs), and (iii) with $M = 2$ observations and separate decoding/fusion. Two values for the observation SNR are considered: (i) 10 dB (dashed lines) and (ii) 20 dB (solid lines). While in the LDPC coded case with standard SP decoding the channel LLRs (input at the variable nodes of the LDPC bipartite graph) do not take into account the observation noise, in the enhanced SP decoding case the channel LLRs are modified by properly taking into account the observation noise. The modified channel LLRs can be expressed as follows:

$$\mathscr{L}^{(i)}_{\text{ch-enhanced}} = \mathscr{L}_{\text{ch}} + \mathscr{L}^{(i)}_{\text{a-priori}} \qquad i = 1, \ldots, n_{\text{cod}}$$

where

$$\mathscr{L}_{\text{ch}} \triangleq \ln \frac{p(r_i | c_i = 0)}{p(r_i | c_i = 1)} = \frac{r_i}{N_0}$$

and

$$\mathscr{L}^{(i)}_{\text{a-priori}} \triangleq \ln \frac{P(c_i = 0)}{P(c_i = 1)} = \begin{cases} \ln \frac{\Upsilon(0, -r_i, 1)}{\Upsilon(1, -r_i, 1)} & \text{if } i = 1, \ldots, n \\ 0 & \text{if } i = n+1, \ldots, n_{\text{cod}} \end{cases}$$
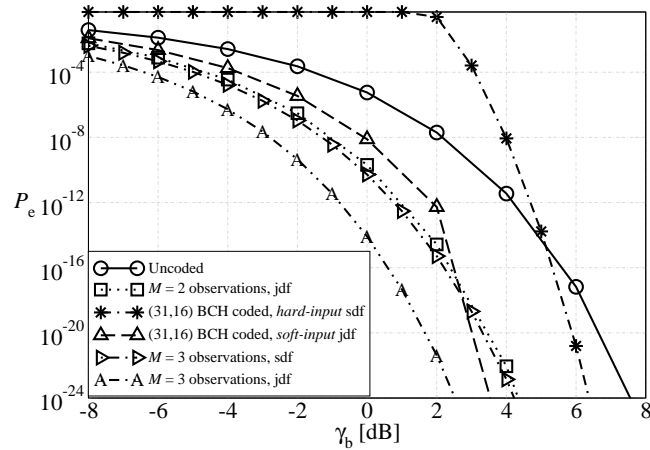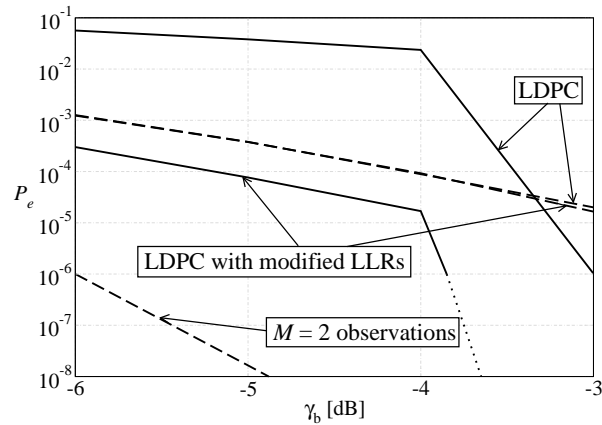
Figure 2.32: Probability of decision error, as a function of the SNR at the AP, in a scenario with $n = 100$ sensors, AWGN communication links, and *noisy* phenomenon observations. Two values for the observation SNR are considered: (i) 10 dB (dashed lines) and (ii) 20 dB (solid lines). Various sensor network architectures are considered.

where Υ has been defined in Section 2.5.3. From the results in Figure 2.32, one can observe that the use of multiple observations is still the winning strategy also in a large-scale sensor network.[12] However, the enhanced LPDC coded scheme (with modified channel LLRs) outperforms the LDPC coded scheme at large observation SNRs, since a statistical knowledge of the observation noise helps the decoding process. In fact, when the communication noise level is too high, a communication error might compensate an error in the phenomenon estimation at the sensors (due to a too high observation noise level). On the other hand, when the communication links to the AP are reliable (i.e., the communication noise is sufficiently small) an error in the phenomenon estimation might not be compensated and, therefore, the AP might not be able to correctly reconstruct the phenomenon status. Finally, note that in the standard LDPC coded case the performance with an observation SNR equal to 10 dB

---

[12]Note that in Figure 2.32 only the curve with observation SNR equal to 10 dB is shown in the case with multiple observations. The curve associated with an observation SNR equal to 20 dB and multiple observations is even lower.

is better than that associated with an observation SNR equal to 20 dB when the SNR at the AP is sufficiently low. This is due to the fact that for small values of the observation SNR a larger number of codewords is actually used by the sensor network and, consequently, the error correction capabilities of the LDPC code are better exploited. However, when the SNR at the AP increases, the "beneficial" impact of the observation noise is reduced by the presence of reliable communication links.

2.6   Concluding Remarks

In this chapter, we have characterized the performance of sensor networks where a spatially constant phenomenon is under observation. First, we have characterized the behavior of clustered sensor networks with distributed detection in the presence of multi-level majority-like information fusion. Upon the derivation of a communication-theoretic analytical framework, we have shown that, in the considered scenarios, uniform clustering, i.e., balanced tree network architectures, leads to a lower probability of decision error than non-uniform clustering, i.e., unbalanced tree network architectures. In the former case, the probability of decision error depends *only* on the number of decision levels and *not* on the specific clustering configuration. An information-theoretic perspective has also been presented. Then, the impact of noisy communication links has then been investigated. Our results show that the presence of noise in the communication links has a strong bearing on the ultimate achievable performance.

Then, an analytical framework to compute the *network lifetime* of clustered sensor networks subject to a physical layer-oriented QoS condition has been derived. In the presence of ideal reclustering, the network lifetime is the longest possible. On the other hand, in the presence of a fixed clustered configuration, our results show that the number of clusters has a strong impact on the network lifetime. More precisely, the network lifetime is maximized if there are a *few large clusters* (at most four). In all cases, the QoS condition has a strong impact on the network lifetime: the more stringent is this condition, the shorter is the network lifetime. We have also evaluated the cost associated with the reclustering procedure, from both *time delay* and *energy*

consumption perspectives. Our results show that reclustering is not useful when phenomenon observations are *rare*, since the network spends more time in transferring control messages than useful data. The impact of noisy communication links, modeled as BSCs, on the network lifetime has also been investigated, showing that the higher is the noise level, the shorter is the network lifetime. However, in this scenario as well reclustering can prolong the network lifetime.

Although the previous analysis was based on the assumption of constant sensor SNR across the sensors, we have proposed an analytical framework to take into account different observation SNRs not known at the AP. In order to model this scenario, four possible sensor SNR profiles (linear, quadratic, cubic, and hyperbolic) have been introduced and we have characterized them by using a *slope coefficient* and the *maximum sensor SNR*. For increasing steepness of the (ordered) sensor SNR profile, i.e., for an increasingly irregular realistic sensor SNR profile, the best performance is obtained by selecting a lower and lower number of sensors (those with highest SNRs). In a scenario with common *average* sensor SNR, the profile which guarantees the best performance is the *cubic*. This is due to the fact that it corresponds to the profile with the largest (in relative terms) number of sensors with SNR higher than the average value. Therefore, a general conclusion is that, for a given *average sensor SNR*, the best performance is obtained when the variance of the sensor SNR is large, i.e., the sensor SNR profile is irregular. The presence of noisy communication links has also been considered. In this case, we have shown that the more irregular is the sensor SNR profile, the milder is the impact of the noise level in the communication links.

The analytical framework has been enriched with simulation and experimental results (in terms of probability of decision error, throughput, and delay) relative to Zigbee and IEEE 802.15.4-based clustered sensor networks with information fusion. The obtained results confirm the validity of our analytical framework in realistic networking scenarios. Moreover, it has been possible to characterize realistic SNR profiles.

Finally, we have studied how to combine detection, decoding, and fusion at the AP in sensor networks for distributed detection of a spatially constant binary phe-

nomenon. To this end, we have embedded simple distributed channel codes (either block or repetition) into sensor network architectures. The performance of the proposed schemes has been analyzed in scenarios with noisy observations and communications. In all cases, the use of *multiple observations* (i.e., repetition coding) guarantees the best performance, with respect to simple systematic block coding strategies, for practical values of the probability of decision error. This leaves the design of powerful distributed channel codes an open problem. Considering scenarios with distributed LDPC coding, our results show that knowledge, at the AP, of the observation noise can significantly improve the decoding process, i.e., it can help in reducing the negative effects of the communication noise.

Chapter 3

Distributed Detection of Spatially Non-Constant Phenomena

3.1 Introduction

In this chapter, we study sensor networks with distributed detection of a *spatially non-constant* phenomenon. In particular, we consider *binary* phenomena characterized by a generic number of status changes (from state "0" to state "1" or vice-versa) across the sensors. We first derive the MMSE fusion algorithm at the AP. Then, we propose simplified (sub-optimum) fusion algorithms at the AP, with a lower computational complexity. While we first consider a scenario with *ideal* communication links between the sensors and the AP, we then extend our framework to scenarios with *noisy* communication links.

The structure of this chapter is the following. In Section 3.2, we derive MMSE and simplified fusion rules at the AP in a scenario with ideal communication links and both single and multi-boundary phenomena. In Section 3.3, we extend the previous fusion rules by taking into account the noise in the communication links between the sensors and the AP. In Section 3.4, numerical results on the performance of the proposed fusion algorithms are presented. In Section 3.5, the computational complexity of the proposed algorithms, in terms of the number of required operations, is

presented. Finally, concluding remarks are given in Section 3.6.

3.2   Ideal Communication Links

In this section, we focus on a network scenario where the status of the phenome-
non under observation is characterized by a *generic* and *a priori known* number
n_{bs} of boundaries. For the ease of simplicity, the status of the phenomenon will be
supposed independent from sensor to sensor. The existence of *correlation* between
sensors would require an extension of the derived algorithms. This extension is in-
vestigated in Chapter 4. Moreover, the proposed simplified algorithms do not require
the knowledge of a possible correlation among the sensors. In particular, we prelimi-
nary investigate the performance when the communication links between the sensors
and the AP are *ideal*, i.e., no noise is introduced during data transmission.

Denote the overall phenomenon status as $\boldsymbol{H} = [H_1, \ldots, H_n]$ with $H_i = H_0$ or $H_i =
H_1$ ($i = 1, \ldots, n$). For the ease of simplicity, we suppose that $H_0 = 0$ and $H_1 = 1$. As
in Chapter 2, the signal observed at the i-th sensor can be expressed, according to the
observable model in (2.1), as

$$r_i = c_{\mathrm{E},i} + n_i \qquad i = 1, \ldots, n$$

and the common SNR at the sensors can be defined as follows:

$$\mathrm{SNR}_{\mathrm{sensor}} = \frac{s^2}{\sigma^2}.$$

Each sensor processes (through proper quantization) the observed signal and the
value output by the i-th sensor is denoted as $d_i \triangleq f_{\mathrm{quant}}(r_i)$, where the function $f_{\mathrm{quant}}(\cdot)$
depends on the specific quantization strategy. In the following, we consider (1) binary
quantization and (2) absence of quantization. In [126], the proposed analytical frame-
work is extended to scenarios with multi-level quantization at the sensors. Upon the
reception of the messages sent by the sensors, the goal of the AP is to reconstruct,
through an MMSE or simplified fusion strategy, the status of the distributed binary
phenomenon $\boldsymbol{H}$. More precisely, in the considered setting the AP needs to estimate
correctly the position of the boundary.

3.2.1   MMSE Fusion Rule

The following assumptions are expedient to simplify the derivation of the MMSE detection strategy:

- changes of the phenomenon status are not admitted in correspondence to the first and last sensors: the number of boundaries must then be such that $1 \leq n_{bs} \leq n - 2$ (in particular, $H_n = H_{n-1}$);

- the phenomenon status is perfectly known at the first sensor. In particular, we assume $H_1 = 0$.

According to the above assumptions, the n_{bs} boundaries $\{\alpha_1, \ldots, \alpha_{n_{bs}}\}$ have to simultaneously satisfy the following inequalities:

$$2 \leq \alpha_1 < \alpha_2 < \ldots < \alpha_{k-1} < \alpha_k < \ldots < \alpha_{n_{bs}} \leq n - 1. \qquad (3.1)$$

Therefore: between 1 and $\alpha_1 - 1$ the phenomenon status is "0;" between α_1 and $\alpha_2 - 1$ the phenomenon status is "1;" and so on. In order for the boundary distribution to be realistic, the following conditions must necessarily hold:

$$\alpha_{k-1} < \alpha_k \leq (n-1) - (n_{bs} - k) = n - n_{bs} + k - 1 \qquad k = 2, \ldots, n_{bs}. \qquad (3.2)$$

For each value of k, condition (3.2) formalizes the intuitive idea that the k-th boundary cannot fall beyond the $(n - 1 - n_{bs} + k)$-th position, in order for the successive (remaining) $n_{bs} - k$ boundaries to have admissible positions.

Binary Quantization

In this scenario, the i-th sensor makes a decision comparing its observation r_i with a threshold value τ_i, and computes a local binary decision $d_i \in \{0, 1\}$, i.e., $f_{quant}(r_i) = U(r_i - \tau_i)$, where $U(\cdot)$ is the unit step function. To optimize the system performance, the thresholds $\{\tau_i\}$ need to be properly selected. As in a scenario with detection of a spatially constant phenomenon, a common value τ at all sensors is considered. This choice is intuitively motivated by the fact that the sensor SNR is constant across

the sensors. In the presence of a spatially non-constant phenomenon, the threshold τ needs to be optimized in order to minimize the distance between the true phenomenon and its estimate at the AP. Our results in [126] show that the optimized value of τ corresponds to $s/2$, for every value of the number of sensors n.

Denoting as $\boldsymbol{\alpha}$ the sequence of boundaries $(\alpha_1, \ldots, \alpha_{n_{bs}})$, the MMSE fusion strategy can be derived obtaining $\widehat{\boldsymbol{\alpha}} = \mathbb{E}[\boldsymbol{\alpha}|\boldsymbol{d}]$ [127]. Using the assumptions introduced at the beginning of this section, the generic component of the vector $\widehat{\boldsymbol{\alpha}}$ can be written as[1]

$$\widehat{\alpha}_k = \mathbb{E}[\alpha_k|\boldsymbol{d}] = \sum_{\alpha_k=1}^{n} P(\alpha_k|\boldsymbol{d}) = \sum_{\alpha_k=k+1}^{n-n_{bs}+k-1} \alpha_k P(\alpha_k|\boldsymbol{d}) \qquad k = 1, \ldots, n_{bs} \qquad (3.3)$$

where the upper and lower bounds of the sum in the last term are properly modified in order to take into account the constraint (3.2). The computation of (3.3) can be carried out by applying the following approach. The probability $P(\alpha_k|\boldsymbol{d})$ $(k = 1, \ldots, n_{bs})$ can be obtained by marginalizing the joint probabilities of proper boundaries' sequences. By applying the Bayes formula and the total probability theorem [94], after a few manipulations the conditional probability mass function (PMF) of $\boldsymbol{\alpha}$ can be expressed as

$$P(\boldsymbol{\alpha}|\boldsymbol{d}) = P(\boldsymbol{d}|\boldsymbol{\alpha})P(\boldsymbol{\alpha}) \left[\sum_{\alpha_1=2}^{n-n_{bs}} \cdots \sum_{\alpha_k=k+1}^{n-n_{bs}+k-1} \cdots \sum_{\alpha_{n_{bs}}=n_{bs}+1}^{n-1} P(\boldsymbol{d}|\boldsymbol{\alpha})P(\boldsymbol{\alpha}) \right]^{-1} . \qquad (3.4)$$

The first multiplicative term at the right-hand side of (3.4) can be written as

$$P(\boldsymbol{d}|\boldsymbol{\alpha}) = \prod_{i=1}^{n} P(d_i|\boldsymbol{\alpha}) = \prod_{i=1}^{\alpha_1-1} \underbrace{P(d_i|\boldsymbol{\alpha})}_{H_i=0} \prod_{j=\alpha_1}^{\alpha_2-1} \underbrace{P(d_j|\boldsymbol{\alpha})}_{H_j=1} \cdots \prod_{q=\alpha_{n_{bs}}}^{n} \underbrace{P(d_q|\boldsymbol{\alpha})}_{H_q=0 \text{ or } 1} \qquad (3.5)$$

where we have used the fact that the sensors' decisions are conditionally independent. Note that, in the last $n - \alpha_{n_{bs}} + 1$ terms, $H_i = 0$ if n_{bs} is *even*, whereas $H_i = 1$ if n_{bs}

---

[1]For ease of notational simplicity, in (3.3) we use the same symbol α_k to denote both the random variable (in the second term) and its realization (in the third and fourth terms). The same simplified notational approach will be considered in the remainder of Section 3.2.1. The context should eliminate any ambiguity.

is *odd*. The component conditional probabilities at the right-hand side of (3.5) can be written as

$$
P(d_i|\boldsymbol{\alpha}) = \begin{cases}
P\left(n_i \overset{d_i=0}{\underset{d_i=1}{\lessgtr}} \tau \right) & \text{if } i \in \mathscr{I}_0(\boldsymbol{\alpha}) \\[4mm]
P\left(n_i \overset{d_i=0}{\underset{d_i=1}{\lessgtr}} \tau - s \right) & \text{if } i \in \mathscr{I}_1(\boldsymbol{\alpha})
\end{cases}
$$

$$
= \begin{cases}
(1-d_i)\left[1-\Phi\left(\frac{\tau}{\sigma}\right)\right] + d_i\Phi\left(\frac{\tau}{\sigma}\right) & \text{if } i \in \mathscr{I}_0(\boldsymbol{\alpha}) \\[2mm]
(1-d_i)\left[1-\Phi\left(\frac{\tau-s}{\sigma}\right)\right] + d_i\Phi\left(\frac{\tau-s}{\sigma}\right) & \text{if } i \in \mathscr{I}_1(\boldsymbol{\alpha})
\end{cases}
$$

where

$$
\mathscr{I}_\ell(\boldsymbol{\alpha}) \triangleq \{\text{indexes } i \text{ such that } H_i = \ell|\boldsymbol{\alpha}\} \qquad \ell = 0,1
$$

and $\Phi(x)$ has been introduced in (2.53).

The second multiplicative term at the right-hand side of (3.4) can be written, using the chain rule [94], as

$$
P(\boldsymbol{\alpha}) = \prod_{i=1}^{n_{\text{bs}}} P(\alpha_i|\alpha_{i-1},\ldots,\alpha_1) = \prod_{i=2}^{n_{\text{bs}}} P(\alpha_i|\alpha_{i-1})P(\alpha_1) \tag{3.6}
$$

where we have used the fact that the position of the i-th boundary depends only on the position of the (previous) $(i-1)$-th boundary. The multiplicative terms at the right-hand side of (3.6) can be evaluated by observing that each boundary is spatially distributed according to the constraints in (3.2). In particular, by using combinatorics, one obtains

$$
P(\alpha_1) = \frac{1}{n - n_{\text{bs}} + 1}
$$

$$
P(\alpha_k|\alpha_{k-1}) = \frac{1}{n - n_{\text{bs}} + k - \alpha_{k-1}} \qquad k = 2,\ldots,n_{\text{bs}}.
$$

The last term at the right-hand side of (3.4) (i.e., the denominator) can be easily computed by observing that it is composed by terms similar to those evaluated in (3.5) and (3.6).

Finally, the a posteriori probabilities of the boundaries' positions in (3.3) can be obtained by proper marginalization of the joint conditional PMF in (3.4):

$$P(\alpha_k|\boldsymbol{d}) = \sum_{\sim\{\alpha_k\}} P(\alpha_1,\ldots,\alpha_{n_{\mathrm{bs}}}|\boldsymbol{d}) \qquad k = 1,\ldots,n_{\mathrm{bs}}$$

where $\sum_{\sim\{y_i\}} f(y_1,y_2,\ldots,y_n)$ is a short-hand notation for $\sum_{y_1} \cdots \sum_{y_{i-1}} \sum_{y_{i+1}} \cdots \sum_{y_n} f(y_1,y_2,\ldots,y_n)$ [1].

Absence of Quantization

In this case, the observations at the sensors are not quantized and a local likelihood value, such as the conditional probability density function (PDF) of the observable, is transmitted from each sensor to the AP. Obviously, this is not a realistic scenario, since an infinite bandwidth would be required to transmit a PDF value. However, investigating this case allows to derive useful information about the limiting performance of the considered distributed detection schemes, since transmission of the PDF of the observables does not entail any information loss at the sensors. The estimated boundaries can be written, according to the assumptions outlined at the beginning of Section 3.2, as

$$\widehat{\alpha}_k = \mathbb{E}\left[\alpha_k|\boldsymbol{r}\right] = \sum_{\alpha_k=k+1}^{n-n_{\mathrm{bs}}+k-1} \alpha_k P\left(\alpha_k|\boldsymbol{r}\right) \qquad k = 1,\ldots,n_{\mathrm{bs}}. \tag{3.7}$$

The probabilities in (3.7) can be obtained, as in Section 3.2.1, through proper marginalization of joint conditional probabilities of the following type:

$$P(\boldsymbol{\alpha}|\boldsymbol{r}) = p(\boldsymbol{r}|\boldsymbol{\alpha})P(\boldsymbol{\alpha}) \cdot \left[\sum_{\alpha_1=2}^{n-n_{\mathrm{bs}}} \cdots \sum_{\alpha_i+1}^{n-n_{\mathrm{bs}}+i-1} \cdots \sum_{\alpha_{n_{\mathrm{bs}}}=\alpha_{n_{\mathrm{bs}}-1}+1}^{n-1} p(\boldsymbol{r}|\boldsymbol{\alpha})P(\boldsymbol{\alpha})\right]^{-1}.$$

Under the assumption of independent sensors' observations, it holds that

$$p(\boldsymbol{r}|\boldsymbol{\alpha}) = \prod_{i=1}^{n} p(r_i|\boldsymbol{\alpha})$$

where

$$p(r_i|\boldsymbol{\alpha}) = \begin{cases} p_{\mathscr{N}}(r_i) & \text{if } i \in \mathscr{I}_0(\boldsymbol{\alpha}) \\ p_{\mathscr{N}}(r_i - s) & \text{if } i \in \mathscr{I}_1(\boldsymbol{\alpha}) \end{cases} \qquad (3.8)$$

and $p_{\mathscr{N}}(u) \triangleq \frac{1}{\sqrt{2\pi\sigma^2}} \exp(-\frac{u^2}{2\sigma^2})$.

3.2.2 Simplified Fusion Rule with a Single Boundary

Since the computational complexity of the MMSE fusion strategy rapidly increases with the number of sensors [58], in this section we derive, under the assumption of single boundary phenomena, a simplified low-complexity fusion algorithm. The key idea of this simplified algorithm consists in approximating the MMSE boundary estimate $\widehat{\alpha} = \mathbb{E}[\alpha|\boldsymbol{d}]$, which involves a *statistical* average, with a simpler *deterministic* expression. Note that the proposed approach relies on the fact that our goal is to estimate a *single* boundary.

Binary Quantization

In this case, the boundary position is estimated as follows:

$$\widehat{\alpha} \simeq \underset{1 \le j \le n}{\operatorname{argmin}} \left\{ \sum_{i=1}^{j-1} |d_i|^2 + \sum_{i=j}^{n} |d_i - 1|^2 \right\}. \qquad (3.9)$$

The intuition behind the estimation strategy in (3.9) is based on the fact that there is a single boundary: the initial sensors' decisions (from the 1-st to the $(j-1)$-th sensor) are compared with "0," whereas the others (from the j-th to the n-th sensor) are compared with "1." The estimated boundary minimizes the simplified cost function $|\boldsymbol{d} - \boldsymbol{d}_j|^2$, where $\boldsymbol{d}_j \triangleq [0, \ldots, 0, \underbrace{1}_{j\text{th position}}, \ldots, 1]$, over all possible values of $j \in \{1, \ldots, n\}$.

Absence of Quantization

In this scenario, the *a posteriori* probabilities of the two hypotheses at each sensor, conditionally on the observables, can be used to derive the proper objective function

to be maximized. In this case, one can write[2]

$$\widehat{\alpha} \simeq \underset{1 \leq j \leq n}{\mathrm{argmax}} \left\{ \sum_{i=1}^{j-1} P(H_i = 0|r_i) + \sum_{i=j}^{n} P(H_i = 1|r_i) \right\} \qquad (3.10)$$

where, using Bayes formula and assuming $P(H_i = 0) = P(H_i = 1)\ \forall i$,

$$P(H_i = \ell|r_i) = \frac{p(r_i|H_i = \ell)}{p(r_i|H_i = 0) + p(r_i|H_i = 1)} = \frac{p_{\mathcal{N}}(r_i - \ell \cdot s)}{p_{\mathcal{N}}(r_i) + p_{\mathcal{N}}(r_i - s)} \quad \ell = 0, 1.$$

3.2.3   Simplified Fusion Rule with Multiple Boundaries

Obviously, the computational complexity of the MMSE distributed detection strategy in scenarios with an arbitrary number of phenomenon boundaries increases more rapidly than in scenarios with a single phenomenon boundary (see Section 3.5 for more details). Therefore, the derivation of simplified fusion algorithms with low complexity (but limited performance loss) is crucial.

A first possible choice is a direct extension of the sub-optimal approach in Section 3.2.2 for scenarios with a single phenomenon status change. However, this class of simplified fusion algorithms is not efficient in a scenario with multiple boundaries, since the number of comparisons with all possible sequences of boundaries increases exponentially with the number of sensors. Therefore, we now introduce another class of reduced-complexity fusion algorithms, which do not make use of these comparisons. As before, we distinguish between two possible quantization strategy at the sensors.

Binary Quantization

Define the following function:

$$f_{\mathrm{bq}}(k, \boldsymbol{d}_1^k) \triangleq \sum_{i=1}^{k} [P(H_i = 0|d_i) - P(H_i = 1|d_i)] \qquad k = 1, \ldots, n \qquad (3.11)$$

---

[2]Note that in (3.10) the "argmax" function is used, instead of the "argmin" function used in (3.9), since the objective function needs to be maximized.

where $\boldsymbol{d}_1^k = (d_1, \ldots, d_k)$. The key idea of our approach is the following. The function $f_{\mathrm{bq}}(k, \boldsymbol{d}_1^k)$ is monotonically increasing (or decreasing), with respect to k, while the phenomenon does not change its status. In correspondence to each change of the phenomenon status, the function $f_{\mathrm{bq}}(k, \boldsymbol{d}_1^k)$ changes its monotonic behavior. More precisely, a phenomenon variation from "0" to "1" corresponds to a change, trend-wise, from increasing to decreasing; a phenomenon variation from "1" to "0" corresponds to a change, trend-wise, from decreasing to increasing. Therefore, by detecting the changes of the monotonic behavior of f_{bq} one can estimate the positions of the boundaries. A graphical description of the behavior of f_{bq} is shown in Figure 3.1, where the phenomenon under observation and the function f_{bq} in equation (3.11) are shown, together with the estimated boundaries. In this pictorial example, the estimated phenomenon coincides with the observed phenomenon.

Note that the proposed algorithm (3.11) does not take into account the number of boundaries n_{bs} in the observed phenomenon. However, as we will highlight in Section 2.5.5, our numerical results show that the algorithm estimates accurately the number of boundaries for sufficiently high values of the sensor SNR, i.e., when the quality of the sensors' observations is sufficiently high. Obviously, one may modify the estimation strategy in order to take into account the value of n_{bs}. This will lead to an improvement for small values of the sensor SNR, i.e., a scenario which is not of interest for practical applications. The same considerations on possible refinement of the estimation strategy also hold in the presence of multi-level or in the absence of quantization.

The probability $P(H_i = \ell | d_i)$ $(\ell = 0, 1; i = 1, \ldots, n)$ in (3.11) can be written, by applying the Bayes formula and following an approach similar to that in Section 3.2.2, as

$$P(H_i = \ell | d_i) = \frac{P(d_i | H_i = \ell)}{P(d_i | H_i = 0) + P(d_i | H_i = 1)}$$
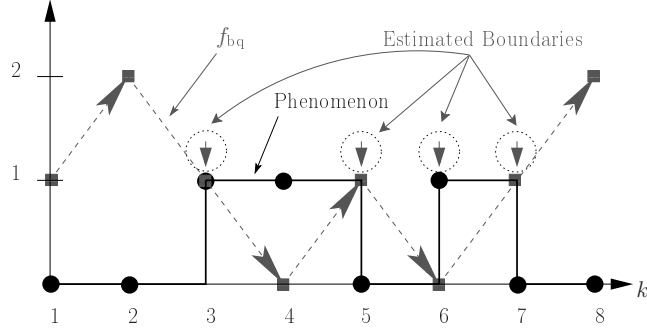
Figure 3.1: Illustrative example: the phenomenon under observation (solid line with circles) and the corresponding function f_{bq} in (3.11) (dashed arrows). The estimated boundaries are indicated by vertical arrows.

where we have used the fact that $P(H_i = 0) = P(H_i = 1)$ and

$$
P(d_i | H_i = \ell) \;=\; \begin{cases} P(s \cdot \ell + n_i < \tau) = P(n_i < \tau - s \cdot \ell) & \text{if } d_i = 0 \\[2mm] P(s \cdot \ell + n_i > \tau) = P(n_i > \tau - s \cdot \ell) & \text{if } d_i = 1 \end{cases}
$$

$$
= \;(1 - d_i)\Phi\left(\frac{\tau - s \cdot \ell}{\sigma}\right) + d_i\left[1 - \Phi\left(\frac{\tau - s \cdot \ell}{\sigma}\right)\right]. \qquad (3.12)
$$

Absence of Quantization

In the absence of quantization at the sensors, one can introduce the following function:

$$
f_{\mathrm{nq}}(k, \boldsymbol{r}_1^k) \triangleq \sum_{i=1}^{k} [P(H_i = 0 | r_i) - P(H_i = 1 | r_i)] \qquad k = 1, \dots, n
$$

where $\boldsymbol{r}_1^k = (r_1, \dots, r_k)$ and

$$
P(H_i = \ell | r_i) = \frac{p(r_i | H = \ell)}{p(r_i | H = 0) + p(r_i | H = 1)} \qquad l = 0, 1; \quad i = 1, \dots, n
$$

with $p(r_i | H = \ell) = p_{\mathscr{N}}(r_i - \ell \cdot s)$. The fusion algorithm at the AP is then identical to that presented in the case with binary quantization, but for the use of f_{nq} at the place of f_{bq}.

3.3   Noisy Communication Links

In this section, we investigate the impact of noisy communication links (between the sensors and the AP) on the structures and performance of the proposed fusion algorithms. In particular, we focus on scenarios with *multi-boundary* phenomena, since the fusion rules for the scenarios with single boundary phenomena and noisy communication links can be easily derived from the equivalent scenarios with ideal communication links.

3.3.1   MMSE Fusion Rule

Binary Quantization

In this case, the noisy communication links between the sensors and the AP are modeled as independent BSCs. Here, we denote as d the sequence of binary decisions at the sensors (as in Section 3.2.1) and as d^{AP} the sequence of binary decisions received at the AP. Because of the presence of BSCs, the received decisions d^{AP} might differ from d (there could be "bit-flipping" in some of the links). In this scenario, the MMSE estimation strategy at the AP becomes:

$$\widehat{\boldsymbol{\alpha}} = \mathbb{E}\left[\boldsymbol{\alpha}|d^{\mathrm{AP}}\right].$$

The analytical framework described in (3.3)-(3.6) can be applied to this scenario as well, by replacing d with d^{AP}. In particular, the *i*-th decision received at the AP can be expressed, using the BSC model, as

$$d_i^{\mathrm{AP}} = \begin{cases} d_i & \text{with probability } (1-p) \\ 1-d_i & \text{with probability } p \end{cases}$$

where p is the cross-over probability of the BSC. After a few manipulations, one obtains:

$$
P(d_i^{AP}|\boldsymbol{\alpha}) = p + (1-2p)P \left(n_i \begin{array}{c} d_i^{AP}=0 \\ \lessgtr \\ d_i^{AP}=1 \end{array} \tau - s\cdot\ell \right) \qquad \text{if } i \in \mathscr{I}_\ell(\boldsymbol{\alpha})
$$

$$
= p + (1-2p)\left\{ (1-d_i^{AP})\Phi\left(\frac{\tau-s\cdot\ell}{\sigma}\right) + d_i^{AP}Q\left(\frac{\tau-s\cdot\ell}{\sigma}\right) \right\} \qquad \text{if } i \in \mathscr{I}_\ell(\boldsymbol{\alpha})
$$

with $\ell = 0,1$.

Absence of Quantization

In a scenario with the absence of quantization, i.e., the sensors transmit real numbers (the likelihood values) to the AP, the BSC model for noisy communication links does not apply. In order to obtain results comparable with those associated with a scenario with binary quantization, we consider AWGN communication links. In other words, the i-th observable at the AP ($i = 1,\dots,n$), denoted as r_i^{AP}, can be written as

$$
r_i^{AP} = r_i^{sensor} + n_i^{comm} \tag{3.13}
$$

where r_i^{sensor} is the observable transmitted by the i-th sensor and n_i^{comm} has a Gaussian distribution $\mathscr{N}(0,\sigma_{comm}^2)$. The value of σ_{comm}^2 is set in order to be consistent with the value of the cross-over probability p in the scenario with BSCs. In particular, in the case with uncoded BPSK transmission over AWGN links, the following relation holds [123]:

$$
p = Q\left(\sqrt{\frac{E_b}{\sigma_{comm}^2}} \right). \tag{3.14}
$$

Therefore, the value of σ_{comm}^2 corresponding to a given value of the cross-over probability p of the equivalent BSC can be obtained from (3.14). This will allow to make a fair performance comparison between the cases with binary quantization and without quantization.

After a few manipulations, one can conclude that the fusion rule described in Section 3.2.1 still holds, by replacing the conditional PDF in (3.8) with the following:

$$p(r_i|\boldsymbol{\alpha}) = \begin{cases} p_{\text{comm}}(r_i) & \text{if } i \in \mathscr{I}_0(\boldsymbol{\alpha}) \\ p_{\text{comm}}(r_i - s) & \text{if } i \in \mathscr{I}_1(\boldsymbol{\alpha}) \end{cases} \qquad i = 1,\dots,n$$

where $p_{\text{comm}}(r) \triangleq \frac{1}{\sqrt{2\pi(\sigma^2+\sigma_{\text{comm}}^2)}} \exp\left[-\frac{r^2}{2(\sigma^2+\sigma_{\text{comm}}^2)}\right]$.

3.3.2 Simplified Fusion Rule

Binary Quantization

In order to extend the reduced-complexity fusion algorithm introduced in Section 3.2.3 for a scenario with ideal communication links to a scenario with BSCs, the objective function in (3.11) must be properly modified. In particular, the following expression for the objective function can be derived:

$$f_{\text{bq}}(k, \boldsymbol{d}_k^{\text{AP}}, p) \triangleq (1-2p) \sum_{i=1}^{k} [P(H_i = 0|d_i^{\text{AP}}) - P(H_i = 1|d_i^{\text{AP}})] \qquad k = 1,\dots,n. \tag{3.15}$$

As one can see, the only difference between (3.11) and (3.15) lies in the term $(1-2p)$. Since $p \in (0, 0.5)$, it follows that the term $(1-2p)$ is always positive. Therefore, this term does not influence the monotonic behavior of the sum at the right-hand side of (3.15) and can be neglected without changing the behavior of f_{bq}. Finally, the conditional probabilities in (3.12) can be extended to a scenario with BSC communication links as follows:

$$P(d_i^{\text{AP}}|H_i = \ell) = p + (1-2p)P\left(n_i \overset{d_i^{\text{AP}}=0}{\underset{d_i^{\text{AP}}=1}{\lessgtr}} \tau - s \cdot \ell\right)$$

$$= (1 - d_i^{\text{AP}})\left[p + (1-2p)\Phi\left(\frac{\tau - s \cdot \ell}{\sigma}\right)\right] + d_i^{\text{AP}}\left\{p + (1-2p)Q\left(\frac{\tau - s \cdot \ell}{\sigma}\right)\right\}.$$

As shown in Section 3.2.3, the evaluation of these conditional probabilities is sufficient for the implementation of the reduced-complexity fusion algorithm illustrated in Figure 3.1.

Absence of Quantization

As previously stated in Section 3.3.1, the fusion rule derived for a scenario with ideal communication links in Section 3.2.3 still applies in the current scenario with noisy communication links, but for the replacement of $P(H_i = \ell | r_i)$ with $P(H_i = \ell | r_i^{AP})(i = 1, \ldots, n; \ell = 0, 1)$, where r_i^{AP} is defined in (3.13). After a few simple manipulations, one obtains:

$$P(H_i = \ell | r_i^{AP}) = \frac{p_{\text{comm}}(r_i^{AP} - s \cdot \ell)}{p_{\text{comm}}(r_i^{AP}) + p_{\text{comm}}(r_i^{AP} - s)} \qquad i = 1, \ldots, n \qquad \ell = 0, 1.$$

3.4 Numerical Results

We now analyze, through Monte Carlo simulations, the performance of the distributed detection schemes previously introduced. We denote as D the following quadratic distance between the observed phenomenon $\boldsymbol{H}$ and its estimate $\widehat{\boldsymbol{H}}$:

$$D(\boldsymbol{H}, \widehat{\boldsymbol{H}}) \triangleq \left| < (\boldsymbol{H} \oplus \widehat{\boldsymbol{H}}); (\boldsymbol{H} \oplus \widehat{\boldsymbol{H}}) > \right|^2 \tag{3.16}$$

where the notation $\oplus$ stands for bit-by-bit ex-or and $\widehat{\boldsymbol{H}}$ is the estimated phenomenon, directly derived from the estimated boundaries' positions $\widehat{\boldsymbol{\alpha}}$. We will simply refer to D as "distance." note that expression (3.16) for the distance reduces to $D(\boldsymbol{H}, \widehat{\boldsymbol{H}}) = |\alpha - \widehat{\alpha}|^2$ in the case of single-boundary phenomena.

The Monte Carlo simulation results are obtained through the following steps:

1. the number of boundaries and their positions are randomly generated according to a uniform distribution[3] (in the case of a single boundary, only its position is randomly generated);

2. the sensors' decisions (or the PDFs of the observables, according to the chosen quantization strategy at the sensors) are transmitted to the AP;

---

[3]Obviously, after the position of a boundary is extracted, the following boundary position is randomly chosen among the remaining positions. After all the boundary positions are extracted, they are ordered. This implies that the multiple conditions in (3.1) are satisfied.

3. the AP estimates the boundaries' positions through either MMSE or simplified fusion algorithms previously proposed;

4. the distance D (between the true phenomenon and its estimate) is evaluated, on the basis of the estimated sequence of boundaries;

5. steps 1÷4 are repeated a sufficiently large number of times, by generating different numbers of boundaries during each simulation run;

6. the average distance $\overline{D}$ is finally computed as the arithmetic average of the distances computed at the previous iterations (in step 4 at each iteration).

We point out that the proposed performance analysis leads to the "average" performance over all possible numbers of boundaries. Should one limit the analysis to a *fixed* number of boundaries, it is expected that the performance will either improve (if the fixed number of boundaries is small) or worsens (if the fixed number of boundaries is large).

3.4.1   Ideal Communication Links

In Figure 3.2, the distance $\overline{D}$ is shown, as a function of the sensor SNR, in a scenario with *single boundary* phenomena and ideal communication links. Two possible values for the number n of sensors are considered: (i) 16 and (ii) 32. The results with both absence of quantization and binary quantization at the sensors are presented. One can observe that the distance reduces to zero for increasing values of the sensor SNR in all considered scenarios; this is to be expected, since the sensors' observations and, consequently, the data sent to the AP are more and more reliable. For low values of the sensor SNR, instead, the distance increases for increasing values of the number of sensors, since larger values for the estimated boundary are possible and, therefore, the distance may become larger. Note, also, that the performance degradation incurred by the use of quantization, with respect to the unquantized case, increases for increasing numbers of sensors. No result in the case of multi-level quantization is reported here. However, the results in [126] show that the use of higher-level quantization (e.g., 2 or 3 quantization bits) leads to a minor performance gain. Finally, the
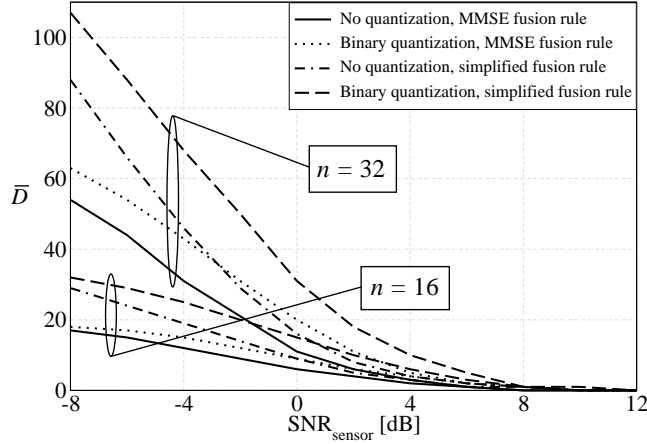
Figure 3.2: Distance, as a function of the sensor SNR, in a scenario with *single boundary* phenomena and ideal communication links. Two possible values for the number *n* of sensors are considered: (i) 16 and (ii) 32. The results with both absence of quantization and binary quantization at the sensors are shown.

scheme with simplified fusion rule at the AP has a performance worse than that of the scheme with the MMSE fusion rule at the AP. However, the performance of the simplified fusion algorithm is close to that of the MMSE fusion rule in the region of interest ($\text{SNR}_{\text{sensor}} \geq 0$ dB) and the performance loss reduces to zero for large values of the sensor SNR.

In order to evaluate the loss incurred by the use of the simplified fusion algorithm, it is expedient to introduce the following percentage loss:

$$
P \triangleq \sqrt{\underbrace{\frac{\overline{D}^{\text{simp}} - \overline{D}^{\text{MMSE}}}{\overline{D}^{\text{MMSE}}}}_{\text{Term}_1} \cdot \underbrace{\frac{\overline{D}^{\text{simp}} - \overline{D}^{\text{MMSE}}}{n^2}}_{\text{Term}_2}}. \tag{3.17}
$$

The intuition behind the definition of P in (3.17), corresponding to the geometric average of Term_1 and Term_2, is the following. Term_1 represents the relative loss of the simplified fusion rule with respect to the MMSE fusion rule. However, using only this term could be misleading. In fact, for high sensor SNRs, the terms $\overline{D}^{\text{simp}}$
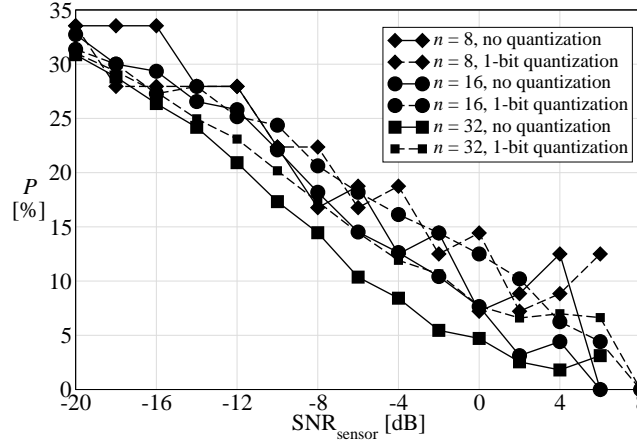
Figure 3.3: Percentage loss, as a function of the sensor SNR, in a scenario with a *single boundary* phenomenon and simplified fusion algorithm at the AP. The communication links are ideal. Three different values for the number n of sensors are considered: (i) 8, (ii) 16, and (iii) 32. The performance in the presence of no quantization (solid lines) is compared with that using binary quantization at the sensors (dashed lines).

and $\overline{D}^{\mathrm{MMSE}}$ are much lower than n^2 (the maximum possible distance). Therefore, even if $\overline{D}^{\mathrm{simp}} > \overline{D}^{\mathrm{MMSE}}$ (for example, $\overline{D}^{\mathrm{simp}} = 4$ and $\overline{D}^{\mathrm{MMSE}} = 1$ with $n = 32$), both algorithms might perform very well. The introduction of Term$_2$ eliminates this ambiguity, since it represents the relative loss (between MMSE and simplified fusion algorithms) with respect to the maximum (quadratic) distance, i.e., n^2. In Figure 3.3, the behavior of P is shown as a function of the sensor SNR. In the region of interest (SNR$_{\mathrm{sensor}} \geq 0$ dB), one can observe that P is lower than 15%, i.e., the proposed simplified fusion algorithm is effective. Note that the same considerations can be carried out in a scenario with noisy communication links.

In Figure 3.4, the distance is shown, as a function of the sensor SNR, in scenarios with multi-boundary phenomena and ideal communication links, with $n = 8$ sensors. no quantization is considered at the sensors and the performance with the simplified fusion algorithm at the AP is compared directly with that obtained using the MMSE
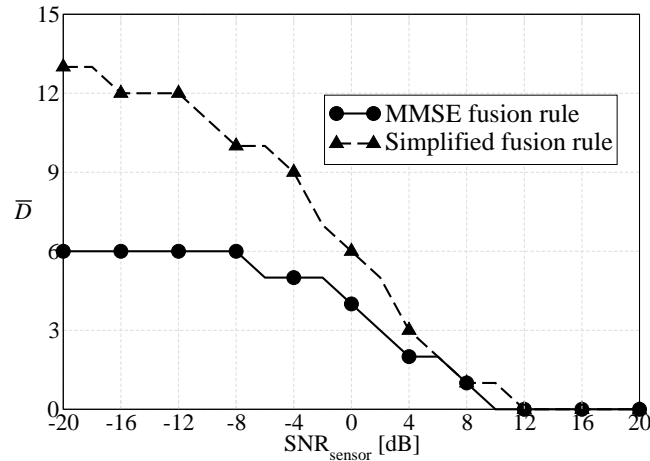
Figure 3.4: Distance, as a function of the sensor SNR, in a scenario with a *multi-boundary* phenomenon, considering $n = 8$ sensors and absence of quantization (MMSE and simplified fusion algorithms at the AP are considered). The communication links are ideal.

fusion rule. As expected, the distance $\overline{D}$ reduces to zero for increasing values of the sensor SNR and the performance with the MMSE fusion algorithm is better than that with the simplified fusion algorithm. We recall that the performance with the MMSE fusion rule can be evaluated only in scenarios with a number n of sensors not larger than 8, since the computational complexity becomes unbearable for values of n larger than 8 (the simulations are too lengthy). In order to investigate scenarios with larger numbers of sensors, the use of the reduced-complexity simplified fusion algorithms derived in Section 3.2.3 is mandatory. Our results presented in [126] show that the proposed simplified fusion rule is effective for all the considered values of the number of sensors n, i.e., the distance reduces to zero for large values of the sensor SNR. Moreover, the performance does not improve by using more than one quantization bit at the sensors. It remains to be investigated what would be the relative loss of the simplified fusion algorithm, with respect to the MMSE fusion algorithm, in scenarios with multi-boundary phenomena. The fact that the quantization strategy at the sensors has little impact seems to suggest that this relative loss might *not* be

Figure 3.5: Distance, as a function of the cross-over probability p, in a scenario with $n = 8$ sensors, binary quantization, and noisy communication links (modeled as BSCs). Three values for the sensor SNR are considered: (i) -10 dB, (ii) 0 dB, and (iii) 10 dB. Both MMSE and simplified fusion algorithms at the AP are considered.

negligible.

3.4.2 Noisy Communication Links

We finally investigate the impact of noisy communication links on the system performance. In Figure 3.5, the distance is shown, as a function of the cross-over probability p, in a scenario with $n = 8$ sensors and binary quantization—in this case, the communication links are modeled as BSCs. Three values for the sensor SNR are considered: (i) -10 dB, (ii) 0 dB, and (iii) 10 dB. Both MMSE and simplified fusion algorithms at the AP are considered. As previously observed in Figure 3.4, the use of the simplified fusion algorithm at the AP leads to a performance worse than that with the MMSE fusion algorithm. However, the higher is the sensor SNR, the lower is the difference between the performance of the two algorithms. Moreover, one can observe that the distance might not converge to zero, due to the presence of two *independent* noise components (i.e., observation and communication noises). For a sufficiently
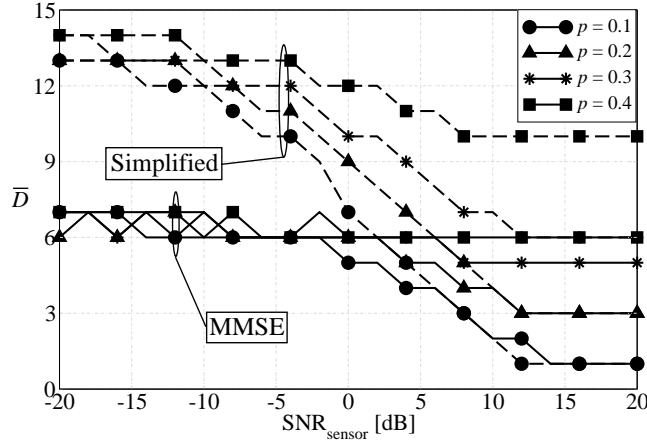
Figure 3.6: Distance, as a function of the sensor SNR, in a scenario with $n = 8$ sensors, binary quantization, and noisy communication links (modeled as BSCs). Four different values of the cross-over probability p are considered: (i) 0.1, (ii) 0.2, (iii) 0.3, and (iv) 0.4. Both MMSE and simplified fusion algorithms at the AP are considered.

high value of the sensor SNR, however, the distance reduces to zero when p tends to zero (as confirmed by the results in Figure 3.4).

In Figure 3.6, the distance $\overline{D}$ is shown, as a function of the sensor SNR, in a scenario with $n = 8$ sensors, noisy communication links (modeled as BSCs), and binary quantization at the sensors. Four different values of the cross-over probability p are considered: (i) 0.1, (ii) 0.2, (iii) 0.3, and (iv) 0.4. The performance with both MMSE and simplified fusion algorithms at the AP is investigated. Unlike the results presented in Section 3.4.1 for a scenario with ideal communication links, there appears to be a distance floor (higher than zero) for larger and larger values of the sensor SNR. This is to be expected, since the communication noise (independent of the observation noise at the sensors) prevents the AP from correctly recovering the data sent by the sensors. In particular, when the cross-over probability is sufficiently high (e.g., $p = 0.4$), the performance does not depend on the value of the sensor SNR, since the noisy communication links make the data sent by the sensors very unreliable. Fi-
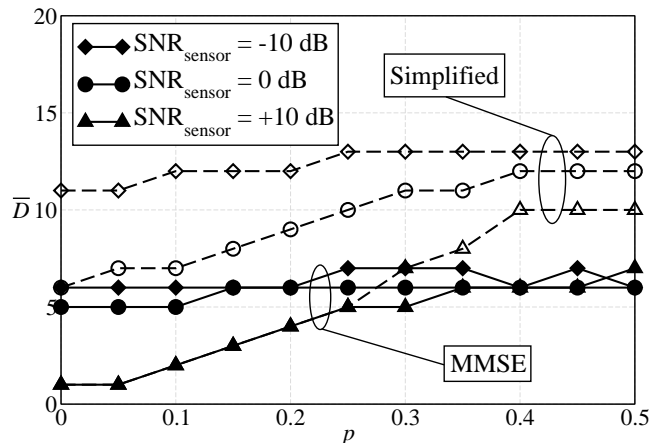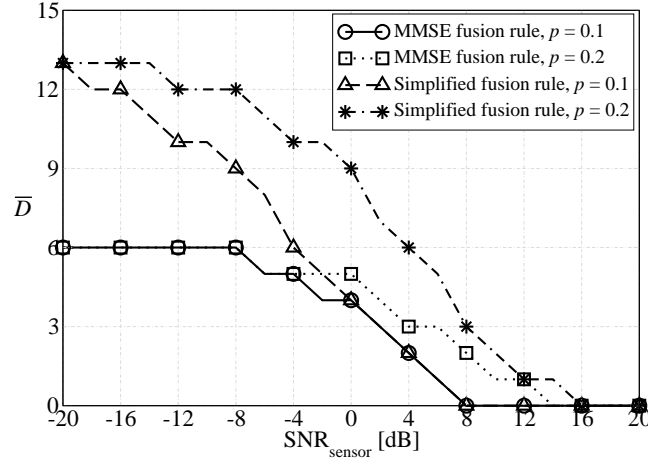
Figure 3.7: Distance, as a function of the sensor SNR, in a scenario with $n = 8$ sensors, absence of quantization, and noisy communication links (modeled as AWGN channels). Two different values of the equivalent bit error rate p (corresponding to different values of σ_{comm}^2 according to (3.14)) are considered: (i) 0.1 and (ii) 0.2. Both MMSE and simplified fusion algorithms at the AP are considered.

nally, one can observe that, for low values of the sensor SNR, the simplified fusion algorithm shows a non-negligible performance loss with respect to the MMSE fusion algorithm. This loss reduces to zero, for increasing values of the sensor SNR, *only* for sufficiently small values of p. In other words, if the communication links are not reliable, then increasing the accuracy of the observations at the sensors is useless.

Finally, in Figure 3.7 the distance $\overline{D}$ is shown, as a function of the sensor SNR, in a scenario with $n = 8$ sensors, absence of quantization, and noisy communication links (modeled as AWGN channels). Two different values of the bit error rate p (corresponding to different values of σ_{comm}^2 according to (3.14)) are considered: (i) 0.1 and (ii) 0.2. The performance of both MMSE and simplified fusion algorithms at the AP is evaluated. One can observe that, unlike the case with binary quantization at the sensors, the distance reduces to zero when the sensor SNR increases, i.e., no floor appears. Moreover, the distance with the simplified fusion rule at the AP approaches

that with the MMSE fusion rule, i.e., it reduces to zero. This means that the proposed simplified fusion algorithm is (asymptotically) effective. Obviously, this is only a theoretical performance limit. In fact, even if the communication links were noisy, the transmission of the "exact" observables (requiring an infinite bandwidth) from the sensors would allow a correct estimation of the true phenomenon. This cannot happen in realistic scenarios with limited transmission bandwidths.

3.5   Computational Complexity

It is now of interest to evaluate the improvement, in terms of computational complexity reduction with respect to the MMSE fusion rule, brought by the use of the simplified fusion algorithms. As complexity indicators, we choose the numbers of additions and multiplications (referred to as n_s and n_m, respectively) required by the considered fusion algorithms, evaluated as functions of the number of sensors n. The following considerations are carried out referring to the formulas relative to the fusion algorithms for the scenario with ideal communication links (i.e., the derivations in Section 3.2). However, the same conclusions still hold for scenarios with noisy communication links, since the structures of the proposed fusion algorithms are the same in both scenarios (i.e., only the expression of the used probabilities and PDFs change).

The numbers of operations (in terms of additions and multiplications) required by the MMSE fusion algorithm are $n_s^{opt} = \Theta(n^{2n_{bs}})$ and $n_m^{opt} = \Theta(n^{2n_{bs}+1})$, respectively—recall that n_{bs} is the number of boundaries. The notation $f(n) = \Theta(g(n))$ means that there exists an n_0 such that for $n > n_0$, $\exists c_1 \in (0,1)$, $c_2 > 1$ such that $c_1 g(n) \leq f(n) \leq c_2 g(n)$ [128]. As described at the beginning of Section 2.5.5, in the considered simulation set-up the number n_{bs} of boundaries is randomly chosen between 1 and $n-2$. Therefore, one can assume that the phenomenon is characterized, on average, by $\frac{n-2}{2}$ boundaries. Under this assumption, the numbers of additions and multiplications required by the MMSE fusion algorithm would be $n_s^{opt} = \Theta(n^{n-2})$ and $n_m^{opt} = \Theta(n^{n-1})$. On the other hand, the reduced-complexity fusion algorithm requires only n additions, since no multiplication has to be performed. Therefore, the

computational complexity of the proposed simplified fusion algorithm is characterized by $n_{\mathrm{m}}^{\mathrm{sub-opt}} = 0$ and $n_{\mathrm{s}}^{\mathrm{sub-opt}} = n$, showing a significant complexity reduction with respect to the MMSE fusion algorithm—this also justifies the non-negligible performance loss at small values of the sensor SNR.

3.6 Concluding Remarks

In this chapter, we have analyzed the problem of distributed detection of spatially non-constant binary phenomena, i.e., phenomena with statuses characterized by single or multiple boundaries. We have proposed an analytical framework considering various quantization strategies at the sensors: (i) no quantization at the sensors and (ii) binary quantization. In all cases, the MMSE fusion algorithm at the AP has been derived and the impact of relevant network parameters (e.g., the sensor SNR, the communication noise level, and the number of sensors) has been investigated. Then, low-complexity fusion rules for scenarios with single-boundary and multi-boundary phenomena have been derived. We have shown that the performance penalty introduced by the simplified fusion algorithms is asymptotically (for high sensor SNR and low communication noise level) negligible. Finally, we have quantified the computational complexity reduction brought by the use of the simplified fusion algorithm with respect to the MMSE algorithm. Our results underline that this complexity reduction is pronounced in scenarios with multi-boundary phenomena.

Chapter 4

Distributed Detection of Correlated Sources

4.1 Introduction

In this chapter, we study the performance of non-cooperative wireless multiple access systems with noisy separated channels, where a generic number of *correlated* sources communicate to an AP. Besides considering a "classical" scenario where the sources are directly connected to the AP, the presence of a relay is taken into account and its impact on the system performance is investigated. In both cases, scenarios with block-faded links are considered. Our goal is to explore the potential benefits which can be obtained when channel coding is used and source correlation is exploited only at the AP (and not at the sources). The AP feeds back to the transmitters simple power control commands in order to counter-act the effects of fading. We consider LDPC-coded communications, and compare different systems (with and without relaying) by keeping fixed the overall coding rate. In relayed scenarios, we develop a novel low-complexity joint detection/decoding iterative algorithm, and the impact of noisy source-relay links on the overall performance is also taken into account. Finally, two simple feedback power control strategies are considered and a simulation-based performance analysis is carried out.

This chapter is structured as follows. In Section 4.2, preliminaries are given. In Section 4.3, the LDPC-coded communication schemes of interest, with and without relaying, are accurately described. In Section 4.4, simple power control strategies are proposed in a scenario with two correlated sources. The performance of the considered schemes is evaluated in Section 4.5, and conclusions are drawn in Section 4.6.

4.2   Preliminaries

Consider n spatially distributed nodes which detect binary information signals $\boldsymbol{x}^{(k)} = [x_0^{(k)}, \ldots, x_{L-1}^{(k)}]$, where $k = 1, \ldots, n$ and L is the signals' length (the same for all sources). The information signals are assumed to be temporally white with $P(x_i^{(k)} = 0) = P(x_i^{(k)} = 1) = 0.5$ and the following simple additive correlation model is considered:

$$x_i^{(k)} = b_i \oplus z_i^{(k)} \qquad\qquad i = 0, \ldots, L-1 \qquad k = 1, \ldots, n$$

where $\{b_i\}$ are independent and identically distributed (i.i.d.) binary random variables and $\{z_i^{(k)}\}$ are i.i.d. binary random variables with probability ρ to be 0 (and $1 - \rho$ to be 1). Obviously, if $\rho = 0.5$ there is no correlation between the binary information signals $\{\boldsymbol{x}^{(k)}\}_{k=1}^{n}$, whereas if $\rho = 1$ the information signals are identical. According to the chosen correlation model, the a-priori joint probability mass function (PMF) of the information signals at the input of the sources at epoch i, with $i = 0, \ldots, L-1$, can be computed. After a few manipulations, one can show that [94]

$$
\begin{aligned}
p(\boldsymbol{x}_i) &= p(\boldsymbol{x}_i|b_i = 0)p(b_i = 0) + p(\boldsymbol{x}_i|b_i = 1)p(b_i = 1) \\
&= \frac{1}{2}\left[\rho^{n_b}(1-\rho)^{n-n_b} + (1-\rho)^{n_b}\rho^{n-n_b}\right] \qquad i = 0, \ldots, L-1 \quad (4.1)
\end{aligned}
$$

where $\boldsymbol{x}_i = (x_i^{(1)}, \ldots, x_i^{(n)})$ and $n_b = n_b(\boldsymbol{x}_i)$ is the number of zeros in $\boldsymbol{x}_i$.

The information signals $\{x_i^{(k)}\}$ have to be delivered to an AP. In order to derive more insights into the benefits of exploiting source correlation at the AP, besides scenarios where the sources transmit directly to the AP, we also consider scenarios with an intermediate node which acts as a *relay* between the sources and the AP. The

use of a relay allows to increase the transmit diversity, under the assumption that the AP can receive information from the sources and the relay. Although we preliminary assume that the communication links between the sources and the relay are *ideal*— this is reasonable, provided that the relay is relatively close to the sources—we then generalize our approach to scenarios with noisy source-relay links.

In the presence of ideal source-relay links, the relay recovers, without errors, the binary information signals $\{\boldsymbol{x}^{(j)}\}_{j=1}^n$, with $\boldsymbol{x}^{(j)} = [x_0^{(j)}, \dots, x_{L-1}^{(j)}]$. For ease of understanding, we denote as "nodes" both the sources and the relay. In general, the proposed scenario may include $n+1$ nodes, where the sources are indexed from 1 to n and the relay is indexed by $n+1$.

Referring to the equivalent low-pass signal representation, we denote as $\boldsymbol{s}^{(k)}$ the complex samples transmitted by the k-th node (either a source or the relay) and as $N^{(k)}$ the length of $\boldsymbol{s}^{(k)}$. In Figure 4.1, we show a pictorial description of the proposed scenario. By $\boldsymbol{f}^{(k)} = [f_0^{(k)}, \dots, f_{N^{(k)}-1}^{(k)}]$ we denote the complex gain vector over the k-th link, which encompasses both path loss and fading, and $\boldsymbol{n}^{(k)} = [n_0^{(k)}, \dots, n_{N^{(k)}-1}^{(k)}]$ is a complex AWGN vector. Regarding the fading affecting the communication links from the nodes to the AP, we assume that the fading is *constant* for the entire duration of a transmission, i.e., $f_i^{(k)} = f^{(k)}$ for $i = 0, \dots, N^{(k)} - 1$, so that the channel link gain can be perfectly estimated at the AP. The fading coefficients $\{f^{(k)}\}$ are assumed to vary independently over consecutive transmitted packets. Moreover, the channel gain is assumed to be Rayleigh distributed (under perfect phase recovery) with $\mathbb{E}[|f^{(k)}|^2] = 1$.

The transmitting rates at the nodes (both at the sources and the relay) depend on the distributed coding strategy: if no relay is used, then the transmitting rate at the k-th source is $h^{(k)} = L/N^{(k)}$, for $k = 1, \dots, n$; if the relay is used, then the transmitting rate at each source node is 1 and the transmitting rate at the relay is $h^{(n+1)} = L \times n/N^{(n+1)}$. In general, there can be distributed channel coding both at the sources and at the relay, so that the network can be characterized by $n+1$ transmitting rates $\{h^{(k)}\}_{k=1}^{n+1}$. We denote as $\boldsymbol{v}^{(k)} = [v_0^{(k)}, \dots, v_{N^{(k)}-1}^{(k)}]$ the binary (not modulated) codeword ($v_i^{(k)} \in \{0, 1\}$) generated at the k-th node.

For simplicity, BPSK is used, i.e., $s_i^{(k)} = y_i^{(k)} \sqrt{E_c^{(k)}}$, where $y_i^{(k)} = 2v_i^{(k)} - 1 = \pm 1$
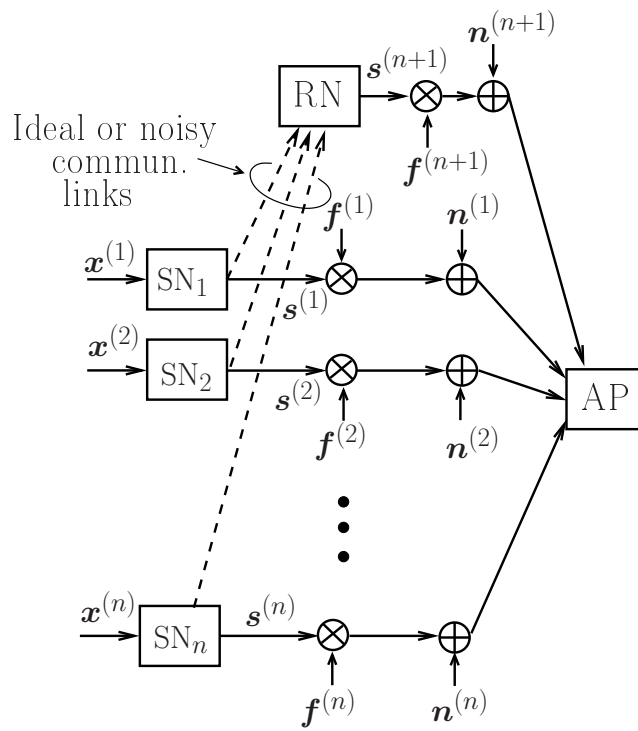
Figure 4.1: Proposed multi-access communication scenario: n source nodes (SNs) communicate directly, and, possibly through a relay node (RN), with the AP.

and $E_c^{(k)}$ is the energy per coded bit transmitted by the k-th node. Therefore, for the sources' transmitters (i.e., for $k = 1, \ldots, n$) $\boldsymbol{y}^{(k)} = [y_0^{(k)}, \ldots, y_{N^{(k)}-1}^{(k)}]$ is a function of the information signal $\boldsymbol{x}^{(k)}$, while for the relay node transmitter (if present) $\boldsymbol{y}^{(n+1)}$ is a function of all the information signals $\{\boldsymbol{x}^{(k)}\}_{k=1}^{n}$. Assuming a perfect channel estimator at the receiver, the real observable at the AP, after matched filtering and carrier-phase estimation, can be expressed as

$$r_i^{(k)} = |f^{(k)}|\sqrt{E_c^{(k)}}y_i^{(k)} + \eta_i^{(k)} \qquad\qquad i = 0, \ldots, N^{(k)} - 1 \quad k = 1, \ldots, n \quad (4.2)$$

where $\eta_i^{(k)}$ is an AWGN variable with zero mean and variance $N_0/2$.

4.3   LDPC-Coded Communication Schemes with and without Relaying

Recent results show clearly that exploiting the source correlation at the receiver leads to an implicit diversity effect which improves the performance in block faded scenarios [129]. Since the use of a *relay* further increases the diversity degree, it is then of interest to evaluate the relative impact of the exploitation of the source correlation in this scenario, and compare directly the obtained performance with that in a scenario without relay.

4.3.1   Scenarios with No Relay

In scenarios with no relay, the information sequences are separately encoded using identical LDPC codes and transmitted over the communication links. In this case, $N^{(k)} = N$ ($k = 1, \ldots, n$), and we assume that the common coding rate at the sources is $L/N = 1/2$. The proposed iterative decoding scheme at the AP is shown in Figure 4.2, where an LDPC decoder per source is considered and the trajectory of the iterative decoding process among these source decoders is highlighted—this decoding scheme is an extension of those, relative to two sources, discussed in [76, 77]. Each LDPC-coded sequence is decoded by using the classical sum-product algorithm [1]. Under
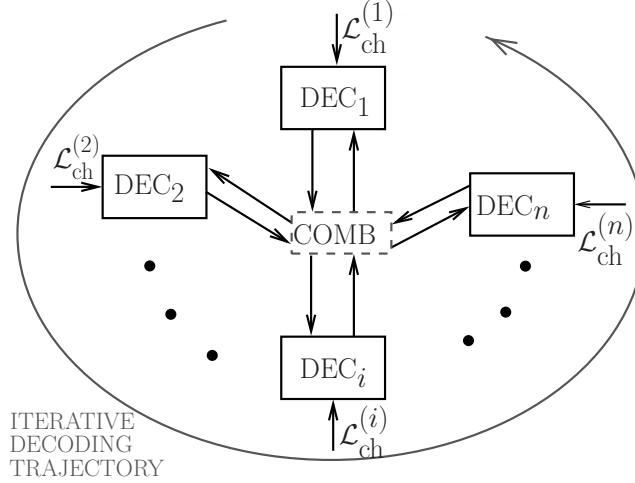
Figure 4.2: Iterative decoding scheme of correlated data in the absence of relay. Each component decoder DEC_i, $(i = 1, \ldots, n)$ is an LDPC decoder, which receives both the channel LLRs and a priori probabilities obtained by properly processing the soft-output reliability values generated by the other decoders. These processing/combining operations are carried out in the central block denoted as "COMB."

the assumption of perfect channel state information (CSI) at the receiver, the channel LLR at the input of the i-th variable node [1] can be expressed as

$$\mathscr{L}_{i,\mathrm{ch}}^{(k)} = \ln \frac{p(r_i^{(k)}|y_i^{(k)} = 1, f_i^{(k)})}{p(r_i^{(k)}|y_i^{(k)} = -1, f_i^{(k)})} = \frac{2r_i^{(k)}\sqrt{E_{\mathrm{c}}^{(k)}}\left|f_i^{(k)}\right|}{\sigma^2} \tag{4.3}$$

where $\sigma^2 = N_0/2$. The maximum number of *internal* decoding iterations in each component LDPC decoder is denoted as $n_{\mathrm{it}}^{\mathrm{int-max}}$.

The a priori information about the correlation between the sources is exploited by applying the following *external* iterative decoding steps between the component LDPC decoders: (i) the a posteriori reliability (i.e., the LLR) on the *information*[1] bits

---

[1]Note that only the information bits are considered in the exchange of reliability information between the component LDPC decoders, since the coded bits are not directly correlated.

of the j-th decoder is properly modified, taking into account the correlation (as will be explained later), and used as a priori reliability for the information bits at the input of the ℓ-th decoder ($j \neq \ell$); (ii) at the first external iteration, the a priori reliability on the information bits at the input of the ℓ-th decoder is obtained by properly modifying the a posteriori reliability of the j-th decoder ($j < \ell$); (iii) the algorithm stops when a maximum number of external iterations (denoted as $n_{\text{it}}^{\text{ext}}$) is reached.

The total LLR at the input of each variable node of the factor graph underlying the ℓ-th LDPC decoder can be expressed as follows:

$$\mathscr{L}_{i,\text{in}}^{(\ell)} = \begin{cases} \mathscr{L}_{i,\text{ch}}^{(\ell)} + \mathscr{L}_{i,\text{ap}}^{(\ell)} & i = 0,\dots,L-1 \\ \mathscr{L}_{i,\text{ch}}^{(\ell)} & i = L,\dots,N-1. \end{cases}$$

In other words, the LLR at the input of the variable nodes associated with the information bits ($i = 0,\dots,L-1$) includes, besides the channel reliability value expressed as in (4.3), the "suggestion" (given by the soft reliability value $\mathscr{L}_{i,\text{ap}}^{(\ell)}$) obtained from a posteriori reliability values output by the other decoders. In particular, the a priori component of the LLR at the input of the ℓ-th decoder can be written as

$$\mathscr{L}_{i,\text{ap}}^{(\ell)} = \ln \frac{P(y_i^{(\ell)} = 1)}{P(y_i^{(\ell)} = -1)} \qquad i = 0,\dots,L-1$$

where $P(y_i^{(\ell)} = \pm 1)$ are derived from the soft-output values generated by the other decoders, as follows. In a straightforward manner, one can rewrite $P(y_i^{(\ell)})$ as

$$P(y_i^{(\ell)}) = \frac{1}{n-1} \underbrace{\left[P(y_i^{(\ell)}) + \dots + P(y_i^{(\ell)}) \right]}_{n-1 \text{ times}}. \tag{4.4}$$

Using Bayes' theorem [94], the probability $P(y_i^{(\ell)})$ can be expressed as

$$P(y_i^{(\ell)}) = \sum_{y_i^{(k)} = \pm 1} P(y_i^{(\ell)}, y_i^{(k)}) = \sum_{y_i^{(k)} = \pm 1} P(y_i^{(\ell)} | y_i^{(k)}) P(y_i^{(k)}) \qquad k = 1,\dots,N \quad \& \quad k \neq \ell.$$
$$\tag{4.5}$$

Approximating the a priori probability $P(y_i^{(k)})$ in (4.5) with the *a posteriori* reliability value, denoted as $\hat{P}(y_i^{(k)})$, output by the k-th decoder ($k \neq \ell$), from (4.5) one obtains:

$$P(y_i^{(\ell)}) \simeq \sum_{y_i^{(k)} = \pm 1} P(y_i^{(\ell)} | y_i^{(k)}) \hat{P}(y_i^{(k)})$$

where

$$\hat{P}(y_i^{(k)}) = \begin{cases} \dfrac{e^{\mathscr{L}_{i,\text{out}}^{(k)}}}{1+e^{\mathscr{L}_{i,\text{out}}^{(k)}}} & \text{if } y_i^{(k)} = +1 \\[3mm] \dfrac{1}{1+e^{\mathscr{L}_{i,\text{out}}^{(k)}}} & \text{if } y_i^{(k)} = -1. \end{cases}$$

At this point, we evaluate the conditional probability $P(y_i^{(\ell)}|y_i^{(k)})$ in (4.5) using the *a priori* distribution (rather than a posteriori reliability values). By using Bayes' theorem, it follows that

$$P(y_i^{(\ell)}|y_i^{(k)}) = \frac{P(y_i^{(\ell)},y_i^{(k)})}{P(y_i^{(k)})} = 2P(y_i^{(\ell)},y_i^{(k)})$$

where we have used the fact that $P(y_i^{(k)} = -1) = P(y_i^{(k)} = +1) = 1/2$, since the BPSK symbols are supposed to be *a priori* equiprobable. Finally, (4.4) can be approximated as

$$P(y_i^{(\ell)}) \simeq \frac{2}{n-1} \sum_{\substack{k=1 \\ k \neq \ell}}^{n} \sum_{y_i^{(k)}=\pm 1} \underbrace{\hat{P}(y_i^{(k)})}_{\text{[from decoder }k]} \cdot \underbrace{P(y_i^{(k)},y_i^{(\ell)})}_{\text{[a priori source correl.]}} \qquad (4.6)$$

where $P(y_i^{(k)},y_i^{(\ell)})$ can be obtained by marginalization of the n-th dimensional a-priori joint PMF $\{P(y_i^{(1)},y_i^{(2)},\ldots,y_i^{(n)})\}$ of the information sequences at the input of the sources.[2] The intuition behind (4.6) consists in modifying the input a priori probability of a single bit by taking into account, through a weighted average, the reliability values (on the same bit) generated by the other decoders. In particular, the weight of the reliability value generated by the k-th decoder is given by the joint a priori probability between the ℓ-th and the k-th decoders.

4.3.2   Scenarios with a Relay and *Ideal* Source-Relay Links

In a scenario with a relay, the uncoded information sequences are transmitted by the sources, and channel coding is considered only at the relay. As anticipated in

---

[2]Since the a priori probabilities need to be evaluated for the systematic bits, in this case $v_i^{(k)} = x_i^{(k)}$ and, therefore, $\{P(y_i^{(1)},y_i^{(2)},\ldots,y_i^{(n)})\} = \{P(2x_i^{(1)}-1,2x_i^{(2)}-1,\ldots,2x_i^{(n)}-1)\}$. The joint PMF of $\{y_i^{(k)}\}_{k=1}^{n}$ can then be obtained directly from (4.1). Note that equation (4.6) is an approximation since, heuristically, the first probability in the summation at the right-hand side is obtained from the reliability values generated by the other decoder, whereas the second probability is a priori.
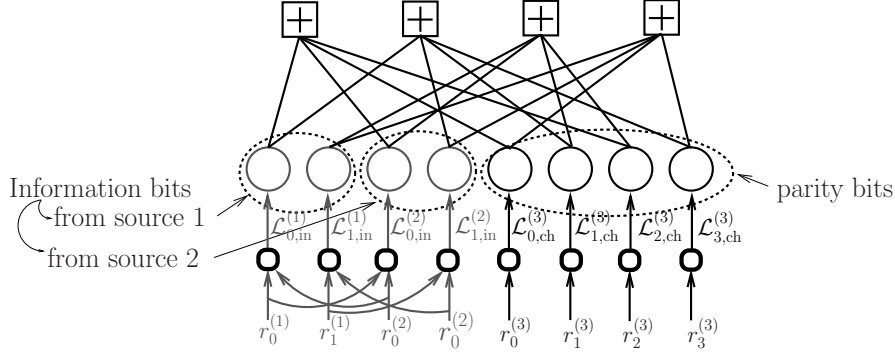
Figure 4.3: Decoding scheme in the presence of two sources and a relay. The modified factor graph for the (2,4) LDPC code presented in [1] is considered.

Section 4.2, due to the broadcast nature of the communication from the sources, we assume that the information sequences are also received by the relay. At this point, the relay multiplexes the data received from the sources to form an information sequence $\boldsymbol{x}$, encodes it using a systematic LDPC code, and sends the parity bits of the codeword to the AP. While the decoding structure proposed in the remainder of this subsection is rigorously valid for error-free source-relay links, in Section 2.5.5 the impact of noisy source-relay links will be evaluated.

At the AP there is a single LDPC decoder. However, the channel LLRs have to be properly modified to take into account the correlation at the sources. A pictorial description of the modified factor graph for the (2,4) LDPC code presented in [1] is shown in Figure 4.3. In particular, there are two sources generating $L = 2$ information bits each and the relay uses a code with rate 1/2. As one can see from Figure 4.3, the factor graph is modified so that the variable nodes corresponding to correlated (information) bits are connected. We now characterize this "connection" in a general scenario with n sources. Since $y_i^{(k)}$ (for the k-th source) is correlated to $\{y_i^{(\ell)}\}$ ($\ell = 1, \ldots, k-1, k+1, \ldots, n$), it follows that $y_i^{(k)}$ depends on $\{r_i^{(\ell)}\}_{\ell=1}^n$: on $(r_i^{(1)}, \ldots, r_i^{(k-1)}, r_i^{(k+1)}, \ldots, r_i^{(n)})$ through $(y_i^{(1)}, \ldots, y_i^{(k-1)}, y_i^{(k+1)}, \ldots, y_i^{(n)})$ and on $r_i^{(k)}$

directly. The LLR at the input of each variable node can be written as

$$\mathscr{L}_{i,\text{in}}^{(k)} = \ln \frac{P(y_i^{(k)} = 1 | \boldsymbol{r}_i, \boldsymbol{f}_i)}{P(y_i^{(k)} = -1 | \boldsymbol{r}_i, \boldsymbol{f}_i)}$$

where $\boldsymbol{r}_i = (r_i^{(1)}, \dots, r_i^{(n)})$ and $\boldsymbol{f}_i = (f_i^{(1)}, \dots, f_i^{(n)})$ are the vectors of the observables and the links' gains on which the k-th information symbol depends. The generic term $P(y_i^{(k)} | \boldsymbol{r}_i, \boldsymbol{f}_i)$ can be computed, by using the total probability theorem and the Bayes formula [94], as[3]

$$
\begin{aligned}
P(y_i^{(k)} | \boldsymbol{r}_i, \boldsymbol{f}_i) &= \sum_{y_i^{(1)}=\pm 1} \cdots \sum_{y_i^{(k-1)}=\pm 1} \sum_{y_i^{(k+1)}=\pm 1} \cdots \sum_{y_i^{(n)}=\pm 1} P(\boldsymbol{y}_i | \boldsymbol{r}_i, \boldsymbol{f}_i) \\
&= \underbrace{\frac{P(\boldsymbol{f}_i)}{p(\boldsymbol{r}_i, \boldsymbol{f}_i)}}_{\Omega_i} \cdot \left[\sum_{y_i^{(1)}=\pm 1} \cdots \sum_{y_i^{(k-1)}=\pm 1} \sum_{y_i^{(k+1)}=\pm 1} \cdots \sum_{y_i^{(n)}=\pm 1} p(\boldsymbol{r}_i | \boldsymbol{y}_i, \boldsymbol{f}_i) P(\boldsymbol{y}_i) \right] \\
&= \Omega_i \sum_{y_i^{(1)}=\pm 1} \cdots \sum_{y_i^{(k-1)}=\pm 1} \sum_{y_i^{(k+1)}=\pm 1} \cdots \sum_{y_i^{(n)}=\pm 1} P(\boldsymbol{y}_i) \prod_{\ell=1}^{n} p(r_i^{(\ell)} | y_i^{(\ell)}, f_i^{(\ell)}) \quad (4.7)
\end{aligned}
$$

where $\boldsymbol{y}_i = (y_i^{(1)}, \dots, y_i^{(n)})$, the conditional independence of $r_i^{(k)}$ and $r_i^{(\ell)}$ ($k \neq \ell$) has been used, and Ω_i *does not* depend on $\boldsymbol{y}_i$. After a few manipulations, one obtains

$$
\mathscr{L}_{i,\text{in}}^{(k)} = \begin{cases} \mathscr{L}_{i,\text{ch}}^{(k)} + \mathscr{L}_{i,\text{corr}}^{(k)} & i = 0, \dots, L-1 \\ \mathscr{L}_{i,\text{ch}}^{(k)} & i = L, \dots, N-1. \end{cases}
$$

where $\mathscr{L}_{i,\text{ch}}^{(k)}$ is defined as in (4.3) and

$$
\begin{aligned}
\mathscr{L}_{i,\text{corr}}^{(k)} =& \ \ln \frac{\sum_{y_i^{(1)}} \cdots \sum_{y_i^{(k-1)}} \sum_{y_i^{(k+1)}} \cdots \sum_{y_i^{(n)}} P(y_i^{(1)}, \dots, y_i^{(k)} = 1, \dots, y_i^{(n)})}{\sum_{y_i^{(1)}} \cdots \sum_{y_i^{(k-1)}} \sum_{y_i^{(k+1)}} \cdots \sum_{y_i^{(n)}} P(y_i^{(1)}, \dots, y_i^{(k)} = -1, \dots, y_i^{(n)})} \\
&+ \ln \frac{\prod_{\substack{\ell=1 \\ \ell \neq k}}^{n} p(r_i^{(\ell)} | y_i^{(\ell)} = +1, f_i^{(\ell)})}{\prod_{\substack{\ell=1 \\ \ell \neq k}}^{n} p(r_i^{(\ell)} | y_i^{(\ell)} = -1, f_i^{(\ell)})}.
\end{aligned}
$$

---

[3]Note that only the LLRs at the input of the variable nodes associated with the information bits has to be modified in order to take into account the correlation between source nodes.

4.3.3   Scenarios with a Relay and *Noisy* Source-Relay Links

The analysis of relayed scenarios has been carried out, so far, in the presence of noiseless links between the sources and the relay. We now generalize this scenario introducing *noisy* source-relay communication links. In this case, we consider two possible relaying strategies: (i) the relay uses the proposed LDPC-coded strategy and adds parity bits, *regardless* of the status of the source-relay links; (ii) the relay is "genie-aided" and adds parity bits *only if* there is no error in the source-relay links; otherwise, no parity bit is added and the AP receives only the information bits from the source. While the system performance with the first strategy (non-genie-aided relay) can be evaluated directly through simulations, in the following paragraph we propose a simple semi-analytical approach to estimating the BER performance with the second strategy (genie-aided relay). We remark that a genie-aided scheme could be implemented by using cyclic-redundancy check (CRC) codes in the transmission from the sources. These codes achieve a very low detection error rate, and its influence on the BER at the AP can be neglected. However, should these codes be used, the overall coding rate would be influenced (reduced) by them. For the sake of simplicity, we simply assume that there is a "genie."

Since we are considering packetized transmissions, we define as $P_{\text{pck}-\text{corr}}$ the probability of correct reception of an information data packet (of L bits) by the relay. Assuming, for simplicity, memoryless[4] source-relay channels with binary modulations (e.g., strong line-of-sight communication channels) and that the relay does not exploit the source correlation, it follows that $P_{\text{pck}-\text{corr}} = (1 - \text{BER}_{\text{s}-\text{r}})^L$, where $\text{BER}_{\text{s}-\text{r}}$ depends on the type of source-relay link: for example, in the case of AWGN links, $\text{BER}_{\text{s}-\text{r}} = Q(\sqrt{2\,\text{SNR}_{\text{s}-\text{r}}})$, where $\text{SNR}_{\text{s}-\text{r}}$ is the SNR at the relay. Given the independence between different source-relay links, the probability of correct reception of all the information packets from all sources is then $P_{\text{corr}} = (P_{\text{pck}-\text{corr}})^n$. The BER at the AP can then be expressed as follows:

$$\text{BER} = \text{BER}_1 \times P_{\text{corr}} + \text{BER}_2 \times (1 - P_{\text{corr}})$$

---

[4]Our approach can be extended to the case of block-faded source-relay links, by properly evaluating the packet error probability.

where BER_1 is given by the BER (previously evaluated through simulations) in the presence of ideal source-relay communication links and BER_2 is the BER influenced by the presence of noise in the source-relay communication links. The value BER_2 depends on the detection strategy followed by the relay, either genie-aided or not. In the presence of errors in the source-relay links, the genie-aided relay does not add any redundancy, so that $BER_2 = BER_{unc}$, where BER_{unc} is the BER with uncoded transmission from sources to AP: if the correlation source is not exploited at the AP, then $BER_{unc} = 0.5 \times [1 - \sqrt{SNR_{s-r}/(1 + SNR_{s-r})}]$; if the correlation is exploited at the AP, then BER_{unc} can be obtained as shown in [129]. In the presence of a non-genie-aided relay, BER_2 is obtained by simulations, using the same iterative decoding strategy developed in the case with ideal source-relay links. Obviously, the AP is assumed to be aware of the coding/no-coding choice of the relay.

4.4   Power Control for Distributed Detection of Correlated Sources

We now focus on scenarios with $n = 2$ spatially correlated sources. As discussed in Section 4.3, we assume that the AP can estimate perfectly the fading coefficients of the wireless links, i.e., $f^{(1)}$, $f^{(2)}$, and, in the presence of a relay, $f^{(3)}$. Considering packetized transmissions, with fading constant for a packet duration, we assume that the fading coefficients are estimated before the transmission of each data packet—for example, through the use of pilot symbols. On the basis of this estimation and a proper decision rule, the AP feeds back to the i-th transmitter ($i = 1, 2, 3$) a power control command. The feedback is assumed to be ideal, i.e., a feedback power control command is received without error. Our approach can be directly extended to scenarios with noisy feedback.

Two possible feedback power[5] control strategies are considered.

- *Balanced SNRs power control strategy*. In this case, the same reference SNR

---

[5]The control power rule can be equivalently expressed as a transmit energy control rule, by taking into account the symbol time interval.

Table 4.1: Balanced SNRs feedback power control strategy. Depending on the value of the instantaneous SNR $\gamma_{\text{b}-\text{inst.}}^{(k)}$ at the end of the k-th link, the AP sends a command (expressed in terms of bit energy correction) to the k-th node.

$\gamma_{\text{b}-\text{inst.}}^{(k)}$ [dB]	ΔE_{b} [dB]
$(\gamma_{\text{ref}} + 2.5, +\infty]$	-3
$(\gamma_{\text{ref}} + 1.5, \gamma_{\text{ref}} + 2.5]$	-2
$(\gamma_{\text{ref}} + 0.5, \gamma_{\text{ref}} + 1.5]$	-1
$(\gamma_{\text{ref}} - 0.5, \gamma_{\text{ref}} + 0.5]$	0
$(\gamma_{\text{ref}} - 1.5, \gamma_{\text{ref}} - 0.5]$	+1
$(\gamma_{\text{ref}} - 2.5, \gamma_{\text{ref}} - 1.5]$	+2
$(-\infty, \gamma_{\text{ref}} - 2.5]$	+3

value, denoted as γ_{ref}, is considered for all links and is set equal to the common average SNR γ_{b}. Then, depending on the value of the instantaneous[6] SNR $\gamma_{\text{b}-\text{inst.}}^{(k)}$, the power control strategy shown in Table 4.1 is applied: depending on the relative values of $\gamma_{\text{b}-\text{inst.}}^{(k)}$ and γ_{ref}, a power control command (expressed in terms of bit energy correction) is chosen.

- *Unbalanced SNRs power control strategy.* In this case, the AP compares the instantaneous SNRs of the links and ranks them from maximum to minimum. Defining $k_{\text{max}} = \arg\max_k \{\gamma_{\text{b}-\text{inst.}}^{(k)}\}$, $k_{\text{min}} = \arg\min_k \{\gamma_{\text{b}-\text{inst.}}^{(k)}\}$, and, in the case with a relay, k_{interm} as the index of the link with intermediate SNR, the AP assigns different reference SNR values $\{\gamma_{\text{ref}}^{(k)}\}$ to the various links. Then, for the k-th link the same power control strategy shown in Table 4.1 is applied, replacing γ_{ref} with $\gamma_{\text{ref}}^{(k)}$.

By trial and error, we found that: in the case without relay, the optimized unbalanced reference SNRs are $\gamma_{\text{ref}}^{(k_{\text{max}})} = \gamma_{\text{b}} + 1.6$ dB and $\gamma_{\text{ref}}^{(k_{\text{min}})} = \gamma_{\text{b}} - 1.6$ dB; in

---

[6]We are implicitly assuming that the AP knows the AWGN variance.

the case with a relay, the optimized unbalanced reference SNRs are $\gamma_{\text{ref}}^{(k_{\max})} = \gamma_b + 1.8$ dB, $\gamma_{\text{ref}}^{(k_{\text{interm}})} = \gamma_b$, and $\gamma_{\text{ref}}^{(k_{\min})} = \gamma_b - 1.8$ dB.

In both the power control strategies outlined above, 7 feedback commands are considered per link. For example, these commands could be implemented considering a 3-bit feedback. For simplicity, we will refer to this case as 3-bit feedback. In Section 4.5, for comparison we will also consider a scenario with infinite-bit feedback commands, i.e., perfect fading compensation.

4.5 Numerical Results

The considered coding schemes are as follows: (i) in scenarios with no relay, each of the source sequences is encoded using a regular (3,6) LDPC code with rate 1/2 and $L = 1000$, and each component decoder performs a maximum number $n_{\text{it}}^{\text{int}-\max}$ of internal iterations set to 50, whereas the number $n_{\text{it}}^{\text{ext}}$ of external iterations between the two decoders is set to 20; (ii) in scenarios with a relay, each of the source sequences has a length $L = 1000$ and the relay uses a regular (3,6) LDPC code with rate 1/2 (the corresponding single LDPC decoder performs a maximum number $n_{\text{it}}^{\text{int}-\max}$ of iterations set to 50) and information sequence length given by $n \times 1000$, so that comparisons between scenarios with and without relay are carried out for the same information rate. The LDPC code is constructed in the same *random* fashion previously explained in Chapter 2.

In Figure 4.4, the BER is shown, as a function of the SNR at the AP. Various systems are considered: (i) without relay, without exploiting the correlation at the AP (W/O R, W/o c); (ii) without relay, exploiting the correlation (W/O R, W c); (iii) with relay, without exploiting the correlation (W R, W/o c), (iv) with relay and exploiting the correlation (W R, W c). In the relayed scenarios, the source-relay links are ideal. The correlation coefficient ρ is set to 0.95. The bit energy $E_{\text{c}}^{(k)}$ is set equal to a common value E_{c} for all the links. Different values for the number n of sources are considered: 2, 3, and 4. As expected, relayed schemes have a higher transmit diversity and, therefore, the performance is better than that in scenarios with no relay. In fact, in relayed scenarios, even if one link is heavily faded, there might be two other reliable
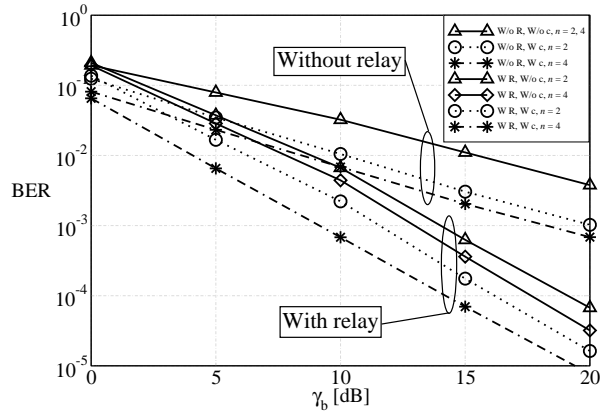
Figure 4.4: BER, as a function of the SNR at the AP, in a scenario with source-AP links with *block-constant* Rayleigh fading (independent from link to link). The correlation coefficient ρ is set to 0.95. Various systems are considered.

communication links available to the AP, allowing the latter to successfully recover the information sequences by exploiting their correlation. On the other hand, in the scenario with no relay, if one link is heavily faded, only one supplementary reliable link could be available and this could not be sufficient for the AP.

In Figure 4.5, the SNR required to achieve a BER equal to 10^{-4} is shown, as a function of the *correlation coefficient* ρ, in various LDPC-coded scenarios. In the relayed cases, the source-relay links are ideal. The number of sources n is either 2 or 4. For comparison, the SNR required when the source correlation is not exploited is also shown, both in the presence and in the absence of a relay. As one can see, in the *presence* of a relay the performance improvement is "smoother" than in the case without a relay and, for any value of ρ, there is approximately the same SNR gain when the number n of sources increases from 2 to 4. In the *absence* of a relay, while the SNR gain is negligible for values of ρ lower than 0.8, for higher values of ρ the gain is more pronounced than in the presence of a relay. In the absence of a relay, however, the number of sources seems to have a limited impact on the SNR gain.

In Figure 4.6, we evaluate the impact of noisy source-relay communication links,
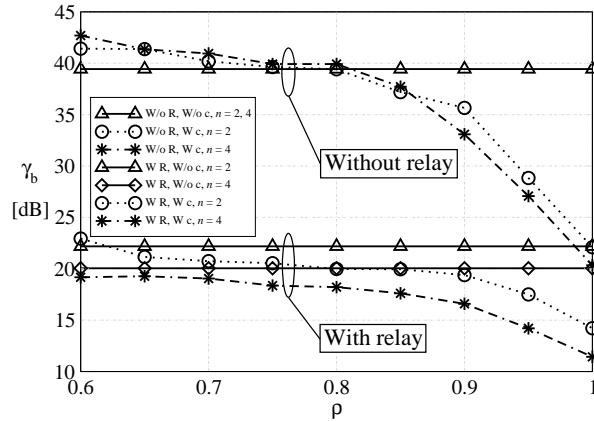
Figure 4.5: SNR, as a function of the *correlation coefficient* ρ, required to achieve a BER equal to 10^{-4} in an LDPC coded scenario with block-faded links. Various systems are considered.
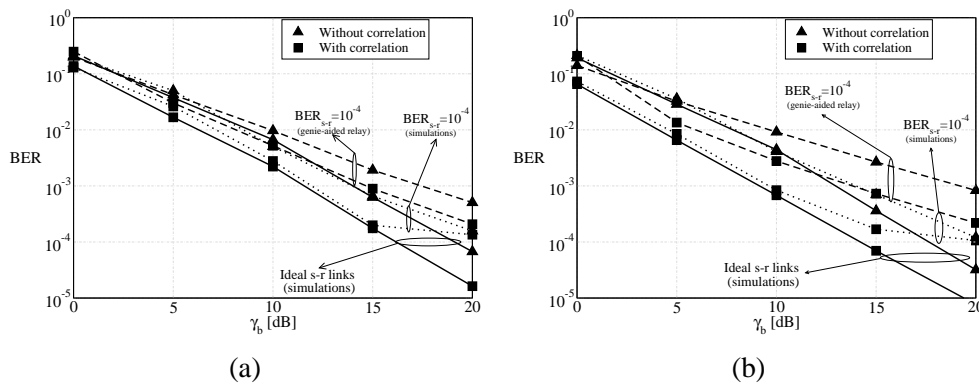
Figure 4.6: Impact of the noise in the source-relay links on the BER performance (at the AP) in scenarios with a relay and (a) $n = 2$ or (b) $n = 4$ sources. The BER at the end of the noisy source-relay links is set to 10^{-4}. The correlation coefficient is set to $\rho = 0.95$. For comparison, the performance in the ideal case with noiseless source-relay links is also shown.

in scenarios with a relay and (a) $n = 2$ or (b) $n = 4$ sources. The correlation coefficient is set to $\rho = 0.95$. As a reference, the performance results in the case of noiseless source-relay links (from Figure 4.4) are also shown. The performance results in the presence of a genie-aided relay correspond to a scenario with $\text{BER}_{s-r} = 10^{-4}$. As one can see, besides a relevant loss, the slope of the BER curves reduces, since the use of the relay is limited only to the cases without source-relay link errors, i.e., the diversity degree reduces. In the same figure, the Monte Carlo simulation results without genie-aided relay selection are shown, considering a source-relay BER equal to 10^{-4}. It can be observed that in the considered SNR range the performance of the coded (with non-genie-aided relay) schemes is better than that of the schemes with a genie-aided relay. However, the BER of the coded schemes reaches a floor, regardless of the use of correlation, equal to $\text{BER}_{s-r} = 10^{-4}$, for both considered values of n. This can be explained as follows. For large values of γ_b, the AP receives correctly the information bits (transmitted by the sources) and the parity bits (transmitted by the relay). If there is a single bit error in the source-relay links, since a (3,6) LDPC code is used, 3 parity bits generated by the relay are "flipped" and received by the AP. At high SNRs, in the LDPC decoder, instead of correcting the three erroneous parity bits, inverts the correct information bit, since the three parity bits have a stronger influence in the message passing-based decoding process. Therefore, at high SNRs the BER at the AP is equal to the probability of bit error in the source-relay links, i.e., BER_{s-r}. Therefore, in the presence of a high noise level in the source-relay links, it follows that the use of a relay is detrimental.

In order to understand further the impact of the noise over the source-relay links, in Figure 4.7 the BER at the AP is shown as a function of the source-relay link BER, considering (a) a coded scheme (with non-genie-aided relay) and (b) a scheme with genie-aided relay. In both cases, the number of sources is set to 2 or 4, and two possible values of the source/relay-AP link SNR are considered. The correlation coefficient is set to $\rho = 0.95$. As one can see comparing Figure 4.7 (a) with Figure 4.7 (b), while for low values of BER_{s-r} the performance of the schemes which make always use of the distributed LDPC coding scheme is better, when the source-relay links become very noisy (for instance, $\text{BER}_{s-r} > 10^{-2}$) then the genie-aided

(a)   (b)
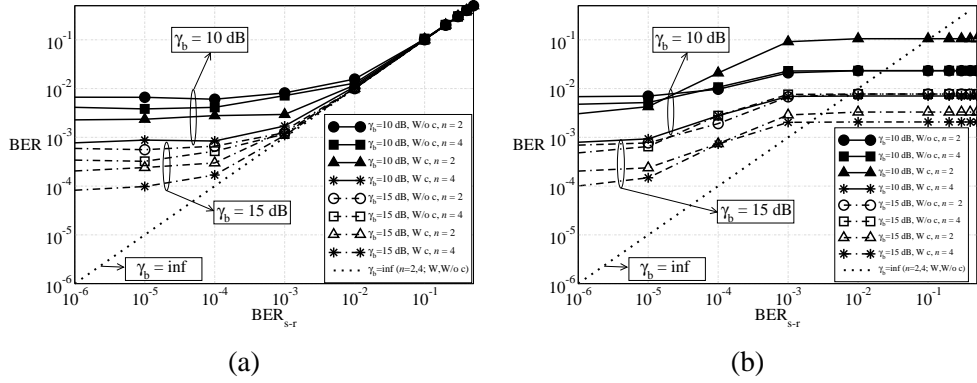
Figure 4.7: BER at the AP, as a function of the source-relay BER, in relayed scenarios (a) with fixed (non-genie-aided) coding at the relay and (b) with the genie-aided approach. In each case, two values of the SNR γ_b at the AP are considered, namely 10 dB and 15 dB, and the number of sources n is either 2 or 4. The correlation coefficient is set to $\rho = 0.95$. In all cases, the performance is evaluated exploiting or not the source correlation at the AP.

scheme is preferable. This result suggests that, in order to optimize the performance of the considered multiple access schemes, an "adaptive" relayed scheme should be used, such that the relay decides which strategy should be adopted depending on the noise level in the source-relay links. In particular, in Figure 4.7 (b) the limiting performance curve in the presence of coding (non-genie-aided) is shown: as one can see, the "switching" point from non-genie-aided to genie-aided corresponds to a scenario in which BER $\simeq$ BER$_{s-r}$. In other words, if BER$_{s-r}$ < BER, then the coded scheme is robust, i.e., the use of a relay leads to a performance improvement; if BER$_{s-r}$ > BER, then the use of a relay is detrimental.

As intuitively expected, the relay should be used only when the quality of the source-relay links is better than the quality of the direct source-AP (and relay-AP) links. While we consider the introduction of redundancy only at the relay, in the presence of noisy source-relay links it is expected that the system performance could be optimized considering also the use of proper channel coding in the source-relay
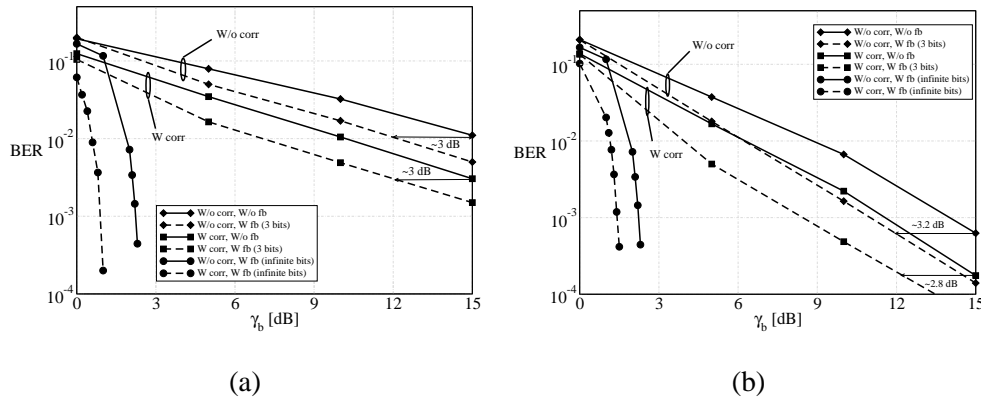
Figure 4.8: BER, as a function of the SNR at the AP, in scenarios (a) without a relay and (b) with a relay. The correlation coefficient ρ is set to 0.95, and the performance is analyzed exploiting or not the correlation at the AP. In the case of feedback, the *balanced* SNRs power control strategy is considered. For comparison, the performance with infinite-bit feedback is also considered.

transmissions, with rate adaptation on a link basis. This goes beyond the scope of our chapter, but represents an interesting extension.

In Figure 4.8, the BER is shown, as a function of the average SNR at the AP, in scenarios (a) without a relay and (b) with a relay. The system performance is analyzed exploiting or not the correlation at the AP. In the case of feedback, the *balanced* SNRs power control strategy is considered: for each value of the average SNR, the associated BER is obtained after feedback power control. As one can see, the use of 3-bit feedback leads to a performance improvement for sufficiently high values of the average SNR, both with and without the exploitation of the correlation at the AP. In particular, the performance improvement, in terms of average SNR, is approximately 3 dB, and for all values of the average SNR the energy saving is between 0.4 dB and 0.6 dB. The energy saving is more pronounced in a scenario with no relay (0.45 dB without and 0.59 dB with exploitation of the correlation at the AP, respectively) with respect to a scenario with relay (0.39 dB without and 0.38 dB with exploitation of the correlation at the AP, respectively). As one can see comparing the results in Fi-

(a)   (b)
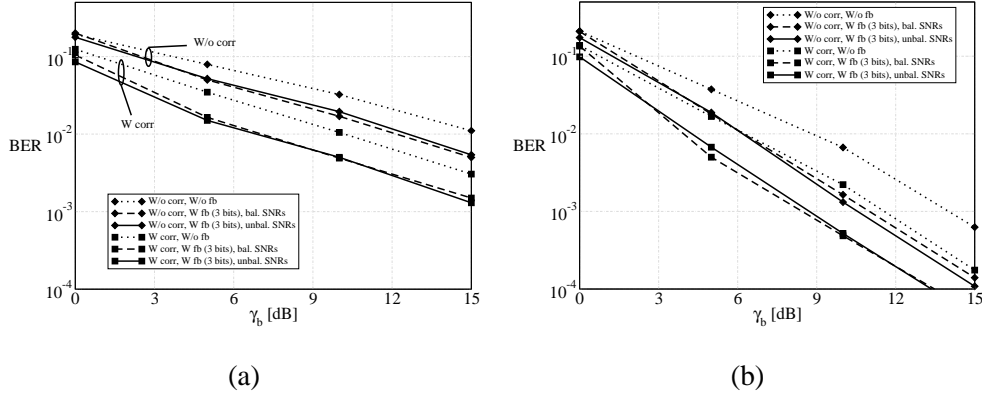
Figure 4.9: BER, as a function of the SNR at the AP, in scenarios (a) without a relay and (b) with a relay, considering *unbalanced* SNR power control strategy. For comparison, the performance results in the presence of a *balanced* SNRs feedback strategy (from Figure 4.8) are also shown. The correlation coefficient ρ is set to 0.95, and the performance is analyzed exploiting or not the correlation at the AP.

gure 4.8 (a) with those in Figure 4.8 (b), the benefits of the use of feedback are slightly reduced in the scenario with a relay. In both subfigures, for comparison, the performance with infinite-bit feedback is also shown. The obtained results correspond to those in a scenario with AWGN communication links, i.e., where the fading has been perfectly recovered.

In Figure 4.9, the BER is shown, as a function of the SNR at the AP, in scenarios (a) without a relay and (b) with a relay, considering an *unbalanced* SNRs 3-bit feedback power control strategy. For comparison, the performance in the presence of a balanced SNRs feedback power control strategy (from Figure 4.8) is also shown. As one can see from the case (a), the use of an unbalanced SNRs rule leads to slightly better performance for low values of the average SNR, and to slightly worse performance for high values of the average SNR. In this case, the energy saving depends on the considered scenario; in particular, there is a gain of 0.15 dB, with respect to the balanced SNRs strategy, in a scenario without exploitation of the correlation at the AP, whereas there is a negligible gain when the correlation is exploited at the AP. In

the case with infinite-bit feedback, the performance with the unbalanced SNRs rule (not reported here for lack of space) is very similar to that shown in Figure 4.8. Unlike the scenario with no relay considered in Figure 4.9 (a), in the presence of a relay the unbalanced SNRs feedback rule leads to a performance improvement, with respect to the balanced SNRs feedback rule, for all the values of the average SNR. However, unlike the scenario with no relay, the unbalanced SNRs feedback rule leads to an energy loss, with respect to the balanced SNRs rule, for all the values of average SNRs. Although this loss is negligible for low values of the SNR, it becomes larger (about 1 dB) for higher values of the SNR (around 10 dB). Therefore, in coded schemes with a relay and a limited feedback, novel feedback power control strategies have to be devised, taking into account the code characteristics (for example, protecting more the parity bits stream, rather than the systematic bit stream).

4.6   Concluding Remarks

In this chapter, we have analyzed wireless multiple access communication systems where a generic number of *correlated* sources communicate, through separated block-faded channels, to an AP, with or without an intermediate relay. *LDPC-coded* transmissions have been considered, and we have derived effective iterative receiver structures at the AP to exploit the source correlation. In particular, the novel iterative receiver for relayed scenarios has a complexity significantly lower than that of the iterative receiver for scenarios with no relay. The impact of noisy source-relay links in relayed coded schemes has also been evaluated. The obtained results show that the relay should add redundancy only if the quality of the source-relay links is better than that of the direct source-AP (and relay-AP) links.

Finally, we have evaluated the impact of feedback. We have considered two simple feedback power control strategies, denoted as balanced SNRs (the quality of all links tend to be equalized to the average link quality) and unbalanced SNRs (the quality of the best link is improved, and viceversa for the worst link). Our results show that the improvement brought by the use of balanced SNRs 3-bit feedback is similar both in the presence or absence of a relay, although the energy savings are

more pronounced in a scenario with no relay. In the case of unbalanced SNRs 3-bit feedback strategy, in the coded case the performance improvement, with respect to the balanced SNRs feedback strategy, is limited in a scenario without a relay and disappears in a scenario with a relay. This suggests that novel feedback power control strategies, with respect to the simple ones proposed in this thesis, should be devised in the presence of a relay.

Chapter 5

Concluding Remarks and Future Work

In this thesis, we have investigated how to incorporate the structural properties of the physical phenomenon under observation into the design of distributed detection algorithms for sensor networks. In particular, three different models have been considered for characterizing the phenomenon under observation.

First, phenomena with the same status across all sensors have been analyzed. In this scenario, distributed detection in the presence of multi-level majority-like information fusion has been proposed, deriving both a communication-theoretic and an information-theoretic analytical framework. We have shown that uniform clustering leads to a lower probability of decision error than non-uniform clustering. The impact of noisy communication links has then been investigated and the analytical results have been confirmed by simulation results. In this scenario, the presence of a non-constant SNR profile at the sensors and the use of a joint detection/decoding/fusion strategy at the AP has been properly taken into account in the design of distributed detection techniques. Our results suggest that the use of repetition codes (i.e., multiple observations) is often the winning choice. The design of more powerful distributed channel codes is an open issue.

In the presence of spatially constant phenomena, an analytical framework to com-

pute the *network lifetime* of clustered sensor networks has also been derived. Reclustering techniques for maximizing the network lifetime have been explored, also evaluating the cost associated with this procedure. The impact of noisy communication links on the network lifetime has also been investigated, showing that the higher is the noise level, the shorter is the network lifetime. However, in this scenario as well reclustering can prolong the network lifetime.

Then, scenarios with phenomenon status independent from sensor to sensor has been considered. We have proposed an analytical framework considering different quantization strategies at the sensors. In all cases, the MMSE fusion algorithm and low-complexity fusion rules at the AP have been evaluated in scenarios with single-boundary and multi-boundary phenomena. We have shown that the performance penalty introduced by the simplified fusion algorithms is asymptotically (for high sensor SNR and low communication noise level) negligible. At the same time, however, we have shown that the computational complexity reduction, with respect to the MMSE algorithm, brought by the use of the simplified fusion algorithm is significant. Our results underline that this complexity reduction is pronounced in scenarios with multi-boundary phenomena.

Finally, the presence of spatial correlation among the sensors has been investigated. LDPC-coded transmissions have been considered, deriving effective iterative receiver structures at the AP to exploit the source correlation, for both scenarios with and without a relay. In the presence of a relay, a novel very effective iterative decoding algorithm with very limited complexity has been proposed. In particular, our results suggest that the relay should add redundancy only if the quality of the source-relay links is sufficiently high. We have also evaluated the impact of feedback. Our results suggest that properly unbalancing the SNRs in the communication links leads to energy savings for a given performance level. In all cases, the performance improvement brought by the exploitation of source correlation at the AP with respect to scenarios with DSC is limited. Therefore, the design of more efficient channel codes for this scenario will be subject of further investigation.

Bibliography

[1] F. R. Kschischang, B. J. Frey, and H. A. Loeliger, "Factor graphs and the sum-product algorithm," *IEEE Trans. Inform. Theory*, vol. 47, no. 2, pp. 498–519, February 2001.

[2] I. Akyildiz, W. Su, Y. Sankarasubramaniam, and E. Cayirci, "A survey on sensor networks," *IEEE Commun. Mag.*, vol. 40, no. 8, pp. 102–114, August 2002.

[3] C. Y. Chong and S. P. Kumar, "Sensor Networks: Evolution, Challanges, and Opportunities," *Proc. IEEE*, vol. 91, no. 8, pp. 1247–1256, August 2003.

[4] S. N. Simic and S. Sastry, "Distributed environmental monitorning using random sensor networks," in *Proc. 2-nd Int. Work. on Inform. Processing in Sensor Networks*, Palo Alto, CA, USA, April 2003, pp. 582–592.

[5] J. N. Tsitsiklis, *Adv. Statist. Signal Process.* Greenwich, CT: JAI Press, 1993, vol. 2, ch. Decentralized detection, pp. 297–344, Eds.: H. V. Poor and J. B. Thomas.

[6] R. Verdone, D. Dardari, G. Mazzini, and A. Conti, *Wireless sensor and actuator networks: Technologies, Analysis and Design.* London, UK: Academic Press, 2008.

[7] R. R. Tenney and N. R. Sandell, "Detection with distributed sensors," *IEEE Trans. Aerosp. Electron. Syst.*, vol. 17, no. 4, pp. 501–510, July 1981.

[8] A. Reibman and L. Nolte, "Design and performance comparison of distribu-ted detection networks," *IEEE Trans. Aerosp. Electron. Syst.*, pp. 2474–2478, December 1987.

[9] R. Viswanathan and P. K. Varshney, "Distributed detection with multiple sensors–Part I: Fundamentals," *Proc. IEEE*, vol. 85, no. 1, pp. 54–63, January 1997.

[10] J. F. Chamberland and V. V. Veeravalli, "Decentralized detection in sensor net-works," *IEEE Trans. Signal Processing*, vol. 51, no. 2, pp. 407–416, February 2003.

[11] H. Gharavi and K. Ban, "Multihop sensor network design for wide-band com-munications," *Proc. IEEE*, vol. 91, no. 8, pp. 1221–1234, August 2003.

[12] I. Y. Hoballah and P. K. Varshney, "An information theoretic approach to the distributed detection problem," *IEEE Trans. Inform. Theory*, vol. 35, no. 5, pp. 988–994, September 1989.

[13] Z.-Q. Luo, "An isotropic universal decentralized estimation scheme for a band-width constrained ad hoc sensor network," *IEEE J. Select. Areas Commun.*, vol. 23, no. 4, pp. 735–744, April 2005.

[14] R. Blum, A. Kassam, and H. Poor, "Distributed detection with multiple sen-sors: Part II," *Proc. IEEE*, vol. 85, no. 1, pp. 64–79, January 1997.

[15] W. Shi, T. W. Sun, and R. D. Wesel, "Quasi-convexity and optimal binary fusion for distributed detection with identical sensors in generalized gaussian noise," *IEEE Trans. Inform. Theory*, vol. 47, no. 1, pp. 446–450, January 2001.

[16] T. S. Rappaport, *Wireless Communications. Principles & Pratice,* 2nd Edition. Uper Saddle River, NJ, USA: Prentice-Hall, 2002.

[17] B. Chen and P. K. Willett, "On the optimality of the likelihood-ratio test for lo-cal sensor decision rules in the presence of nonideal channels," *IEEE Trans. In-form. Theory*, vol. 51, no. 2, pp. 693–699, February 2005.

[18] M. Madishetty, V. Kanchumarthy, C. H. Gowda, and R. Viswanathan, "Distributed detection with channel errors," in *Proc. Thirty-Seventh Southeastern Symposium on System Theory* (SSST), Tuskegee University, AL, USA, March 2005, pp. 302–306.

[19] A. R. Reibman and L. W. Nolte, "Optimal design and performance of distributed signal detection systems with faults," *IEEE Trans. Acoust., Speech, Signal Processing*, vol. 38, no. 10, pp. 1771–1782, October 1990.

[20] S. C. A. Thomopoulos and L. Zhang, "Distributed decision fusion in the presence of networking delays and channel errors," *Information Sciences*, vol. 66, no. 1-2, pp. 91–118, December 1992.

[21] G. Ferrari and R. Pagliari, "Decentralized binary detection with noisy communication links," *IEEE Trans. Aerosp. Electron. Syst.*, vol. 42, no. 4, pp. 1554–1563, October 2006.

[22] N. Patwari and A. O. Hero, "Hierarchical censoring for distributed detection in wireless sensor networks," in *Proc. ICASSP*, vol. 4, Hong Kong, April 2003, pp. 848–851.

[23] M. Gastpar, M. Vetterli, and P. L. Dragotti, "Sensing reality and communicating bits: a dangerous liaison," *IEEE Signal Processing Mag.*, vol. 23, no. 4, pp. 70–83, April 2006.

[24] K. Yamasaki and T. Ohtsuki, "Design of energy-efficient wireless sensor networks with censoring, on-off, and censoring and on-off sensors based on mutual information," in *Proc. IEEE Vehicular Tech. Conf.* (VTC), vol. 2, Stockholm, Sweden, May 2005, pp. 1312 – 1316.

[25] Y. Lin, B. Chen, and P. K. Varshney, "Decision fusion rules in multi-hop wireless sensor networks," *IEEE Trans. Aerosp. Electron. Syst.*, vol. 41, no. 2, pp. 475–488, April 2005.

[26] N. A. C. Cressie, *Statistics for Spatial Data.* New York, NY, USA: John Wiley & Sons, Inc., 1993.

[27] C. Guestrin, A. Krause, and A. P. Singh, "Near-optimal sensor placement in gaussian processes," in *Proc. International Conference on Machine Learning*, vol. 119, Bonn, Germany, August 2005, pp. 265 – 272.

[28] H. Wang, K. Yao, and D. Estrin, "Information-theoretic approaches for sensor selection and placement in sensor networks for target localization and tracking," *Journal of Communications and Networks*, vol. 7, no. 4, pp. 438–449, December 2005.

[29] T. Ikeda, H. Ishiguro, and M. Asada, "Adaptive fusion of sensor signals based on mutual information maximization," in *Proc. Int. Conference on Robotics and Automation* (ICRA'03), vol. 3, Taipei, Taiwan, September 2003, pp. 4398–4402.

[30] F. Gini, F. Lombardini, and L. Verrazzani, "Decentralised detection strategies under communication constraints," *IEE Proc.-Radar, Sonar Navig.*, vol. 145, no. 4, pp. 199–208, August 1998.

[31] B. Chen, R. Jiang, T. Kasetkasem, and P. K. Varshney, "Channel aware decision fusion in wireless sensor networks," *IEEE Trans. Signal Processing*, vol. 52, no. 12, pp. 3454–6458, December 2004.

[32] R. Jiang and B. Chen, "Fusion of censored decisions in wireless sensor networks," *IEEE Trans. Wireless Commun.*, vol. 4, no. 6, pp. 2668–2673, November 2005.

[33] R. Ahlswede, N. Cai, S.-Y. R. Li, and R. W. Yeung, "Network information flow," *IEEE Trans. Inform. Theory*, vol. 46, no. 4, pp. 1204–1216, July 2000.

[34] S.-Y. R. Li, R. W. Yeung, and N. Cai, "Linear network coding," *IEEE Trans. Inform. Theory*, vol. 49, no. 2, pp. 371–381, February 2003.

[35] R. Koetter and M. Medard, "An algebraic approach to network coding," *IEEE/ACM Trans. Networking*, vol. 11, no. 5, pp. 782–795, October 2003.

[36] X. Bao and J. Li, "Matching code-on-graph with network-on-graph: Adaptive network coding for wireless relay networks," in *Proc. Allerton Conf. on Comm., Control and Computing* (ALLERTON), Urbana Champaign, IL, USA, September 2005.

[37] C. Fragouli and E. Soljanin, "Information flow decomposition for network coding," *IEEE Trans. Inform. Theory*, vol. 52, no. 3, pp. 829–848, March 2006.

[38] D. Tuninetti and C. Fragouli, "On the throughput improvement due to limited complexity processing at relay nodes," in *Proc. IEEE Symposium on Information Theory* (ISIT), Adelaide, Australia, September 2005, pp. 1081–1085.

[39] M. Xiao and T. Aulin, "A physical layer aspect of network coding with statistically independent noisy channels," in *Proc. IEEE International Conf. on Commun.* (ICC), vol. 9, Instanbul, Turkey, June 2006, pp. 3996–4001.

[40] C. Hausl and P. Dupraz, "Joint network-channel coding for the multiple-access relay channel," in *Proc. Int. Workshop on Wireless, Ad hoc and Sensor Networks* (IWWAN'06), vol. 3, New York, NY, USA, June 2006, pp. 817–822.

[41] C.-C. Chang and H.-N. Lee, "Space-time mesh codes for the multiple-access relay network: space vs. time diversity benefits," in *Proc. Workshop on Network Coding, Theory, and Applications* (NetCod), San Diego, CA, USA, January 2007.

[42] A. Kansal, A. Ramamoorthy, M. Srivastava, and G. Pottie, "On sensor network lifetime and data distortion," in *Proc. IEEE Symposium on Information Theory* (ISIT), Adelaide, Australia, September 2005, pp. 6–10.

[43] S. Arnon, "Deriving an upper bound on the average operation time of a wireless sensor network," *IEEE Commun. Lett.*, vol. 9, no. 2, pp. 154–156, February 2005.

[44] F. Ordonez and B. Krishnamachari, "Optimal information extraction in energy-limited wireless sensor networks," *IEEE J. Select. Areas Commun.*, vol. 22, no. 6, pp. 1121–1129, August 2004.

[45] H. Zhang and J. Hou, "On deriving the upper bound of lifetime for large sensor networks," in *Proc. ACM Int. Symp. on Mobile Ad Hoc Network. and Comput.* (MOBIHOC), Tokyo, Japan, May 2004, pp. 121–132.

[46] Z. Hu and B. Li, "On the fundamental capacity and lifetime limits of energy-constrained wireless sensor networks," in *Proc. 10th IEEE Real-Time and Embedded Technology and Applications Symp.* (RTAS), Toronto, Canada, May 2004.

[47] D. M. Blough and P. Santi, "Investigating upper bounds on network lifetime extension for cell-based energy conservation techniques in stationary ad-hoc networks," in *Proc. ACM Intern. Conf. on Mobile Comput. and Networking* (MOBICOM), Atlanta, GA, USA, September 2002, pp. 183 – 192.

[48] M. Bhardwaj, T. Garnett, and A. P. Chandrakasan, "Upper bounds on the lifetime of sensor networks," in *Proc. IEEE International Conf. on Commun.* (ICC), vol. 119, Helsinki, Finland, June 2001, pp. 785–790.

[49] M. Bhardwaj and A. P. Chandrakasan, "Bounding the lifetime of sensor networks via optimal role assignments," in *Proc. IEEE Conf. on Computer Commun.* (INFOCOM), vol. 3, New York, NY, USA, June 2002, pp. 1587–1596.

[50] V. Rai and R. N. Mahapatra, "Lifetime modeling of a sensor network," in *Proc. Design, Automation and Test in Europe 2006* (DATE'05), vol. 1, Messe Munich, Germany, March 2003, pp. 202–203.

[51] Y. Chen and Q. Zhao, "On the lifetime of wireless sensor networks," *IEEE Commun. Lett.*, vol. 9, no. 11, pp. 976–978, November 2005.

[52] Q. Zhao, A. Swami, and T. Long, "The interplay between signal processing and networking in sensor networks," *IEEE Signal Processing Mag.*, vol. 23, no. 4, pp. 84–93, 2006.

[53] K. Kalpakis, K. Dasgupta, and P. Namjoshi, "Maximum lifetime data gathering and aggregation in wireless sensor networks," Uni-

versity of Maryland, Baltimore, Tech. Rep., 2002, available at
`www.csee.umbc.edu/ kalpakis/`.

[54] M. E. S. Coleri and T. J. Koo, "Lifetime analysis of a sensor network with
hybrid automata modelling," in *Proc. First Int. Workshop on Wireless Sensor
Networks and Applications 2002* (WSNA'02), Atlanta, USA, September 2002,
pp. 98–104.

[55] M. Franceschetti and R. Meester, "Critical node lifetime in random networks
via the Chen-Stein method," *IEEE Trans. Inform. Theory*, vol. 52, no. 6, pp.
2831–2837, June 2006.

[56] N. F. Timmons and W. G. Scanlon, "Analysis of the performance of IEEE
802.15.4 for medical sensor body area networking," in *Proc. IEEE Conference
on Sensor and Ad Hoc Communications and Networks* (SECON), Santa Clara,
CA, USA, October 2004, pp. 16–24.

[57] IEEE 802.15.4 Std: Wireless Medium Access Control (MAC) and Physi-
cal Layer (PHY) Specifications for Low-Rate Wireless Personal Area Net-
works (LR-WPANs), *IEEE Computer Society Press*, pp. 1–679, October 2003,
ISBN: 0-7381-3677-5.

[58] R. Nowak and U. Mitra, "Boundary estimation in sensor networks: Theory and
methods," in *Proc. 2-nd Int. Work. on Inform. Processing in Sensor Networks*,
Palo Alto, CA, USA, April 2003.

[59] R. Nowak, U. Mitra, and R. Willett, "Estimating inhomogeneous fields using
wireless sensor networks," *IEEE J. Select. Areas Commun.*, vol. 22, no. 6, pp.
999–1006, August 2004.

[60] J. Barros and M. Tückler, "Scalable Decoding on Factor Trees: A Practical
Solution for Wireless Sensor Networks," *IEEE Trans. Commun.*, vol. 54, no. 2,
pp. 284–294, February 2006.

[61] J.-J. Luo and Z.-Q. Luo, "Universal decentralized detection in a bandwidth constrained sensor network," *IEEE Trans. Signal Processing*, vol. 53, no. 8, pp. 2617–2624, August 2005.

[62] S. Duttagupta and K. Ramamritham, "Distributed boundary estimation using sensor networks," Indian Institute of Technology, Mumbai, India, Tech. Rep., 2006, available at `www.it.iitb.ac.in/research/techreport/`.

[63] S. Duttagupta, K. Ramamritham, and P. Ramanathan, "Distributed boundary estimation using sensor networks," in *Proc. Int. Conference on Mobile Ad-hoc and Sensor Systems* (MASS), Vancouver, Canada, October 2006, pp. 316–325.

[64] J. Barros and S. D. Servetto, "On the capacity of the reachback channel in wireless sensor networks," in *Proc. IEEE Workshop on Multimedia Signal Processing*, St. Thomas, US Virgin Islands, December 2002, pp. 408–411.

[65] P. Gupta and P. Kumar, "The capacity of wireless networks," *IEEE Trans. Inform. Theory*, vol. 46, no. 2, pp. 388–404, March 2000.

[66] H. El Gamal, "On the scaling laws of dense wireless sensor networks," *IEEE Trans. Inform. Theory*, vol. 51, no. 3, pp. 1229–1234, March 2005.

[67] J. Barros and S. D. Servetto, "Network information flow with correlated sources," *IEEE Trans. Inform. Theory*, vol. 52, no. 1, pp. 155–170, January 2006.

[68] S. Shamai and S. Verdù, "Capacity of channels with uncoded side information," *European Trans. Telecommun.*, vol. 6, no. 5, pp. 587–600, September-October 1995.

[69] A. Aaron and B. Girod, "Compression with side information using turbo codes," in *Proc. IEEE Data Compression Conference*, Snowbird, UT, USA, April 2002, pp. 252–261.

[70] J. Bajcsy and P. Mitran, "Coding for the Slepian-Wolf problem with turbo codes," in *Proc. IEEE Global Telecommun. Conf.* (GLOBECOM), vol. 2, San Antonio, TX, USA, November 2001, pp. 1400–1404.

[71] I. Deslauriers and J. Bajcsy, "Serial turbo coding for data compression and the Slepian-Wolf problem," in *Proc. IEEE Information Theory Workshop*, Paris, France, March 2003, pp. 296–299.

[72] Z. Xiong, A. D. Liveris, and S. Cheng, "Distributed source coding for sensor networks," *IEEE Signal Processing Mag.*, vol. 21, no. 5, pp. 80–94, September 2004.

[73] J. Garcia-Frias and Y. Zhao, "Compression of correlated binary sources using turbo codes," *IEEE Commun. Lett.*, vol. 5, no. 10, pp. 417–419, October 2001.

[74] Q. Zhao and M. Effros, "Lossless and near-lossless source coding for multiple access networks," *IEEE Trans. Inform. Theory*, vol. 49, no. 1, pp. 112–128, January 2003.

[75] J. Maramatsu, T. Uyematsu, and T. Wadayama, "Low-density parity-check matrices for coding of correlated sources," *IEEE Trans. Inform. Theory*, vol. 51, no. 10, pp. 3645–3654, October 2005.

[76] Y. Zhao, W. Zhong, and J. Garcia-Frias, "Transmission of correlated senders over a Rayleigh fading multiple access channel," *Elsevier Signal Processing*, vol. 86, pp. 3150–3159, November 2006.

[77] J. Garcia-Frias, Y. Zhao, and W. Zhong, "Turbo-like codes for transmission of correlated sources over noisy channels," *IEEE Signal Processing Mag.*, vol. 24, no. 5, pp. 58–66, September 2007.

[78] J. Castura and Y. Mao, "Rateless coding and relay network," *IEEE Signal Processing Mag.*, vol. 24, no. 5, pp. 27–35, September 2007.

[79] F. Daneshgaran, M. Laddomada, and M. Mondin, "LDPC-based channel coding of correlated sources with iterative joint decoding," *IEEE Trans. Commun.*, vol. 54, no. 4, pp. 577–582, April 2006.

[80] C. Hausl, F. Schreckenbach, I. Oikonomidis, and G. Bauch, "Iterative network and channel decoding on a Tanner graph," Monticello, IL, USA, September 2005.

[81] T. M. Cover and A. A. El Gamal, "Capacity theorems for the relay channel," *IEEE Trans. Inform. Theory*, vol. 25, no. 5, pp. 572–584, September 1979.

[82] M. Gastpar and M. Vetterli, "On the capacity of large Gaussian relay networks," *IEEE Trans. Inform. Theory*, vol. 51, no. 3, pp. 765–779, March 2005.

[83] A. Sendonaris, E. Erkip, and B. Aazhang, "User cooperation diversity—Part I and Part II," *IEEE Trans. Commun.*, vol. 51, no. 11, pp. 1927–1948, November 2003.

[84] A. Stefanov and E. Erkip, "Cooperative coding for wireless networks," *IEEE Trans. Commun.*, vol. 52, no. 9, pp. 1470–1476, September 2004.

[85] G. Kramer, M. Gastpar, and P. Gupta, "Cooperative strategies and capacity theorems for relay networks," *IEEE Trans. Inform. Theory*, vol. 51, no. 9, pp. 3037–3063, September 2005.

[86] A. Chakrabarti, E. Erkip, A. Sabharwal, and B. Aazhang, "Code designs for cooperative communication," *IEEE Signal Processing Mag.*, vol. 24, no. 5, pp. 16–26, September 2007.

[87] C. E. Shannon, "The zero-error capacity of a noisy channel," *IRE Trans. Inform. Theory*, vol. 2, pp. 8–19, September 1956.

[88] T. Gaarder and J. K. Wolf, "The capacity region of a multiple-access channel can increase with feedback," *IEEE Trans. Inform. Theory*, vol. 21, pp. 100–102, January 1975.

[89] T. M. Cover and C. S. K. Leung, "A rate region for the multiple access channel with feedback," *IEEE Trans. Inform. Theory*, vol. 27, pp. 292–298, May 1981.

[90] A. D. Murugan, P. K. Gopala, and H. El-Gamal, "Correlated sources over wireless channels: Cooperative source-channel coding," *IEEE J. Select. Areas Commun.*, vol. 22, no. 6, pp. 988–998, August 2004.

[91] L. Ong and M. Motani, "Coding strategies for multiple-access channels with feedback and correlated sources," *IEEE Trans. Inform. Theory*, vol. 53, no. 10, pp. 3476 – 3497, October 2007.

[92] G. Ferrari and R. Pagliari, *Distributed Cooperative Laboratories: Networking, Instrumentation, and Measurements (Signals and Communication Technology).* Springer-Verlag, 2006, ch. "Decentralized Detection in Sensor Networks with Noisy Communication Links", Eds.: F. Davoli, S. Palazzo, and S. Zappatore.

[93] G. Ferrari, M. Martalò, and R. Pagliari, "Decentralized detection in clustered sensor networks," *IEEE Trans. Aerospce and Electronic Systems*, submitted February 2008. Revised November 2008.

[94] A. Papoulis, *Probability, Random Variables and Stochastic Processes.* New York, NY, USA: McGraw-Hill, 1991.

[95] B. Chen, L. Tong, and P. K. Varshney, "Channel aware distributed detection in wireless sensor networks," *IEEE Signal Processing Magazine,* Special issue on "Distributed Signal Processing for Sensor Networks, vol. 23, no. 4, pp. 16–26, July 2006.

[96] Q. Cheng, B. Chen, and P. K. Varshney, "Detection performance limits for distributed sensor networks in the presence of non-ideal channels," *IEEE Trans. Wireless Commun.*, vol. 5, no. 11, pp. 3034–3038, November 2006.

[97] R. Niu, B. Chen, and P. K. Varshney, "Fusion of decisions transmitted over Rayleigh fading channels in wireless sensor networks," *IEEE Trans. Signal Processing*, vol. 54, no. 3, pp. 1018–1027, March 2006.

[98] R. Meester and R. Roy, *Continuum Percolation*. Cambridge, U.K.: Cambridge University Press, 1996.

[99] G. R. Grimmet, *Percolation*. New York, NY, USA: Springer-Verlag, 1999.

[100] O. Dousse, F. Baccelli, and P. Thiran, "Impact of interferences on connectivity in ad hoc networks," in *Proc. IEEE Conf. on Computer Commun.* (INFO-COM), San Francisco, USA, April 2003, pp. 1724 – 1733.

[101] L. Booth, J. Brook, M. Franceschetti, and R. Meester, "Continuum percolation and the geometry of wireless networks," *Annals of Applied Prob.*, vol. 13, no. 2, pp. 722–733, May 2003.

[102] O. K. Tonguz and G. Ferrari, *Ad Hoc Wireless Networks: A Communication-Theoretic Perspective*. Chichester, UK: John Wiley & Sons, Inc., 2006.

[103] T. M. Cover and J. A. Thomas, *Elements of Information Theory*. New York, NY, USA: John Wiley & Sons, Inc., 1991.

[104] G. Ferrari, M. Martalò, and R. Pagliari, "On multi-level decentralized detection in sensor networks," in *Proc. Int. Conference on Intelligent Systems And Computing: Theory And Applications* (ISYC'06), Ayia Napa, Cyprus, July 2006.

[105] Opnet Website, `http://www.opnet.com`.

[106] N. I. of Standards and T. N. Website, `http://www.nist.gov`.

[107] G. Ferrari, P. Medagliani, M. Martalò, and A. Muzzini, "Zigbee wireless sensor networks with data fusion," in *Proc. Int. Symposium on Communications, Control and Signal Processing* (ISCCSP'08), St. Julians, Malta, March 2008, pp. 472–477.

[108] Cross-Bow, "Wireless Sensor Networks," Website: `http://www.xbow.org`.

[109] Atmel Corporation, "Atmel Microcontroller," Website: www.atmel.com/atmel/acrobat/doc2467.pdf.

[110] Texas Instruments, " RF/IF and ZigBee Solutions," Website: http://www.ti.com/.

[111] R. E. Ziemer, *Elements of Engineering Probability & Statistics*. Upper Saddle River, NJ, USA: Prentice-Hall, 1997.

[112] G. Ferrari and M. Martalò, "Extending the lifetime of sensor networks through adaptive reclustering," *Eurasip J. Wireless Commun. and Networking,* Special Issue on "Novel Techniques for Analysis & Design of Cross-Layer Optimized Wireless Sensor Networks", vol. 2007, article ID 31809, 20 pages. doi:10.1155/2007/31809.

[113] J. H. Conway and R. K. Guy, *The Book of Numbers*. New York, NY, USA: Springer-Verlag, 1996.

[114] G. Ferrari, P. Medagliani, S. Di Piazza, and M. Martalò, "Wireless sensor networks: Performance analysis in indoor scenarios," *EURASIP J. Wireless Commun. and Networking,* Special Issue on "MobileMAN (Mobile Multi-hop Ad Hoc Networks): From Theory to Reality", vol. 2007, 2007, article ID 81864, 14 pages, 2007. doi:10.1155/2007/81864.

[115] J. Ma, M. Gao, Q. Zhang, L. M. Ni, and W. Zhu, "Localized low-power topology control algorithms in IEEE 802.15.4-based sensor networks," in *Proc. IEEE International Conference on Distributed Computing Systems*, Columbus, OH, USA, June 2005, pp. 27–36.

[116] G. Ferrari, P. Medagliani, and M. Martalò, "Performance analysis of Zigbee wireless sensor networks with relaying," in *Proc. Int. Workshop on Distributed Cooperative Laboratories* (Ingrid), Santa Margherita Ligure, Italy, April 2007.

[117] G. Ferrari, R. Pagliari, and M. Martalò, "Decentralized binary detection with non-constant SNR profile at the sensors," *Int. Journal on Sensor Networks,*

Special Issue *on "Energy-Efficient Algorithm and Protocol Design in Sensor Networks"*, vol. 4, no. 1, pp. 23–36, 2008.

[118] J. Tsitsiklis, "Decentralized detection by a large number of sensor," *Mathematics of Control, Signals, and Systems* (MCSS), vol. 1, no. 2, pp. 167–182, 1988.

[119] S. Alhakeem and P. K. Varshney, "A unified approach to the design of decentralized detection systems," *IEEE Trans. Aerosp. Electron. Syst.*, vol. 31, no. 1, pp. 9–20, January 1995.

[120] P. Willett, B. Tober, and P. Swaszek, "Fully-connected non-hierarchical decentralized detection networks," in *Proc. IEEE Conf. on Control Applications*, Dayton, OH, USA, September 1992, pp. 404–409.

[121] A. B. Carlson, P. B.Crilly, and J. C. Rutledge, *Communication Systems, An Introduction to Signals and Noise in Electrical Communication, 4th Edition.* New York, NY, USA: McGraw-Hill, 2002.

[122] A. F. Molisch, *Wireless Communications.* Chichester, UK: John Wiley & Sons, 2005.

[123] J. G. Proakis, *Digital Communications,* 4th Edition. New York, NY, USA: McGraw-Hill, 2001.

[124] X. Hu, E. Eleftheriou, and D. Arnold, "Regular and irregular progressive edge-growth tanner graphs," *IEEE Trans. Inform. Theory*, vol. 51, no. 1, pp. 386–398, January 2005.

[125] R. G. Gallager, *Low Density Parity Check Codes.* Cambridge, MA, USA: MIT Press, 1963.

[126] G. Ferrari, M. Martalò, and M. Sarti, "Reduced-complexity decentralized detection of spatially non-constant phenomena," in *Proc. Int. Workshop on Distributed Cooperative Laboratories* (Ingrid), Santa Margherita Ligure, Italy, April 2007.

[127] S. M. Kay, *Fundamentals of Statistical Signal Processing, Volume I: Estimation Theory*. Upper Saddle River, NJ, USA: Prentice-Hall, 1993.

[128] T. H. Cormen, C. E. Leiserson, R. L. Rivest, and C. Stein, *Introduction to Algorithms,* 2nd Edition. Cambridge, MA, USA: MIT Press, 2002.

[129] A. Abrardo, G. Ferrari, and M. Martalò, "Non-cooperative wireless orthogonal multiple access schemes with and without relaying," in *IEEE International Symposium on Communications, Control and Signal Processing* (ISCCSP), St. Julians, Malta, March 2008, pp. 455–460.

Acknowledgments

This thesis would be impossible to develop without the unvaluable guide of my advisor, Dr. Gianluigi Ferrari. His presence and advices have been a constant motivation for my research. He spent a lot of his time trying to push me at my best, also encouraging me during all the difficult moments. I hope I am repaying him for his trust in me and my skills.

Together with Gianluigi, I have to thank all the members (present and past) of the WASN lab, whose affiliation I am very proud. I think that it is impossible to find a similar place where doing high-level research and having funny moments at the same time. Paolo and Busa are the best office mates I could ask.

I would like also to thank all the member of the Information Engineering Department at the University of Parma and, in particular, Prof. Alberto Bononi and Riccardo Raheli who inspired my research with their precious help and comments. The material presented in Chapter 4 has been obtained with the help of Prof. Andrea Abrardo from University of Siena, Italy, whose collaboration has been very profitable from the beginning.

I would like to thank Prof. Christina Fragouli for hosting me during my 6-month internship at the EPFL and introducing me into the interesting world of network coding. Although the large amount of her engagements, she spent a lot of time with me, giving a lot of useful indications and comments to my work. *Un très grand merci* also to Christina's secretary Françoise and all the guys at the ARNI lab of the EPFL, who made my time in Lausanne easier and funnier.

All the work during the last years was impossible to be finished without all my

friend. They were always present to encourage me during the difficult moments and celebrate the victories. Therefore, thanks to my friend living in my native town, Andrea, Chiara, and Roberta, who are still important friends although the life has separeted us. Thank also to Claudio, Emanuela, Giovanni, Michele, and Rocco, who spent some or all these years in Parma with me, making these years "a bed of roses." The months living in Switzerland have been hard and, therefore, I would like to thank my relatives in Basel, who were my second family for those months. It is difficult for me to imagine my period at the EPFL without them. This final year has been so complicated and difficult. The presence of my girlfriend is helping me in quietly living this so important period of my life. Thanks Alba, I think that there is no other to say!!!

Finally, this thesis is dedicated to my parents (Luigi and Maria) and my brothers (Giorgio and Mauro). Simply, I could not be here and I would not have all these possibilities for my future life without their presence and their unconditioned support. Without them, I would be lost...